DIPLOMARBEIT

Investigation of Polarization Modulation in Optical Free Space Communications through the Atmosphere

ausgeführt zum Zwecke der Erlangung des akademischen Grades
einer Diplom-Ingenieurin
unter der Leitung von

Univ.-Ass. Dr. Franz Fidler
Univ.-Prof. Dr. Walter R. Leeb
E389
Institut für Nachrichtentechnik und Hochfrequenztechnik

eingereicht an der Technischen Universität Wien
Fakultät für Elektrotechnik und Informationstechnik

von

Jasmin Grosinger
Matrikelnummer 9925521
Hohe Gasse 9
7441 Pilgersdorf

Wien, im Februar 2008

Danksagung

Ich möchte mich auf diesem Weg bei allen bedanken, die durch ihre fachliche und persönliche Unterstützung zum Gelingen dieser Diplomarbeit beigetragen haben.

Ich danke meinen Eltern, Christine und Manfred Grosinger, die mir das Studium der Elektrotechnik ermöglicht haben und mir dabei immer tatkräftig zur Seite standen.

Ein herzliches Dankeschön auch an Prof. Dr. Walter Leeb, der mir in den wöchentlichen Treffen die richtigen Anregungen gegeben hat um diese Arbeit zu verwirklichen. Durch sein Vorbild wurde mir wissenschaftliches Arbeiten vor Augen geführt.

Ganz besonders möchte ich mich bei Herrn Dr. Franz Fidler bedanken, für die unermüdliche Betreuung und Hilfe, die vielen aufschlussreichen Diskussionen und Ratschläge sowie seine freundschaftliche Unterstützung, die wesentlich zum Gelingen dieser Arbeit beigetragen haben.

Ich danke besonders auch meinen Großeltern, Anna und Franz Morth, meinen Brüdern, Bernhard und Wilfrid Grosinger, meiner Großtante, Sr. Margareta, sowie allen lieben Freunden und Studienkollegen, die mich während meines Studiums immer unterstützt haben.

Jasmin Grosinger

Kurzfassung

Um den ständig steigenden Bandbreitebedarf abzudecken, der mit der Entstehung immer neuerer Kommunikationsanwendungen verbunden ist, werden innovative Technologien benötigt. Optische Freistrahlkommunikation mit Hilfe von Lasern ist eine viel versprechende Kandidatin für diese Anwendungen, sie erlaubt das Übertragen von Informationen bei hohen Datenraten mittels eines kollimierten Laserstrahls. Dabei werden kompakte und leichte Endgeräte verwendet. Im Vergleich zu Mikrowellensystemen treten weniger Interferenzprobleme mit anderen Systemen auf, außerdem liegen die optischen Frequenzen außerhalb der regulierten Frequenzbänder. Während optische Kommunikationsverbindungen zwischen Satelliten bereits Standard sind, kommt es bei Laserkommunikation durch die Atmosphäre zu Leistungseinbußen aufgrund von Bewölkung, schlechten Wetterverhältnissen und atmosphärischen Turbulenzen. Wissenschaftliche Arbeiten zu diesem Thema beschäftigten sich bisher hauptsächlich mit intensitätsmodulierten Systemen. Ob Systeme basierend auf Polarisationsmodulation intensitätsmodulierte Systeme übertreffen, soll in dieser Arbeit untersucht werden, da die Polarisation eines der stabilsten Eigenschaften des Laserstrahls bei Durchgang durch die Atmosphäre zu sein scheint. Ein genauer und detaillierter Vergleich der beiden Modulationsarten ist daher von großem Interesse.

In meiner Diplomarbeit habe ich ein digitales Polarisationsmodulationssystem (PolSK) mit direktem Empfänger entworfen. Dazu habe ich eine kommerziell erhältliche Software verwendet, die die Simulation von optischen Nachrichtentechniksystemen erlaubt. Zwei Empfängerstrukturen wurden realisiert, eine mit und eine ohne optischen Vorverstärker. Ein Vergleich mit einem intensitätsmodulierten System (OOK) hat gezeigt, dass PolSK in spitzenleistungsbegrenzten Systemen um $3\,\mathrm{dB}$ besser ist als OOK. Besonderes Augenmerk ist auf optisch vorverstärkte Empfänger und deren Nichtidealitäten gelegt worden. Nichtidealitäten sind zum Beispiel eine nicht ideale Polarisationsweiche, eine nicht ideale PIN Photodiode mit Transimepedanzverstärker oder nicht ideale optische und elektrische Leitungen. Diese Simulationen haben auch bei der Abschätzung des Einflusses der Atmosphäre im Bezug auf die Empfängersensitivität geholfen.

Ein Einfluss der Atmosphäre auf die Polarisation eines Laserstrahls wird mit Hilfe von polarimetrischen Messungen abgeschätzt. Die Polarimetrie ist ein Forschungsgebiet in der Astronomie. Ein Vergleich von Messungen von teilweise polarisiertem Sternenlicht auf der Erde und im Weltall (Hubble Space Telescope) gibt Aufschluss über einen solchen Einfluss. Basierend auf diesen Daten habe ich einen geringen und vernachlässigbaren atmosphärischen Einfluss auf die Polarisation festgestellt.

Für eine praktische Realisierung von PolSK-Systemen mit optischen Vorverstärkern habe ich eine Marktstudie gemacht, um die geeigneten Komponenten dafür zu finden. Zwei Realisierungsarten für hochempfindliche Empfänger mit PIN Photodioden werden präsentiert.

Obwohl die Komplexität eines PolSK-Systems größer ist als bei einem OOK-System überwiegen die Vorteile in spitzenleistungsbegrenzten Systemen, wie zum Beispiel die konstante Einhüllende des Sendesignals und der $3\,\mathrm{dB}$ Gewinn in der Empfängersensitivität. Daher ist Polarisationsmodulation eine viel versprechende Kandidatin um Systeme mit Intensitätsmodulation in der optischen Freistrahlkommunikation durch die Atmosphäre abzulösen.

Abstract

Innovative technologies are required to satisfy the ever increasing bandwidth demand associated with new communication services. Optical free space laser communications - with its ability to transmit information via a collimated laser beam at high data rates using compact, low-mass terminals, while avoiding interference problems and without exhausting the radio-frequency bandwidths - is a promising candidate in the field. While optical intersatellite links are state-of-the-art technology, laser communications from ground suffers from cloud coverage, harsh weather conditions, and atmospheric turbulence. Most of the previous work on optical free space laser communications through the atmosphere was concentrated on intensity modulated systems. However, polarization modulated systems may be more appropriate for such communication links, because the polarization seems to be the most stable characteristic of a laser beam while propagating through the atmosphere. Thus, a detailed comparison between intensity and polarization modulated systems is of big interest.

In my thesis I have implemented a direct detection digital *polarization shift keying* (PolSK) system with the aid of a commercially available software to simulate the behavior of optical transmission systems. Two receiver structures are realized, for the absence and for the presence of optical amplification in the receiver. A comparison with intensity modulated systems shows that PolSK outperforms *on-off keying* (OOK) systems in terms of peak optical power by about $3\,\mathrm{dB}$. Special attention is given to the PolSK receiver with optical preamplification and the non-idealities which arise in such systems, e.g., a non-ideal polarization beam splitter, a non-ideal PIN photodiode with transimpedance amplifier, or non-ideal optical and electrical wires. The simulations also help to assess penalties in the receiver's sensitivity when investigating the influence of the atmosphere.

The influence of the atmosphere on the polarization of a laser beam is assessed in terms of polarimetry, a field of research in astronomy. A comparison between ground based and space based (Hubble Space Telescope) polarimetric measurements of partially polarized stars gives further information about such an influence. Based on these measurements I showed that the atmospheric influence on the polarization in rather small and thus negligible.

For a practical implementation of an PolSK system with optical amplifier a market study is done to list appropriate devices. Two realizations of high sensitivity receivers, which use PIN photodiodes as detectors, are presented.

Although the complexity of an PolSK system is higher than that of an OOK system, the advantages of PolSK in peak power limited systems such as the constant envelope of the transmit signal and the $3\,\mathrm{dB}$ sensitivity gain predominate the disadvantages. Thus, PolSK is a promising candidate to replace OOK as modulation system in optical free space communications through the atmosphere.

Contents

Chapter 1

Polarization Shift Keying Systems

1.1   Introduction

The investigation of polarization modulation in optical free space communications through the atmosphere is of particular interest, because systems based on polarization modulation show some advantages in comparison with other modulation formats. It is assumed that the polarization is the most stable characteristic of a laser beam while propagating through the atmosphere (see Chapter 2). Furthermore, polarization modulation features a constant envelope of the transmitted optical power, which makes it especially attractive for peak power limited systems.

Various studies on polarization modulation in optical transmission systems have been published. In 1992, a polarization modulated direct detection optical transmission system was researched by Betti [1], suitable for binary and multilevel transmission. The receiver was proposed to extract the Stokes parameters of the transmitted light (Stokes receiver). The system's performance was analyzed for the absence and for the presence of optical amplifiers. In 1995, results by Benedetto [2] show that the performance of a binary polarization modulated direct detection system is approximately $3\,dB$ better in terms of peak optical power than an intensity modulated direct detection system. In 2003, a 4-level direct detection polarization modulated system realized with phase modulators was presented by Hu [3]. The use of polarization modulation in long-haul fiber transmission systems was carried out by Carena [4]. Lepley [5] reported about the influence of polarization mode dispersion in polarization modulated fiber link transmission systems. Dispersion-tolerant transmission over a standard single mode fiber using a duobinary polarization modulated transmission system was proposed by Siddiqui [6]. In 2005, Chi [7] presented a scheme for the generation of a $40\,Gbit/s$ binary polarization modulated signal, which was successfully transmitted over a $50\,km$ standard single mode fiber with a penalty of $0.6\,dB$. An investigation of digital coherent optical polarization modulation schemes was also done by Benedetto [8][9].

The aim of my diploma thesis is to assess the performance of a direct detection digital modulation system based on polarization modulation. The implementation is done in VPItransmissionMaker from VPI photonics, a commercially available software to simulate the behavior of optical transmission systems. Moreover, I will investigate the impact of the atmosphere on the polarization based on information given in literature. For a practical realization of polarization modulated systems I perform a market research to find appropriate devices.

The polarization modulated system, introduced in this chapter, is composed of a transmit-

ter, a free space channel which attenuates the mean received power by a variable value, and a receiver. The transmitter imprints digital data on the optical signal by means of a polarization modulator. Two receiver structures are implemented, for the absence and for the presence of optical amplification. The receivers performances are compared to the performances of intensity modulated systems. Another objective of my diploma thesis is to model non-idealities within the receiver structures. Penalties in the receivers performances, when real, non-ideal optic and electronic devices are used, can be estimated. In the second chapter, I present the literature research on the impact of the atmosphere on the polarization. In the third chapter, I discuss the realization of a receiver. Some appropriate optic and electronic devices are presented.

1.2 Polarization modulation

In telecommunications, modulation is the process of varying a carrier signal to transmit information. In optics this carrier signal is a light beam. The physical characteristics of the signal, on which the information is modulated, can be the amplitude, the phase, the frequency, or the polarization. It is also distinguished between analog and digital transmission [10].

The most important digital modulation formats are *amplitude shift keying* (ASK), *frequency shift keying* (FSK), *phase shift keying* (PSK) and *differential PSK* (DPSK). ASK modulates digital data ('1's and '0's) as variations in the amplitude onto the optical carrier. The simplest and most common form of ASK is *on-off keying* (OOK), the optical signal is simply turned on and off in response to whether the data is a '1' or a '0'. In an FSK system the transmitter generates a specific frequency for a '1' and a different frequency for a '0'. In PSK, the transmitter sends an in-phase signal for a '1' and an out-of-phase signal for a '0' (or vice-versa). A variation of PSK is DPSK, where a phase change is used to indicate transition from a '1' to a '0' or a '0' to a '1' [11]. As an alternative to the standard digital modulation techniques in optical communications *polarization shift keying* (PolSK) is proposed, where the digital information is encoded in the *state of polarization* (SOP) of the launched light.

1.2.1 Polarization

The study of the vectorial nature of light has shown that a planar electro-magnetic wave is a solution to Maxwell's equations in free space. This subsection is addressed to the evolution of the electric field in the plane perpendicular to the propagation direction $\vec{e}_z$ (see Fig.(1.1)). The motion of the electric field in this plane governs the polarization of the wave [12].

Maxwell's equations

Light propagates in the form of waves [13]. Maxwell's equations completely describe the propagation and spatial extent of electromagnetic waves in free space and in any medium [12].

They establish a relationship between the electric field $\vec{E}(\vec{r}, t)$ and the magnetic field $\vec{H}(\vec{r}, t)$ at a fixed point in time and space. The following equations are not the original ones, they are adopted for ideal (electric conductivity $\kappa = 0$) dielectric materials, where charge density and
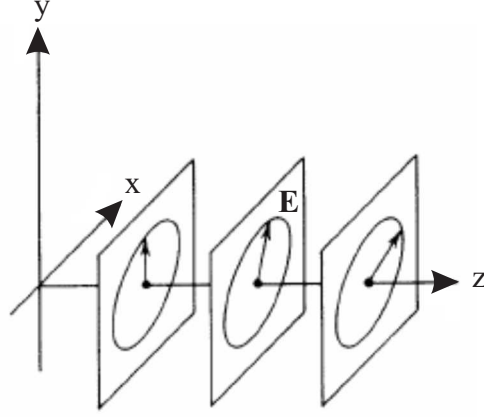
Figure 1.1: Plane wave traveling in z-direction $\vec{e}_z$ (**E** ... electric field vector) [13]

current density are set to zero [14][15]:

$$
\begin{aligned}
\vec{\nabla} \cdot \varepsilon \vec{E}(\vec{r},t) &= 0, & (1.1)\\
\vec{\nabla} \cdot \mu \vec{H}(\vec{r},t) &= 0, & (1.2)\\
\vec{\nabla} \times \vec{E}(\vec{r},t) &= -\mu\frac{\partial \vec{H}(\vec{r},t)}{\partial t}, & (1.3)\\
\vec{\nabla} \times \vec{H}(\vec{r},t) &= \varepsilon\frac{\partial \vec{E}(\vec{r},t)}{\partial t}, & (1.4)
\end{aligned}
$$

where t represents the time and the position vector is $\vec{r} = x\vec{e}_x + y\vec{e}_y + z\vec{e}_z$ in the cartesian coordinate system with $\vec{e}_x$, $\vec{e}_y$, and $\vec{e}_z$ being the basis vectors of the coordinate system. The vectorial differential operator Nabla $\vec{\nabla}$ is defined as $\vec{\nabla} = \partial_x\vec{e}_x + \partial_y\vec{e}_y + \partial_z\vec{e}_z$, ε is the electric field permittivity, and μ is the magnetic field permeability. In vacuum, $\varepsilon = \varepsilon_0 = 8.854 \cdot 10^{-12}$ As/Vm and $\mu = \mu_0 = 4\pi \cdot 10^{-7}$ Vs/Am [15].

The ideal dielectric medium is presumed to be homogeneous, isotropic, linear, and time-invariant [14]. It is now possible to merge the coupled equations to get one expression for the electric field based on Eqn.(1.3) inserting Eqn.(1.1) and (1.4) [15],

$$
\nabla^2 \vec{E}(\vec{r},t) - \mu\varepsilon\frac{\partial^2 \vec{E}(\vec{r},t)}{\partial t^2} = 0. \tag{1.5}
$$

In Equation (1.5) the identity $\vec{\nabla} \times (\vec{\nabla} \times \vec{E}) = \vec{\nabla}(\vec{\nabla} \cdot \vec{E}) - \nabla^2\vec{E}$ was used, where ∇^2 is the Laplace operator in cartesian coordinates [15],

$$
\nabla^2 = \frac{\partial^2}{\partial x^2} + \frac{\partial^2}{\partial y^2} + \frac{\partial^2}{\partial z^2}. \tag{1.6}
$$

Using the Maxwell relation $c^2\varepsilon\mu = 1$ with phase velocity c in Eqn.(1.5), the result is the well-known homogenous wave equation [15],

$$
\nabla^2 \vec{E}(\vec{r},t) - \frac{1}{c^2}\frac{\partial^2 \vec{E}(\vec{r},t)}{\partial t^2} = 0. \tag{1.7}
$$

For time-harmonic processes the electric field vector is written as [14]

$$\vec{E}(\vec{r}, t) = \Re\left[\vec{E}(\vec{r})e^{j\omega t}\right] = \frac{1}{2}\left(\vec{E}(\vec{r})e^{j\omega t} + \vec{E}^{\star}(\vec{r})e^{-j\omega t}\right), \tag{1.8}$$

where ω represents the angular frequency, $j = \sqrt{-1}$, and $\Re[\cdot]$ denotes the real part of a complex number. Applying time-harmonic processes to Eqn.(1.7) ($\partial/\partial t \to j\omega$, $\partial^2/\partial t^2 \to -\omega^2$, vector $\to$ phasor) yields the Helmholtz equation [14][15],

$$\nabla^2\vec{E}(\vec{r}) + \frac{\omega^2}{c^2}\vec{E}(\vec{r}) = 0. \tag{1.9}$$

The derivation for the magnetic field is analogue.

The most simple solution for Eqn.(1.9) is the plane wave given by [15]

$$\vec{E}(\vec{r}) = \vec{E}(\vec{k})e^{-j\vec{k}\cdot\vec{r}}, \tag{1.10}$$

where $\vec{k}$ is the wave vector, which denotes the propagation direction of the wave, and $\vec{k} \cdot \vec{r}$ denotes the scalar product of the vectors $\vec{k}$ and $\vec{r}$. The Expression (1.10) can be directly inserted into Eqn.(1.8) to get an equation for the electric field in the time domain [15][16],

$$\vec{E}(\vec{r}, t) = \Re\left[\vec{E}(\vec{k})e^{j(\omega t - \vec{k}\cdot\vec{r})}\right] = \Re\left[\vec{E}_c(\vec{r}, t)\right], \tag{1.11}$$

where [16]

$$\vec{E}(\vec{k}) = \begin{pmatrix} E_x e^{j\phi_x} \\ E_y e^{j\phi_y} \\ E_z e^{j\phi_z} \end{pmatrix} \tag{1.12}$$

is the complex envelope of the electric field, which is composed of the magnitudes E_x, E_y, and E_z and the phases ϕ_x, ϕ_y, and ϕ_z. The complex electric field vector can be denoted with

$$\vec{E}_c(\vec{r}, t) = \begin{pmatrix} \tilde{E}_x(t) \\ \tilde{E}_y(t) \\ \tilde{E}_z(t) \end{pmatrix}. \tag{1.13}$$

The planes of constant phase of Eqn.(1.11), $\omega t - \vec{k} \cdot \vec{r} = const.$, are orthogonal to the wave vector $\vec{k}$. The wavenumber $k = |\vec{k}|$ can not be chosen independently of ω, the dispersion relation $k^2 = \omega^2/c^2$ has to be met to let Eqn.(1.10) solve Eqn.(1.9). The physical meaning of k is that of a spatial frequency, e.g., two planes of constant phase are separated by the distance $\lambda = 2\pi/k$, which is called the wavelength. In vacuum, the wavelength is $\lambda_0 = 2\pi/k_0 = 2\pi c_0/\omega = c_0/f$, where $c_0 \approx 3 \cdot 10^8$ m/s is the velocity of light in vacuum and $f = \omega/2\pi$ is the frequency.

Elliptical polarized light

Consider a time-harmonic monochromatic plane wave in an ideal dielectric medium traveling in the z-direction of the Cartesian coordinate system, i.e., $\vec{k} \cdot \vec{r} = kz$ with $\vec{k} = k\vec{e_z}$ (see Fig.(1.1)). The electric field lies in the (x,y) plane, i.e., $\vec{k} \cdot \vec{E} = 0$, and is generally described by [13][12]

$$\vec{E}(z, t) = \Re\left[\begin{pmatrix} E_x e^{j\phi_x} \\ E_y e^{j\phi_y} \end{pmatrix} e^{j(\omega t - kz)}\right]. \tag{1.14}$$

The complex 2-row column vector in Eqn.(1.14) is called the Jones polarization vector, $\vec{E}_J$. The plane wave propagates along the z-axis with a wavelength $\lambda = 2\pi/k$. The two field components in the (x,y) plane complete full cycles with the angular frequency ω. The polarization of the wave is governed by the electric field evolution in the (x,y) plane [12].

Converting Eqn.(1.14) to its real-valued counterpart, the electric field vector is [12]

$$\vec{E}(z,t) = E_x \cos{(\omega t - kz + \phi_x)}\vec{e_x} + E_y \cos{(\omega t - kz + \phi_y)}\vec{e_y}. \tag{1.15}$$

Since only the relative phase positions are important, ϕ_x is set to zero and ϕ_y is set to the phase difference $\phi = \phi_y - \phi_x$ [13]. Equation (1.15) describes an ellipse in the plane perpendicular to $\vec{e_z}$. The light is elliptical polarized. That is, at a fixed value of z, the tip of the electric field vector rotates periodically in the (x,y) plane, tracing out an ellipse (see Fig.(1.2a)). When the electric field vector at a fixed position z rotates in a clockwise direction when viewed from the direction toward which the wave is approaching, the light is said to be right-hand elliptical polarized. While in the case of counterclockwise rotation the light is said to be left-hand elliptical polarized. At a fixed time t, the locus of the tip of the electric field vector follows a helical trajectory in space lying on the surface of an elliptical cylinder. The electric field rotates as the wave advances, repeating its motion periodically for each distance corresponding to the wavelength λ (see Fig.(1.2b)) [13].

(a)   (b)
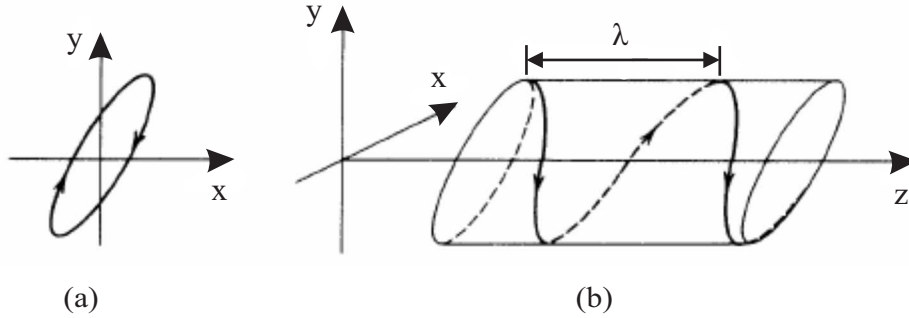
Figure 1.2: (a) Rotation of the endpoint of the electric field vector in the (x,y) plane at a fixed position z and (b) a snapshot of the trajectory of the endpoint of the electric field vector at a fixed time t of elliptical polarized light (λ ... wavelength) [13]

The field amplitudes as projected along the $\vec{e_x}$ and $\vec{e_y}$ directions are

$$x = E_x \cos{(\omega t - kz)}, \tag{1.16}$$
$$y = E_y \cos{(\omega t - kz + \phi)}. \tag{1.17}$$

Equation (1.16) and (1.17) are the parametric equations of an ellipse [13],

$$\frac{x^2}{E_x^2} + \frac{y^2}{E_y^2} - \frac{2xy}{E_x E_y}\cos\phi = \sin^2\phi. \tag{1.18}$$

There are three independent variables that govern the shape of the ellipse: E_x, E_y, and ϕ. Because as any ellipse has a major and a minor axes, a coordinate system, (u, v), can be defined to align to these axes. In the (u, v) basis the elliptical equation is

$$\frac{u^2}{a^2} + \frac{v^2}{b^2} = 1, \tag{1.19}$$

where the major and minor axes of the ellipse, (a, b), are the projections onto the u and v axes [12].

The *state of polarization* (SOP) of the wave is determined by the shape of the ellipse, i.e. by the parameters ϵ and η of the polarization ellipse (see Fig.(1.3)): The ellipticity ϵ is defined as [12]

$$\tan \epsilon = \frac{b}{a} \tag{1.20}$$

and describes the length ratio of the minor to the major axis of the ellipse. The ellipses

Figure 1.3: Polarization ellipse (a ... major axis, b ... minor axis, ϵ ... ellipticity, η ... azimuth) [17]
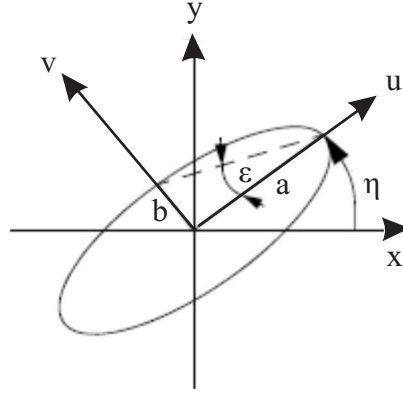
described by equation (1.18) and (1.19) are related by a rotation η, called azimuth, i.e. [12],

$$\begin{pmatrix} u \\ v \end{pmatrix} = \begin{pmatrix} \cos \eta & \sin \eta \\ -\sin \eta & \cos \eta \end{pmatrix} \begin{pmatrix} x \\ y \end{pmatrix}. \tag{1.21}$$

There are three general categories of polarization states depending on the shape of the ellipse: elliptical, linear, and circular SOPs.

Linear polarized light

If one of the components E_x or E_y vanishes, the light is *linear polarized*. The wave is also linear polarized if the phase difference ϕ equals 0 or π, since Eqn.(1.17) gives $y = \pm (E_y/E_x)x$. As illustrated in Fig.(1.4a), latter is the equation of a straight line with a slope $\pm E_y/E_x$ (the $+$ and $-$ signs correspond to $\phi = 0$ or π). The elliptical cylinder in Fig.(1.2b) collapses into a plane as illustrated in Fig.(1.4b). If $E_y = E_x$ the plane of polarization is offset by an angle of $\eta = +45°$ from the x axis, if $E_y = -E_x$, the wave is said to be $-45°$ linear polarized [13].

Circular polarized light

If $\phi = \pm \pi/2$ and $E_x = E_y = E_0$, Eqn.(1.16) and Eqn.(1.17) read $x = E_0 \cos(\omega t)$ and $y = \mp E_0 \sin(\omega t)$, from which $x^2 + y^2 = E_0^2$ can be deduced, which is the equation of a circle (see Fig(1.5a)). The elliptical cylinder in Fig.(1.2b) becomes circular and the wave is said to be circular polarized (see Fig.(1.5b)). In the case of $\phi = +\pi/2$, the electric field vector at a fixed

Figure 1.4: (a) Time course at a fixed position z and (b) a snapshot at a fixed time t of the electrical field vector of linear polarized light [13]

position z rotates in a clockwise direction when viewed from the direction toward which the wave is approaching. The light is then said to be *right-hand circular* (RHC) polarized [13]. The case of $\phi = -\pi/2$ corresponds to a counterclockwise rotation of the electric field vector and *left-hand circular* (LHC) polarized light (see Fig.(1.5)).

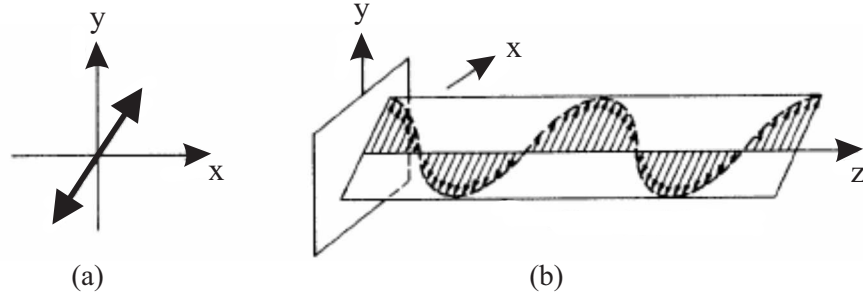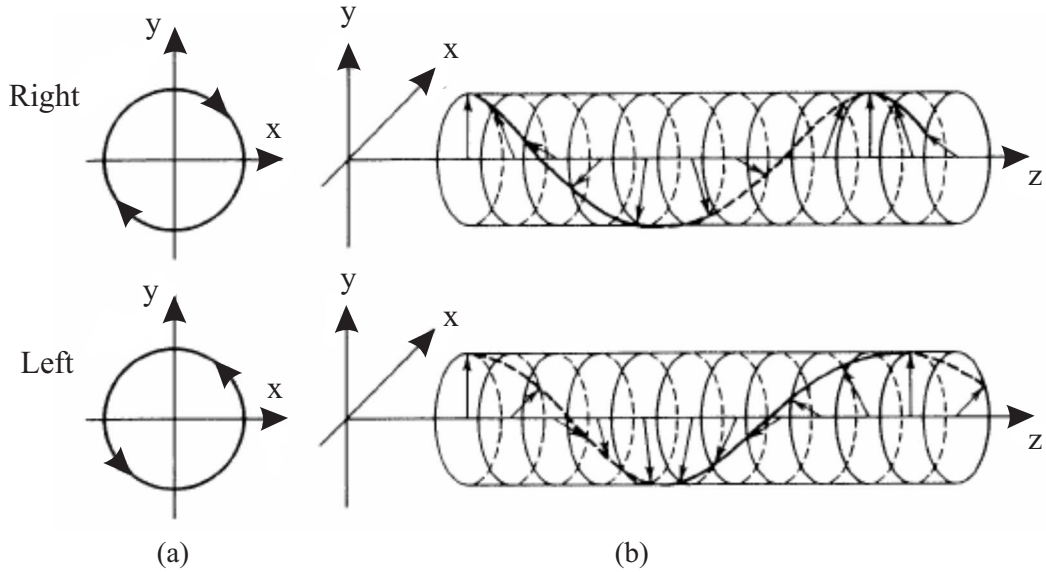Figure 1.5: (a) Time courses at a fixed position z and (b) snapshots at a fixed time t of the electrical field vector of right-hand and left-hand circular polarized light [13]

The Poincaré sphere

For a fixed polarization state, the *Jones vector* [12],

$$\vec{E}_J = \begin{pmatrix} E_x \\ E_y e^{j\phi} \end{pmatrix},$$

(1.22)

defines unambiguously the SOP of light at any instant of time.

Another conventional description of the polarization state is based on the *Stokes vector*, defined as [12]

$$\vec{S} = \begin{pmatrix} S_0 \\ S_1 \\ S_2 \\ S_3 \end{pmatrix}. \tag{1.23}$$

The components of the vector are called Stokes parameters and can be calculated as [12]

$$\begin{aligned} S_0 &= (E_x^2 + E_y^2)/2, \\ S_1 &= (E_x^2 - E_y^2)/2, \\ S_2 &= E_x E_y \cos \phi, \\ S_3 &= E_x E_y \sin \phi. \end{aligned} \tag{1.24}$$

The components have the following physical interpretations [17]:

- S_0 is the optical intensity,

- S_1 is the intensity difference between horizontal and vertical polarized components. When S_1 is positive, the preference is for horizontal polarization (i.e., for linear polarization in x-direction) and when it is negative, the preference is for vertical polarization (i.e., for linear polarization in y-direction).

- S_2 indicates the preference for $+45\,^\circ$ or $-45\,^\circ$ SOPs. A positive S_2 implies a preference towards $+45\,^\circ$ linear polarization.

- S_3 gives the preference for RHC and LHC polarization. A positive S_3 implies a preference towards RHC polarization.

Every possible polarization state for completely polarized light (see Section 2.2.3) can be represented on the surface of an unit sphere called the *Poincaré sphere* (see Fig.(1.6)), where the Stokes components S_i with $i = 1, 2, 3$ are normalized by the intensity component S_0 [12][17],

$$s_i = \frac{S_i}{S_0}. \tag{1.25}$$

The equator of the sphere represents various forms of linear polarizations. Right-hand and left-hand circular SOPs are located at the poles of the sphere. Other points represent elliptical polarized light, where right-hand elliptical SOPs are in the northern hemisphere and left-hand elliptical SOPs are in the southern hemisphere. Points at the opposite ends of a line passing through the center of the sphere represent orthogonal polarization states [17].

It is useful to connect the Stokes vector with the parameters of the polarization ellipse (see Fig.(1.3)):

$$\begin{aligned} s_1 &= \cos 2\eta \cos 2\epsilon, \\ s_2 &= \sin 2\eta \cos 2\epsilon, \\ s_3 &= \sin 2\epsilon. \end{aligned} \tag{1.26}$$

Azimuth, η, and ellipticity, ϵ, can be interpreted as angles in the Poincaré sphere (see Fig. (1.6)) [17].
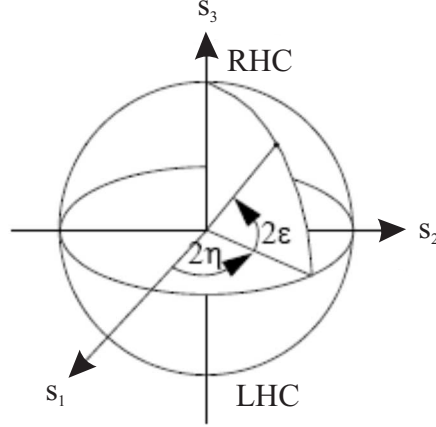
Figure 1.6: Poincaré sphere (RHC ... right-hand circular, LHC ... left-hand circular, ϵ ... ellipticity, η ... azimuth) [17]

1.2.2 PolSK transmitter

In this section I will present a *polarization shift keying* (PolSK) system, which I implemented in VPItransmissionMaker. VPItransmissionMaker is a software helping to design and to simulate optical transmission systems. First I want to describe the modeling of the transmitter of the PolSK system where the optical field is polarization modulated by means of a *polarization modulator* (PolM) module. Starting from a linear polarized laser field, the polarization modulator generates two orthogonal polarization states, which correspond to '1' and '0' bits [1]. Then two receiver structures for the absence and the presence of optical amplification will be presented and their performances are compared with the performances of OOK receivers. Finally, non-idealities are included in the PolSK receiver to estimate penalties in its performance, when real, non-ideal optical and electrical devices are used.

Polarization modulator

The VPI PolM module shown in Fig.(1.7) applies polarization modulation to encode digital data in orthogonal SOPs of an optical carrier. For a logical '1' the output signal is linear polarized ($\epsilon = 0°$) at an angle of $\eta = -45°$ and for a logical '0' the output signal is linear polarized at an angle of $\eta = +45°$ [18].

Figure 1.7: VPI photonics polarization modulator module [18]

Figure (1.8) shows the implementation of the PolM module within VPI. The polarization state of the input signal is adjusted to a linear polarization at an angle of $+45°$ by means of a polarization controller (ellipticity: $\epsilon = 0°$, azimuth: $\eta = +45°$) [18]. The $+45°$ linear
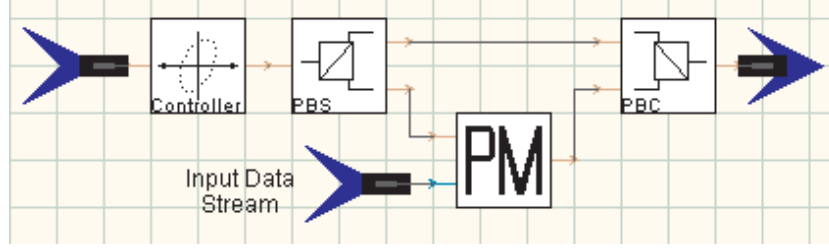
Figure 1.8: Implementation of the PolM module (PBS ...   polarization beam splitter, PM ... phase modulator, PBC ... polarization beam combiner) [18]

polarized light then enters a *polarization beam splitter* (PBS), which can be considered as two ideal linear polarizers oriented orthogonal to each other. The function of an ideal polarizer is to transmit the linear polarized component of the input light which coincides with the transmission axis of the polarizer and to completely remove the orthogonal component (see Fig.(1.9)) [18]. The output ports of the PBS then correspond to the x- and y-polarization
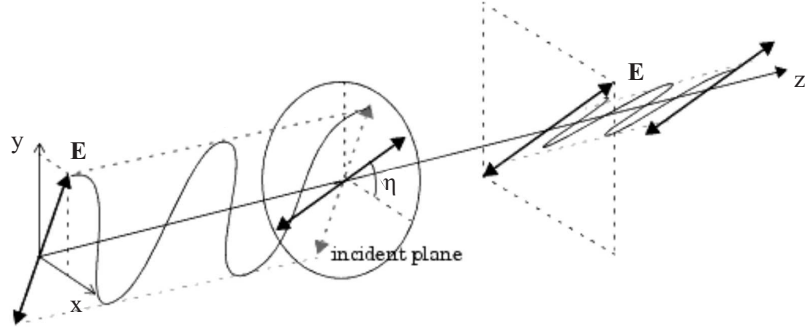
Figure 1.9: Function of a linear polarizer ($\mathbf{E}$ ... electric field vector, η ... azimuth) [18]

components of the incident light. Depending on the input data stream, phase modulation is applied to the y-component of the signal (see Fig.(1.8)). The output signal of the *phase modulator* (PM), $\vec{E}_{out}(t)$, is given by

$$\vec{E}_{out}(t) = \vec{E}_{in}(t) \cdot \exp[j\Delta\varphi \, data(t)], \tag{1.27}$$

where $\vec{E}_{in}(t)$ denotes the input optical signal of the PM, $data(t)$ can be '1' or '0', and $\Delta\varphi = 180°$ denotes the phase difference between marks and spaces [18]. A *polarization beam combiner* (PBC) then combines the x- and phase modulated y-component at the output of the polarization modulator. When the input data is '0' no phase modulation is applied and $45°$ linear polarized light appears at the output of the PolM. If there is a '1' at the input data, the y-polarization component is phase shifted by $180°$, and $-45°$ linear polarized light appears at the output of the PolM.

The realization of an PolM module to transmit any orthogonal SOPs is possible in VPI by adjusting the polarization controller and the PBS. For example, '0' bits can be transmitted via left-hand circular polarized light and '1' bits via right-hand circular polarized light when

the ellipticity of the polarization controller is set to $\epsilon = +45°$, the azimuth is set to $\eta = 0°$, and the linear PBS is replaced with an PBS for circular polarized light.

Transmitter

The implementation of the whole PolSK *transmitter* (TX) is shown in Fig.(1.10), using the parameters as given in Tab.(1.1).
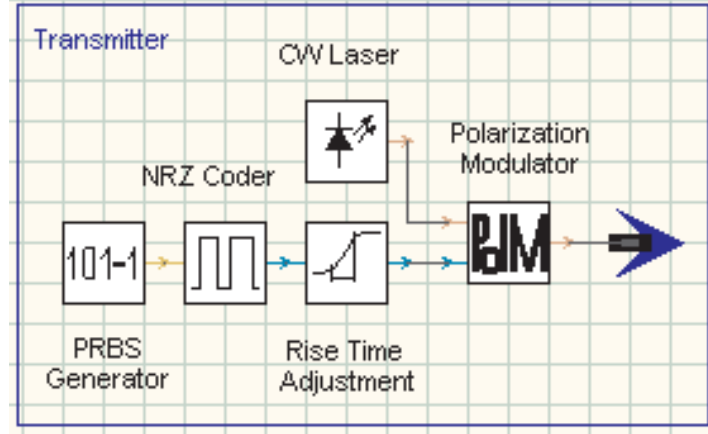
Figure 1.10: Implementation of PolSK transmitter (CW ... continuous wave, PRBS ... pseudo random bit sequence, NRZ ... non return to zero)

	Parameter	*Value*
	Emission frequency	$f = 193.1\,\text{THz}$
	Average power	$P = 1\,\text{mW}$
	Linewidth	$\Delta f = 0\,\text{Hz}$
Laser	Azimuth	$\eta = 0°$
	Ellipticity	$\epsilon = 0°$
	Output data type	Blocks (see Appendix A.2)
	Bit rate	$R = 1\,\text{Gbit/s}$
PRBS	Type of bit stream	PRBS (see Appendix B.1)
	Mark probability	0.5
Rise time adjustment	10/90-Rise time	$\Delta t_{10/90} = 0.25\,\text{ns}$

Table 1.1: Parameters of PolSK transmitter (PRBS ... pseudo random bit sequence)

A *continuous wave* (CW) laser emits light at the wavelength $\lambda = 1.55\,\mu\text{m}$ and is feed to the carrier input of the PolM. A *pseudo random bit sequence* (PRBS) generator creates the data bit sequence which is then encoded by a *non return to zero* (NRZ) coder. An NRZ pulse remains at a constant value over the entire bit duration, i.e., the '1' is coded by a power level P_1 with non-zero amplitude and the '0' by a power level P_0 with zero amplitude (see Fig.(1.11)) [18]. The module to adjust the rise time of NRZ pulses is a Gaussian filter that transforms rectangular electrical input pulses into smoother output pulses with a user-defined
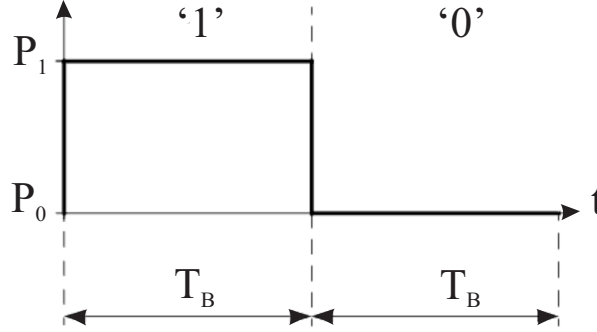
Figure 1.11: NRZ coded '1' and '0' bits (P_1 ... power level '1' bit, P_0 ... power level '0' bit, T_B ... bit duration, t ... time) [18]

10/90-rise time $\Delta t_{10/90}$ (see Fig.(1.12)) [18]. As illustrated in Fig.(1.10) the NRZ coded bit
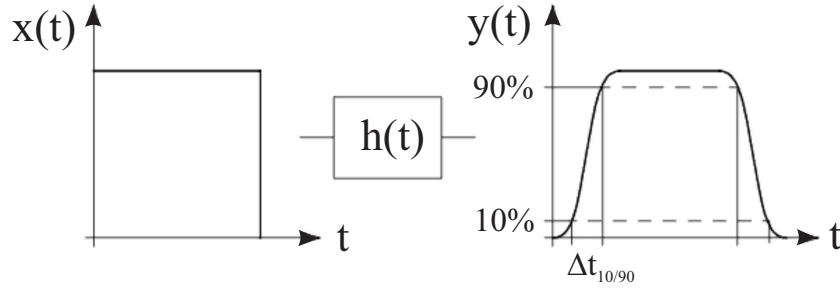
Figure 1.12: Output pulses $y(t)$ with an user-defined rise-time $\Delta t_{10/90}$ are generated by filtering input pulses $x(t)$ with a Gaussian-shaped filter $h(t)$ [18].

sequence generated by the PRBS module is modulated onto the SOP of the light produced by the CW laser by means of the PolM module.

At the output of the PolSK TX the SOP of '1' and '0' bits as determined by the Stokes parameters can be visualized in the Poincaré sphere. For binary PolSK the information is sent by switching the polarization of the transmitted lightwave between two orthogonal SOPs. In the Poincaré sphere two orthogonal SOPs map onto opposite points with respect to the origin [8]. In my work the SOPs of '1' and '0' bits are located at $-S_2$ on the equator of the Poincaré Sphere equivalent to $-45\,^\circ$ linear polarized light and at $+S_2$ equivalent to $+45\,^\circ$ linear polarized light (see Fig.(1.13)).

The optical power at the output of the PolSK TX stays constant over time (see Fig.(1.14)). Thus, fullest utilization of the output power of a laser transmitter is obtained by polarization modulation [19].

1.3   Receivers without optical amplification

Receiver structures for the direct detection of binary digital optical modulation schemes employing polarization modulation can be realized as shown in Fig.(1.15), the logical '0' and
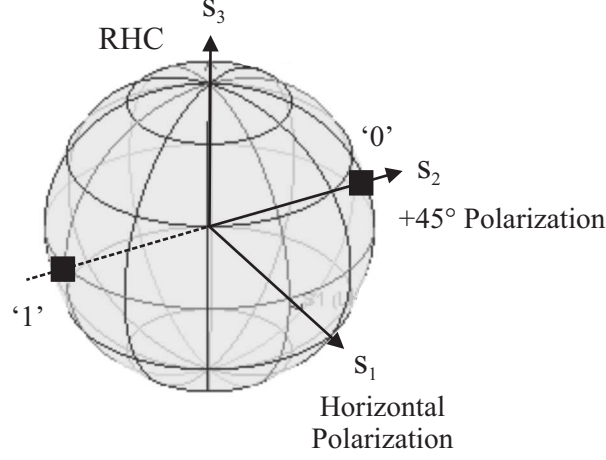
Figure 1.13: SOPs after the PolSK TX: '0' bit at $+45\,^\circ$ and '1' bit at $-45\,^\circ$ (RHC ... right-hand circular)
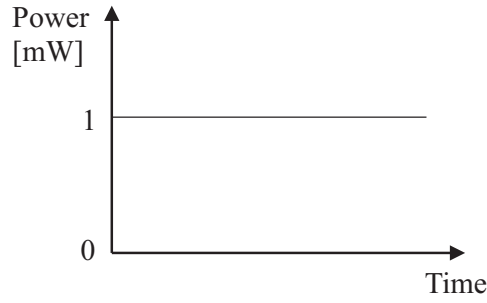
Figure 1.14: Optical signal over time after PolSK TX

'1' are represented by orthogonal SOPs, which are received by two photodetectors. The output signals from these photodetectors are fed to a subtractor, which is then connected to a decision circuit [19]. I will present three different *receiver* (RX) structures to detect polarization modulated light and compare these with *on-off keying* (OOK) systems: The *single PolSK* (SPolSK) receiver using only one photodiode with transimpedance amplifier, the *balanced PolSK* (BPolSK) receiver with two photodiodes and transimpedance amplifiers in the '0' and '1' branches, and an BPolSK receiver with differential amplifier.

1.3.1 Introduction

All functional components of a digital receiver without optical amplification as implemented in VPI are illustrated in Fig.(1.16). The photodiode converts the optical input signal into an electrical current, I. The electrical signal resulting from photodetection is then amplified by means of a *transimpedance amplifier* (TIA). The lowpass filter determines the electrical bandwidth of the receiver. The digital information present in the received signal and the digital clock must then be recovered. The recovered clock signal must have a stable and well defined time relationship with the data bits because it is used by the decision circuit to examine the optimum sampling instance. The decision circuit is intended to turn the analog electrical
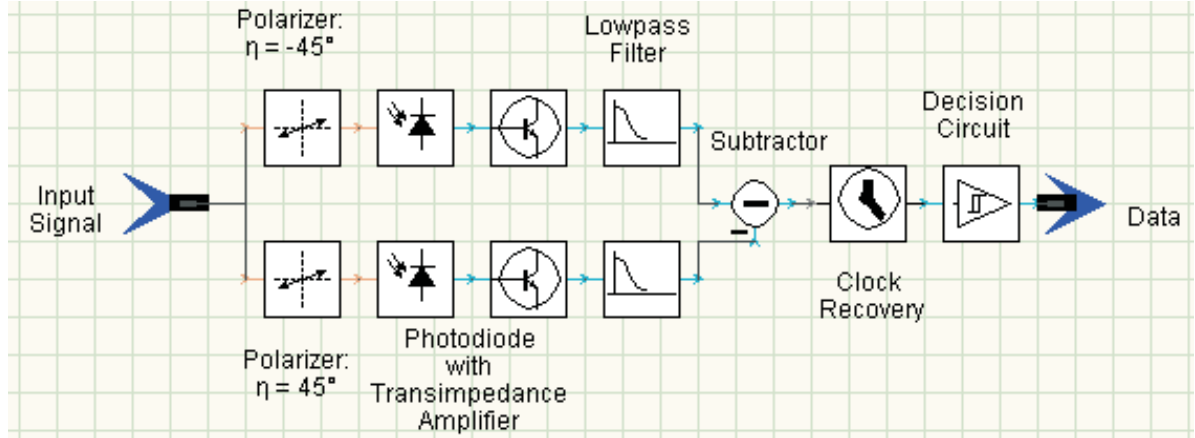
Figure 1.15: Balanced PolSK RX (η ... azimuth)

signal into a digital signal with well-defined current levels. All input levels exceeding a certain threshold level will result in a logical '1', all input levels below the threshold will produce a logical '0' [18].
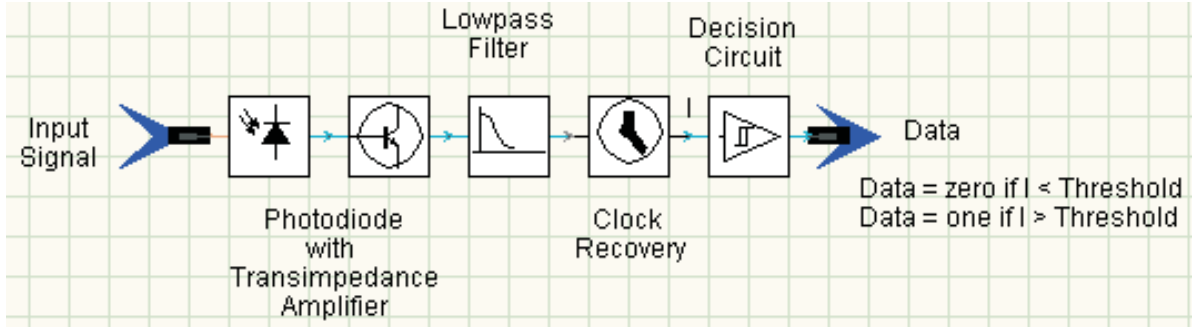
Figure 1.16: Digital receiver (I ... current)

PIN photodiode

The photodiode is one of the key components of the optical receiver, converting optical power, P, into electrical current, I, due to the photoelectric effect. The fluctuations of the electric current are regarded as noise, which is characterized by the standard deviation, σ_I, where the variance is $\sigma_I^2 = \langle (I - \mu_I)^2 \rangle$ with mean μ_I and $\langle \cdot \rangle$ denotes the expectation value [13].

$I(t)$ is the current due to the optical input signal $P(t)$. The optical signal is converted into an electrical signal by the photodiode with finite conversion efficiency, ζ, called quantum efficiency. The quantum efficiency is defined as [11][20]

$$\zeta = \frac{\text{number of photocarriers produced}}{\text{number of incident photons}} = \frac{I(t)/e}{P(t)/hf}, \qquad \eta \leq 1, \qquad (1.28)$$

where $e = 1.6 \cdot 10^{-19}$ C is the charge of a single electron and hf given in [J] is the photon energy with *Planck's constant* $h = 6.626 \cdot 10^{-34}$ Js and frequency f. The photocurrent produced by

the photodiode is then given by [11][20]

$$I(t) = \zeta \frac{e}{hf} P(t) = SP(t). \tag{1.29}$$

The responsivity S given in [A/W] of the photodiode is known as the current generated per unit optical power.

Several sources of noise are inherent in the process of photon detection of an PIN photodiode [13]:

- *Photon noise*: The most fundamental source of noise is associated with the random arrivals of the photons themselves, which are usually described by Poisson statistics.

- *Photoelectron noise*: For a photon detector with finite conversion efficiency ζ ($0 \leq \zeta \leq 1$), a single photon generates a photoelectron-hole pair with probability ζ but fails to do so with probability $1 - \zeta$. Because of the inherent randomness in this process of carrier generation, it serves as a source of noise.

- *Receiver circuit noise*: The various components in the electrical circuitry of an optical receiver, such as resistors and transistors, contribute to the receiver circuit noise. Circuit noise results from the thermal motion of charged carriers in resistors and other dissipative elements (thermal noise), and from fluctuations of charge carriers in transistors used in the receiver amplifier. Thermal noise can be described by Gaussian statistics.

The output noise current of an PIN photodiode is therefore described by the sum of shot noise, I_{sh}, and thermal noise, I_{th} [18],

$$I_n^2(t) = I_{sh}^2(t) + I_{th}^2(t): \tag{1.30}$$

- $I_{sh}^2(t)$ given in [A^2] is the generated shot noise current associated with the quantum nature of light (photon noise and photoelectron noise). The one-sided spectral density, $N_{sh}(t)$ given in [A/$\sqrt{\text{Hz}}$], for an PIN photodiode is related to signal current and dark current [18],

$$N_{sh}(t) = \sqrt{2e(I(t) + I_D)}. \tag{1.31}$$

A dark current, I_D, results from random electron-hole pairs generated thermally or by tunneling [13]. It can be described by

$$I_D = I_{sat} \left(\exp^{\frac{e}{k_B T} V_d} - 1 \right), \tag{1.32}$$

where I_{sat} is the temperature dependent reverse saturation current of the photodiode, $k_B = 1.38 \cdot 10^{-23}$ J/K is the *Boltzmann constant*, T is the absolute temperature in Kelvin and V_d is the voltage at the photodiode [18][11]. The current-noise according to shot-noise is then [11]

$$I_{sh}^2(t) = 2e(I(t) + I_D)B_e = N_{sh}^2(t)B_e, \tag{1.33}$$

where B_e is the electrical filter bandwidth after photodetection.

- $I_{th}^2(t)$ given in [A^2] is the thermal noise current, which arises from the random motions of mobile carriers in resistive electrical materials at finite temperatures even in the absence of an external electrical power source [13]. The current-noise according to thermal noise is given by [18]

$$I_{th}^2(t) = N_{th}^2(t)B_e, \tag{1.34}$$

where $N_{th}(t)$ is the one-sided spectral density in [A/$\sqrt{\text{Hz}}$].

Receiver noise

In Tab.(1.2) the most important parameters of the PIN photodiode with TIA and the electrical lowpass filter as used for my simulations are listed.

	Parameter	Value
PIN photodiode with TIA	Responsivity	$S = 1.05 \, \text{A/W}$
	Dark current	$I_D = 1 \, \text{nA}$
	Thermal noise one-sided spectral density	$N_{th} = 31.5 \, \text{pA}/\sqrt{Hz}$
	Gain transimpedance amplifier	$G_{TIA} = 26 \, \text{dB}$
Electrical lowpass filter	Transfer function	Bessel
	3 dB bandwidth	$B_e = 0.75 \, \text{GHz}$
	Filter order	5

Table 1.2: Parameters of digital receiver as used for VPI simulations

The thermal noise current produced according to Eqn.(1.34) is

$$I_{th}^2 = 7.44 \cdot 10^{-13} \; \text{A}^2, \tag{1.35}$$

with $N_{th} = 31.5 \cdot 10^{-12} \, \text{A}/\sqrt{Hz}$ and $B_e = 0.75 \, \text{GHz}$ (see Tab.(1.2)). The shot noise current at an input power of $P = -33 \, \text{dBm}$ according to Eqn.(1.33) and the parameters in Tab.(1.2) is

$$I_{sh}^2 = 1.27 \cdot 10^{-16} \; \text{A}^2. \tag{1.36}$$

In receivers without optical preamplification, the dominant source of noise usually is the thermal noise in the electronics of the receiver [11]. Thermal noise is Gaussian in nature, and if the noise power is known, one can calculate the spreads in '0' and '1' signals. These spreads cause errors, as '1' bits will occasionally be detected as '0' bits, and vice versa. When the noise probability density functions are known, the *bit error ratio* (BER) can be calculated analytically (see Appendix B.2.1).

1.3.2 On-off keying system

In my work I compare the performance of the PolSK systems to an intensity modulated OOK system. Latter is the most frequently used technique in direct detection optical communication systems [4].

Transmitter

The parameters of the OOK transmitter are similar to the PolSK transmitter (see Tab.(1.1)). The most important difference is the used modulator. OOK transmitters use an *amplitude modulator* (AM), where the output signal of the AM, $\vec{E}_{out}(t)$, is given by

$$\vec{E}_{out}(t) = \vec{E}_{in}(t) \cdot \sqrt{data(t)}, \tag{1.37}$$

with the optical input signal, $\vec{E}_{in}(t)$, and the electrical modulation signal, $data(t)$. The power of the output signal, $\vec{P}_{out}(t) = |\vec{E}_{out}(t)|^2$, is then given by

$$\vec{P}_{out}(t) = \vec{P}_{in}(t) \cdot data(t) \tag{1.38}$$

with $\vec{P}_{in}(t) = |\vec{E}_{in}(t)|^2$ being the input power of the optical carrier [18].

For comparison with SPolSK the optical signal at the output of the OOK transmitter is $-45\,^\circ$ linear polarized by a polarization controller (ellipticity: $\epsilon = 0\,^\circ$, azimuth: $\eta = -45\,^\circ$) (see Fig.(1.17)).
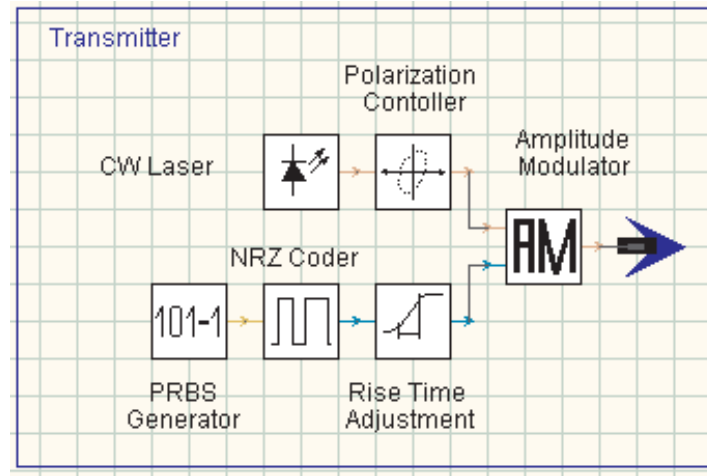
Figure 1.17: Implementation of OOK transmitter (CW ... continuous wave, PRBS ... pseudo random bit sequence, NRZ ... non return to zero)

Receiver

Figure (1.18) shows the whole OOK system as implemented in VPI. It comprises an OOK transmitter module, which has been presented in Fig.(1.17), an attenuator to emulate the free-space loss, the OOK receiver, and an BER estimator. The attenuator at the RX input is
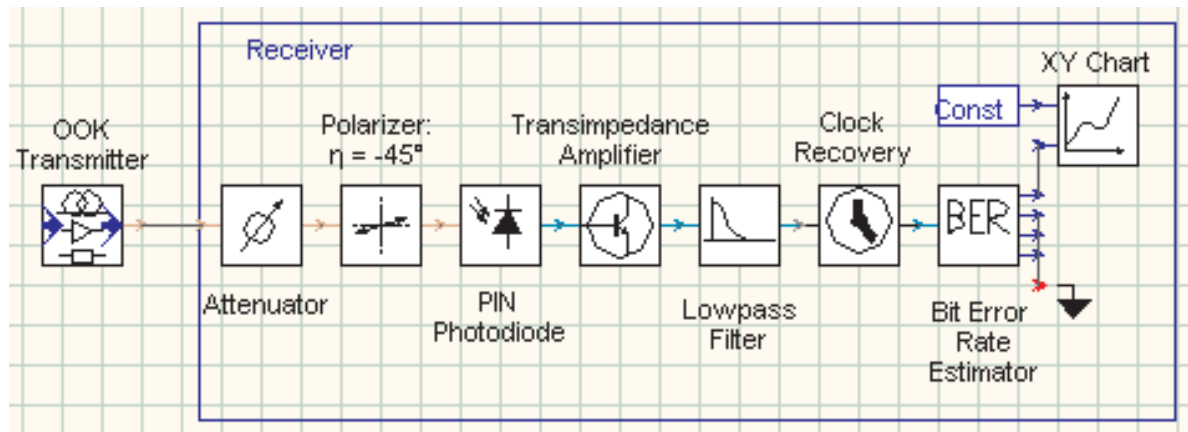
Figure 1.18: OOK system (η ... azimuth)

required for the variation of the *receiver input power* (RIP) and is essential for most simulations of the system, e.g., a simulation of BER versus RIP (which is seen later in this section). A polarizer, which only transmits $-45\,°$ linear polarized light, is situated behind the attenuator. Thus, the OOK and SPolSK RX setup are identical. The PIN photodiode with transimpedance amplifier, the lowpass filter, and the clock recovery are the same components as shown in Fig.(1.16) with the same parameters as presented in Tab.(1.2). The decision element of the OOK RX is situated in the BER estimator, it defines the sample time and the decision threshold (see Appendix B.2) [18]. The BER estimator evaluates the bit error probability in the digital

direct detection optical transmission system, where the statistics of the received optical signal, as said in Section 1.3.1, are assumed to be Gaussian (see Appendix B.2.1).

The receiver input power corresponds to the peak power of the OOK system (which is thus denominated as peak power limited). For example, if the peak power is $P_{peak} = 1\,\mathrm{mW}$ and given that the mark probability in the PRBS generator is 0.5 (see Tab.(1.1)), the average power is equivalent to $P_{average} = 0.5\,\mathrm{mW}$. This is shown in Fig.(1.19). The calculated OOK
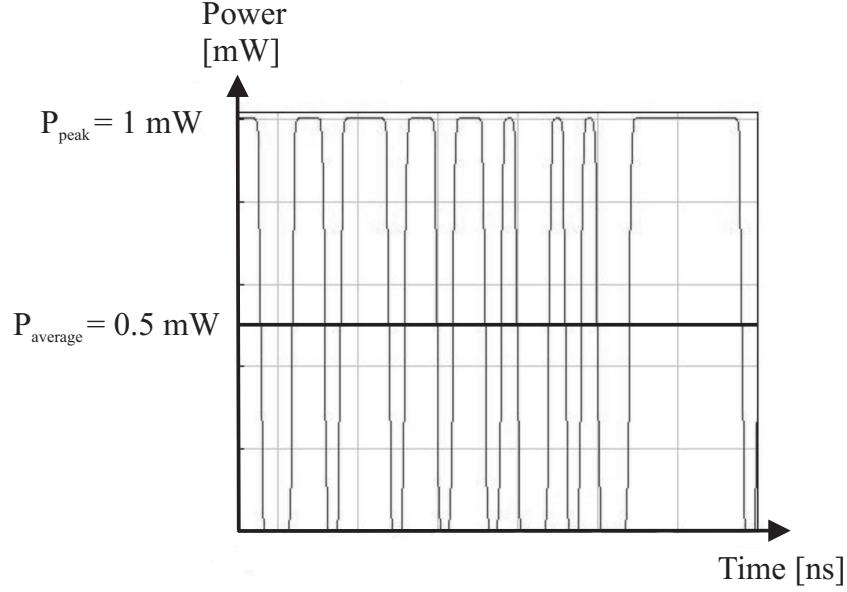
Figure 1.19: Example of OOK receiver input power versus time (P_{peak} ... peak power, $P_{average}$ ... average power)

receiver sensitivity (which is the receiver input power at a data rate of $R = 1\,\mathrm{Gbit/s}$ and at an $BER = 10^{-9}$) is $S_{RX} = -33\,\mathrm{dBm}$.

1.3.3 Single polarization shift keying system

The single PolSK system (shown in Fig.(1.20)) consists of an PolSK TX as introduced in Subsection 1.2.2. The receiver is the same like in the OOK system presented above. The SPolSK receiver is implemented with a single polarizer, which transmits only the '1's and discards the '0's. The receiver sensitivity at a data rate of $R = 1\,\mathrm{Gbit/s}$ and at an $BER = 10^{-9}$ in this peak-power limited system is $S_{RX} = -33\,\mathrm{dBm}$, which is equal to OOK.

1.3.4 Balanced polarization shift keying system

Balanced PolSK systems use two polarizers to detect both '1's and '0's. In Fig.(1.21) an BPolSK system denoted as BPolSK1 is sketched. A -45° polarizer in the first branch passes through the '1's, which are -45° linear polarized and are detected by the PIN photodiode with an TIA in the upper branch. A $+45^\circ$ polarizer in the second branch passes through the '0's, which are $+45^\circ$ linear polarized and are detected by the PIN photodiode with an TIA in the lower branch. The subtractor subtracts the electrical signal of the '1' branch from the electrical signal of the '0' branch, doubling the amplitude of the received signal compared
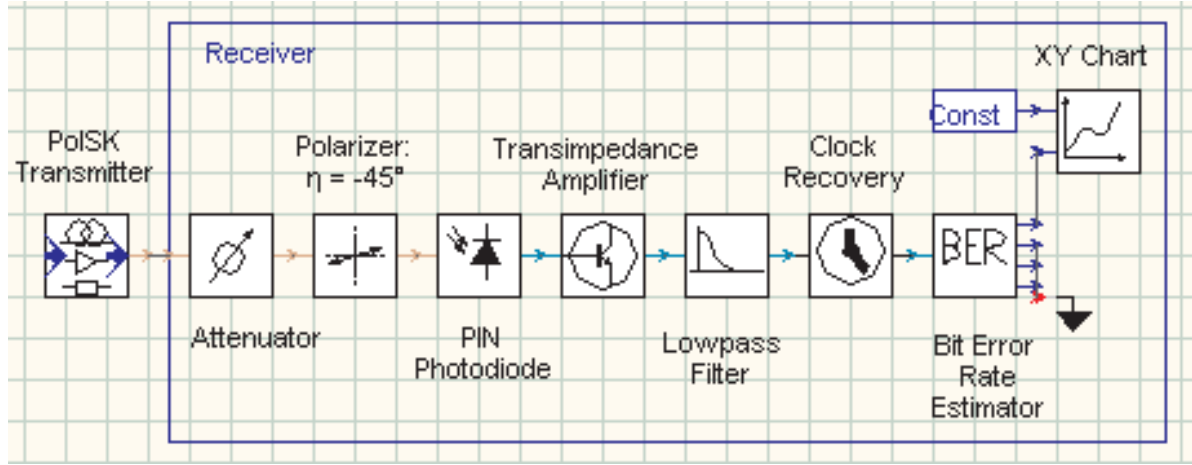
Figure 1.20: Single PolSK system (η ... azimuth)
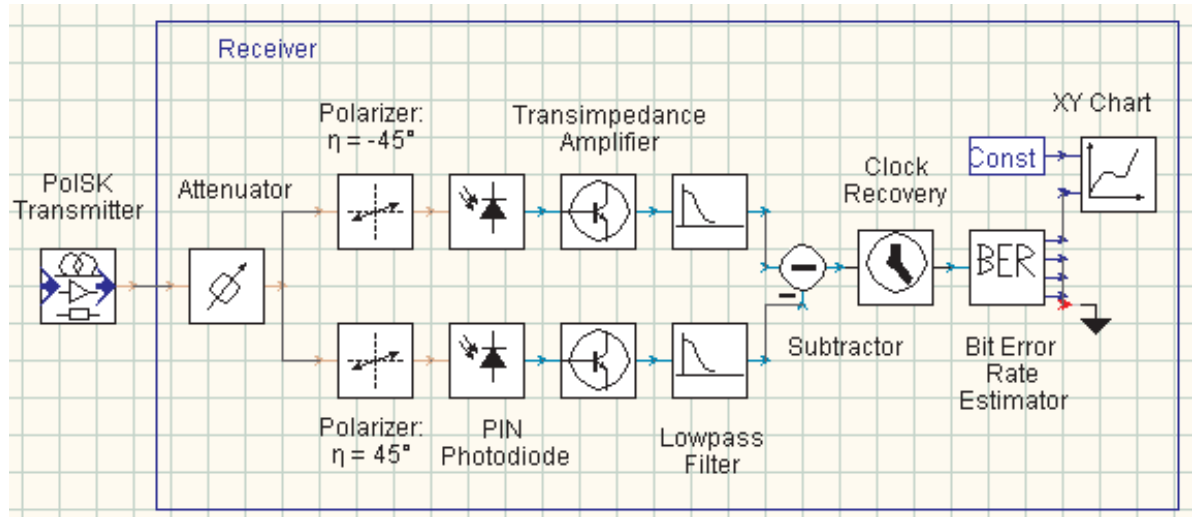
Figure 1.21: Balanced PolSK system (BPolSK1) with photodiode and transimpedance amplifier in both detector branches (η ... azimuth)

to SPolSK or OOK systems (see Fig.(1.22)). A drawback in the BPolSK1 RX is the doubled noise as compared to SPolSK or OOK receivers. Due to two photodiodes with transimpedance amplifiers the influence of the dark current, the shot noise, and the thermal noise has to be counted twice. The receiver sensitivity of the BPolSK1 RX at a data rate of $R = 1\,\text{Gbit/s}$ and at an $BER = 10^{-9}$ is $S_{RX} = -34.5\,\text{dBm}$. Thus, a gain in receiver sensitivity of $1.5\,\text{dB}$ is reached with this system in comparison to SPolSK and OOK RXs.

Another implementation of a balanced PolSK system can be seen in Fig.(1.23). The receiver is implemented with two photodiodes and a differential amplifier, this system is denoted as BPolSK2 system. The differential amplifier is implemented within VPI with a subtractor and subsequent transimpedance amplifier. The receiver sensitivity of the BPolSK2 system at a data rate of $R = 1\,\text{Gbit/s}$ and at an $BER = 10^{-9}$ is $S_{RX} = -36\,\text{dBm}$, provided that the gain
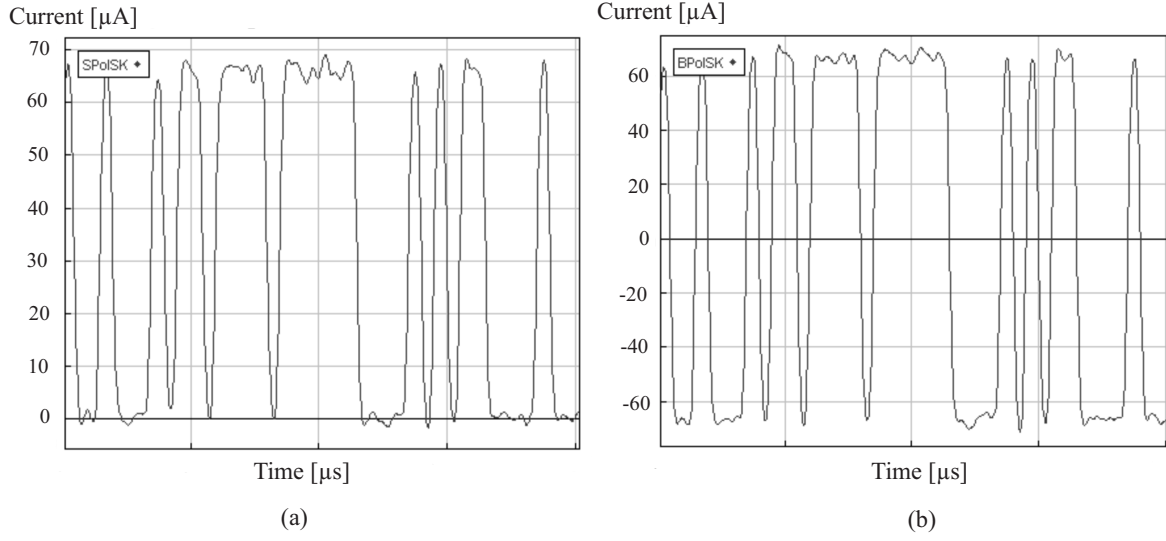
Figure 1.22: Time signals after clock recovery at a receiver input power of $P = -25\,\mathrm{dBm}$: (a) SPolSK and (b) BPolSK1
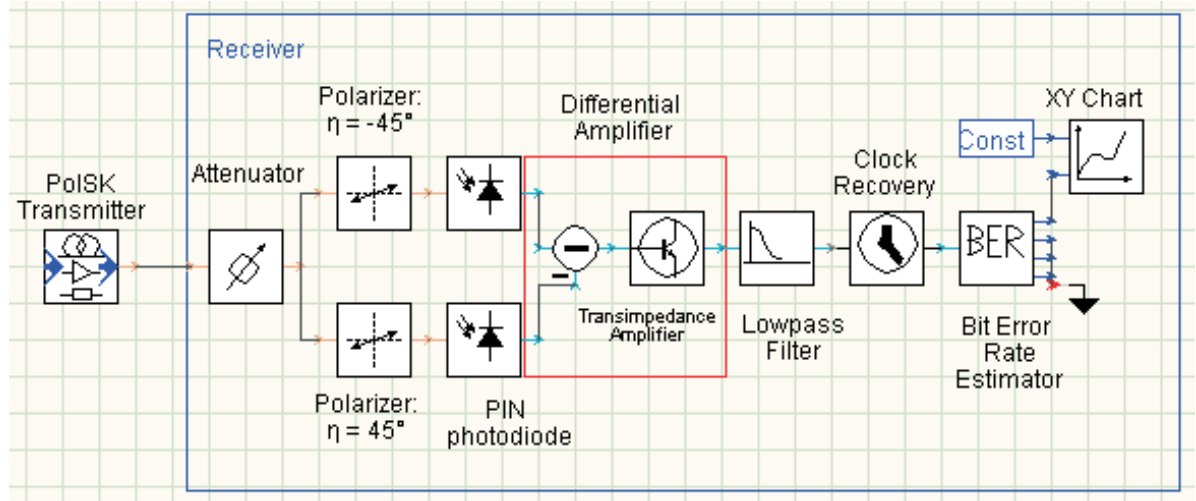
Figure 1.23: Balanced PolSK system (BPolSK2) with two photodiodes and one differential amplifier (η ... azimuth)

and the noise spectral density of the differential amplifier is equal to the TIA used in BPolSK1, i.e., a gain of $G_{TIA} = 26\,\mathrm{dB}$ and a noise current density of $N_{th} = 31.5 \cdot 10^{-12}\,\mathrm{A}/\sqrt{Hz}$. Thus, compared to SPolSK a receiver sensitivity gain of 3 dB is achieved. The 1.5 dB gain over the BPolSK1 system is caused by the reduction of the thermal noise by a factor of 2.

Comparison of systems

In Table (1.3) the required receiver input power (peak power) at a $BER = 10^{-9}$ and a data rate $R = 1\,\mathrm{Gbit/s}$ for thermal noise limited systems is listed.

	Noise statistics	*RX sensitivity* [dBm]	*RX sensitivity* [ppb]
OOK	Gaussian	−33	3921
SPolSK	Gaussian	−33	3921
BPolSK1	Gaussian	−34.5	2776
BPolSK2	Gaussian	−36	1965

Table 1.3: Receiver sensitivity in the case of thermal noise limited operation (ppb ... photons per bit)

In Tab.(1.4) the gain in receiver sensitivities of PolSK systems compared to OOK systems is itemized.

	Gain in receiver sensitivity [dB]
OOK	0
SPolSK	0
BPolSK1	1.5
BPolSK2	3

Table 1.4: Gain in receiver sensitivity in the case of thermal noise limited operation relative to OOK system with polarization control

This shows that in thermal noise limited systems BPolSK2 clearly outperforms OOK systems in terms of peak power by some 3 dB. However, in average power limited systems, like when using a booster *Erbium-doped fiber amplifier* (EDFA) in the transmitter, OOK and BPolSK2 show similar performance.

1.4 Receivers with optical amplification

1.4.1 Introduction

Optical preamplification can be used to improve the receiver performance [11]. A simplified diagram of an optically preamplified receiver is shown in Fig.(1.24): After the light is amplified by means of an EDFA, it is optically bandpass filtered to suppress *amplified spontaneous emission* (ASE) and background noise. The optical-to-electrical conversion again is done by a photodiode module.
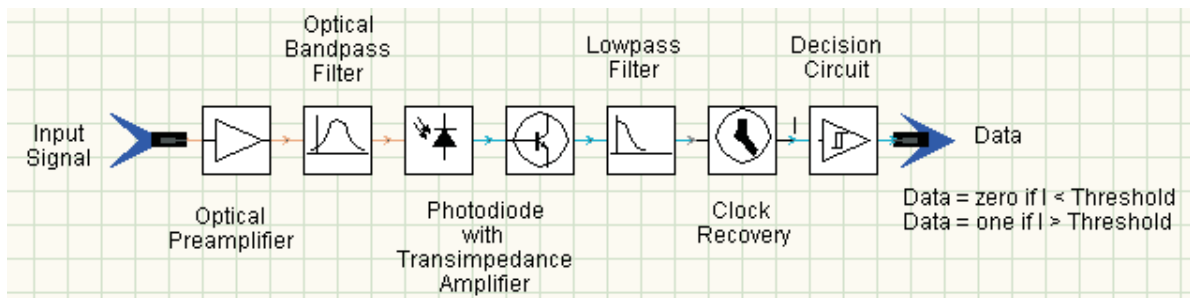
Figure 1.24: Optically preamplified receiver (I ... current)

Optical amplifier

The underlying principle for achieving optical amplification of light is stimulated emission of radiation [13]. Stimulated emission allows a photon in a given mode to induce an electron in an upper energy level (E_2) to undergo a transition to a lower energy level (E_1) and, in the process, to emit a clone photon into the same mode as the initial photon (a photon with the same frequency, direction and polarization). These two photons can serve to stimulate the emission of two additional photons, and so on. The result is light amplification. An essential ingredient for achieving laser amplification is the presence of a greater number of atoms in the upper energy level than in the lower level, denoted as population inversion [13].

The resonant medium that provides amplification by the process of stimulated emission also generates spontaneous emission. If the electron is initially in the upper energy level, it may drop spontaneously to the lower energy level and release its energy in the form of a photon. The light arising from this process, which is independent of the input to the amplifier, represents a fundamental source of laser amplifier noise. Whereas the amplified signal has a specific frequency, direction and polarization, the ASE noise is broadband, multidirectional and unpolarized. As a consequence it is possible to filter out some of this noise by a narrow bandpass optical filter and a polarizer [13].

It is seen that a conventional optical amplifier has an associated ASE noise that is inherent in the optical amplification process. An optical amplifier can therefore be modeled as a noise-free linear amplifier combined with an additive white Gaussian noise source that extends over the amplifier's bandwidth [11].

The single-sided spectral density of the ASE noise, N_{ASE} in $[\text{W}/\text{Hz}]$, at the output of the optical amplifier is given by [11][20]

$$N_{ASE} = p\,(G-1)hf\frac{N_2}{N_2 - N_1} = p\,(G-1)hfn_{sp}, \tag{1.39}$$

where $p = 1$ if only a single polarization is present at the amplifier's output, G is the linear gain of the amplifier, and n_{sp} is the spontaneous emission factor [11]. The spontaneous emission factor is determined by the population densities N_1 of the lower energy level and N_2 of the upper energy level [20].

The amplifier's noise figure, F, can be related to the spontaneous emission factor, n_{sp}, via [11]

$$F = 10\log_{10}\left[\frac{2n_{sp}(G-1)}{G} + \frac{1}{G}\right] \cong 10\log_{10}[2n_{sp}], \tag{1.40}$$

in which the approximation is valid for a gain much larger than 1.

For optical amplifiers with a noise-bandwidth, which is equal to the optical bandwidth of the subsequent bandpass filter, B_o, the total amount of noise power caused by ASE is [11]

$$P_{ASE} = p\,n_{sp}(G-1)hfB_o = p\,N_{ASE}B_o. \tag{1.41}$$

Because the PIN photodiode is a square-law detector for electric fields, the received signal field mixes with the components of the ASE noise field which are polarized in the same direction as the signal. This is called signal-ASE beat noise. The ASE noise will also mix with itself, resulting in ASE-ASE beat noise [11][20]. The quadratic noise current $I^2_{Signal-ASE}$ in $[\text{A}^2]$ associated with the Signal-ASE term is given by [11][20][21]

$$I^2_{Signal-ASE} = 4S^2GPN_{ASE}B_e, \tag{1.42}$$

and the quadratic noise current for the ASE-ASE term, $I_{ASE-ASE}^2$, in $[\,A^2]$ is [11][20][21]

$$I_{ASE-ASE}^2 = p \cdot 2S^2 N_{ASE}^2 B_o B_e, \tag{1.43}$$

where S is the photodiode's responsivity, P is the receiver input power, and B_e is the electrical bandwidth of the RX.

Receiver noise

In Tab.(1.5) the most important parameters of the implemented receiver with optical preamplification are listed.

	Parameter	*Value*
PIN photodiode with TIA	Responsivity	$S = 1.05\,\text{A/W}$
	Dark current	$I_D = 1\,\text{nA}$
	Thermal noise one-sided spectral density	$N_{th} = 31.5\,\text{pA}/\sqrt{Hz}$
	Gain transimpedance amplifier	$G_{TIA} = 26\,\text{dB}$
Electrical lowpass filter	Transfer function	Bessel
	3 dB bandwidth	$B_e = 0.75\,\text{GHz}$
	Filter order	5
Optical amplifier	Amplifier type	gain controlled (see Appendix B.3)
	Gain	$G = 39\,\text{dB}$
	Maximum output power	$P_{out(max)} = 14.5\,\text{dBm}$
	Noise figure	$F = 3.8\,\text{dB}$
	Noise bandwidth	$B_{ASE} = 64\,\text{GHz}$
Optical bandpass filter	Transfer function	Gaussian
	Optical bandwidth	$B_o = 1.6\,\text{GHz}$
	Gaussian order	1

Table 1.5: Parameters of receiver with optical amplification as used for simulations

As mentioned in Section 1.3.1 the amount of noise present in the receiver determines the receivers sensitivity. In the system with optical preamplification the single-sided spectral density of ASE noise is given according to Eqn.(1.39) and Tab.(1.5) with

$$N_{ASE} = p \cdot 8.82 \cdot 10^{-16}\ \text{W/Hz}, \tag{1.44}$$

where the spontaneous emission factor is $n_{sp} = 0.87$ (see Eqn.(1.40)). The quadratic noise current for the signal-ASE term and a receiver input power of $P = -45\,\text{dBm}$ is (see Eqn.(1.42))

$$I_{Signal-ASE}^2 = 7.33 \cdot 10^{-10}\ \text{A}^2, \tag{1.45}$$

and the current noise for the ASE-ASE term is (see Eqn.(1.43))

$$I_{ASE-ASE}^2 = p \cdot 2.06 \cdot 10^{-12}\ \text{A}^2. \tag{1.46}$$

The shot-noise term as given by Eqn.(1.33) for an input power of $P = -45\,\text{dBm}$ is

$$I_{sh}^2 = 8.22 \cdot 10^{-18}\ \text{A}^2, \tag{1.47}$$

and the noise current according to thermal noise is given by Eqn.(1.34) as

$$I_{th}^2 = 7.44 \cdot 10^{-13} \text{ A}^2. \tag{1.48}$$

For systems using optically preamplified receivers the ASE noise dominates all other noise sources [22]. It is well known that in a baseband, direct-detection optical communication system, the statistics of a received optical signal accompanied by optical noise, such as ASE noise from optical amplifiers, are non-Gaussian [11]. In fact, since the total optical field in this case consists of a signal field accompanied by a noise field with Gaussian-distributed amplitude, the statistics of the electrical current after square law detection will follow a chi-squared (χ^2) distribution. The χ^2 probability density function will be affected by the process of electrical low-pass filtering that typically follows detection. In the special case of the ideal integrate-and-dump receiver (where the filtering action is performed by an integrator), it has been shown that the statistics of the electrical signal remain χ^2 [18]. It is therefore reasonable to assume that in a wide range of receiver configurations, in which the ideal integrate-and-dump system is approximated by a low pass filter followed by a sampling circuit, a χ^2 model for the received optical beat noise statistics will be more suitable than the common Gaussian approximation (see Appendix B.2.1) [18].

1.4.2 On-off keying system

In Figure (1.25) an OOK system using a receiver with optical preamplification is depicted. The major difference to the OOK transmitter and receiver as given in Section 1.3.2 is the existence of an optical amplifier and an optical bandpass filter in front of the PIN photodiode. The parameters used for my simulation of the transmitter and the receiver are listed in Tab.(1.1) and Tab.(1.5).
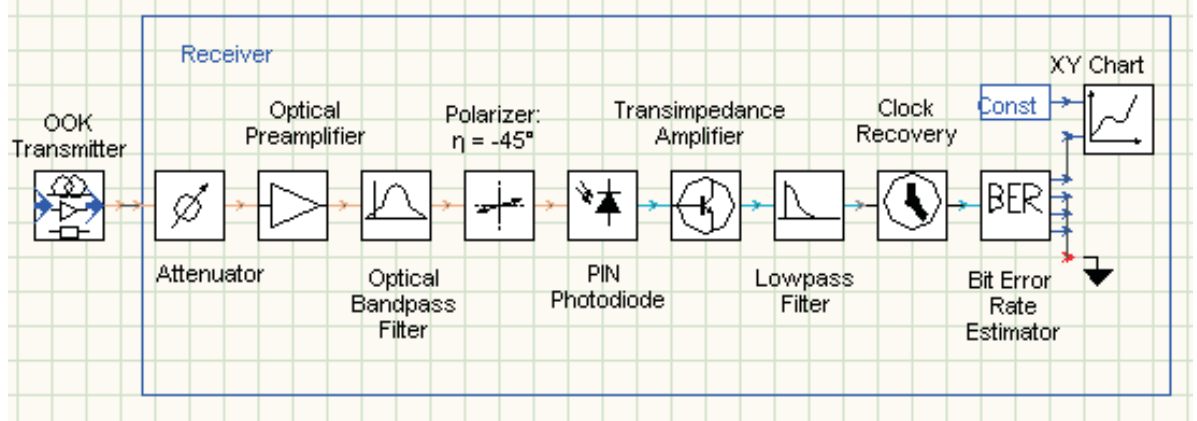
Figure 1.25: OOK system with optical amplifier (η ... azimuth)

For comparison with PolSK systems, polarized light is used also within the OOK system. The receiver sensitivity for the OOK system at a data rate of $R = 1$ Gbit/s and at an $BER = 10^{-9}$ without polarized light is $S_{RX} = -48.24$ dBm. The receiver sensitivity for the OOK system with polarization control is $S_{RX} = -48.7$ dBm. Since the optical field at the input of the OOK receiver has a given polarization state while the ASE noise is completely unpolarized, the performance of the OOK system can be improved by placing a polarization filter in front of the photodetector. The polarizer then reduces the ASE noise by a factor of 2 [1].

In Fig.(1.26), the RX sensitivity in photons per bit [ppb] versus the optical filter bandwidth of the bandpass given in multiples of the bit rate [R] is depicted. The optimum filter bandwidth is $B_o = 1.6\,\mathrm{GHz}$, where 106 photons per bit ($S_{RX} = -48,7\,\mathrm{dBm}\ @\ R = 1\,\mathrm{Gbit/s}$) are necessary to achieve an $BER = 10^{-9}$.
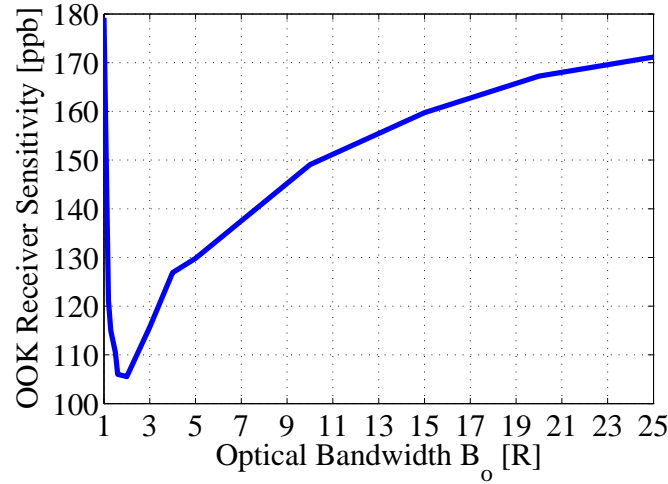
Figure 1.26: OOK receiver sensitivity in photons per bit [ppb] versus optical filter bandwidth (R ... bit rate)

1.4.3 Single polarization shift keying system

An SPolSK system using a receiver with optical preamplification can be seen in Fig.(1.27). The PolSK transmitter was already presented in Section 1.2.2. The RX is almost the same as the SPolSK RX presented in Section 1.3.3, but contains an additional optical preamplifier and a bandpass filter. The BER estimator uses χ^2 noise statistics to account for the ASE noise. Parameters of TX and RX as used for my simulations are listed in Tab.(1.1) and Tab.(1.5).
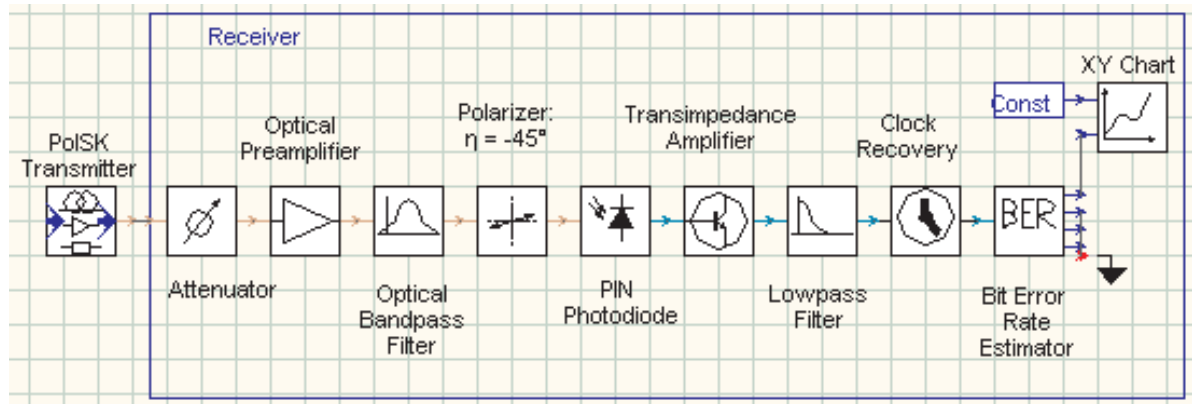
Figure 1.27: Single PolSK system with optical preamplification (η ... azimuth)

The simulated receiver sensitivity for the SPolSK system with optical amplification is $S_{RX} = -49.09 \, \text{dBm}$. The SPolSK RX shows a slightly better performance than the OOK RX because if perfect extinction is assumed at the polarizer, beating at the photodiode only produces an ASE/2-ASE/2 term at the '0' level (see Fig.(1.28)), while in OOK systems a signal-ASE/2 and ASE/2-ASE/2 term is produced during a logical '0' (see Fig.(1.29)). As presented in Section 1.4.1 the noise current of the signal-ASE term (Eqn.(1.45)) usually is higher than the term due to ASE-ASE beating (Eqn.(1.46) with $p = 1$) for small optical filter bandwidths [23]. The beating noise after the photodiode in SPolSK systems with perfect polarization extinction is thus smaller than in OOK systems, which is the reason for the better performance of the SPolSK receiver.
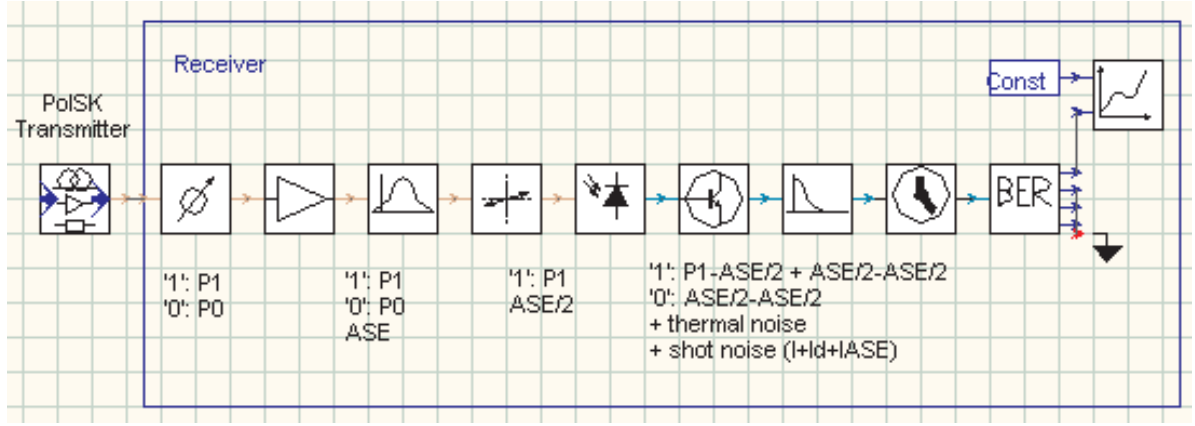
Figure 1.28: SPolSK system with optical amplification (P_0 ... power level '0' bit, P_1 ... power level '1' bit, ASE ... amplified spontaneous emission, I ... electrical current due to signal, I_D ... dark current, I_{ASE} ... electrical current due to ASE noise)
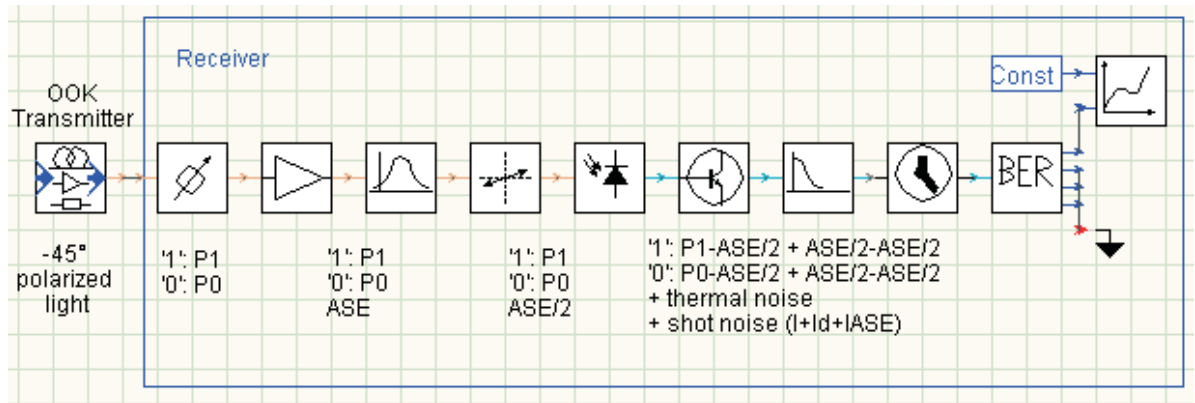
Figure 1.29: OOK system with optical amplification (P_0 ... power level '0' bit, P_1 ... power level '1' bit, ASE ... amplified spontaneous emission, I ... electrical current due to signal, I_D ... dark current, I_{ASE} ... electrical current due to ASE noise)

Figure (1.30) shows the *probability density function* (PDF) of the '0' bits for SPolSK and OOK at an $RIP = -49.1 \, \text{dBm}$. It can be seen that the mean value of the '0' bits for SPolSK

is 39.4 μA (ASE/2-ASE/2 beating), which is less than the mean value for OOK of 48.2 μA (signal-ASE/2 and ASE/2-ASE/2 beating).
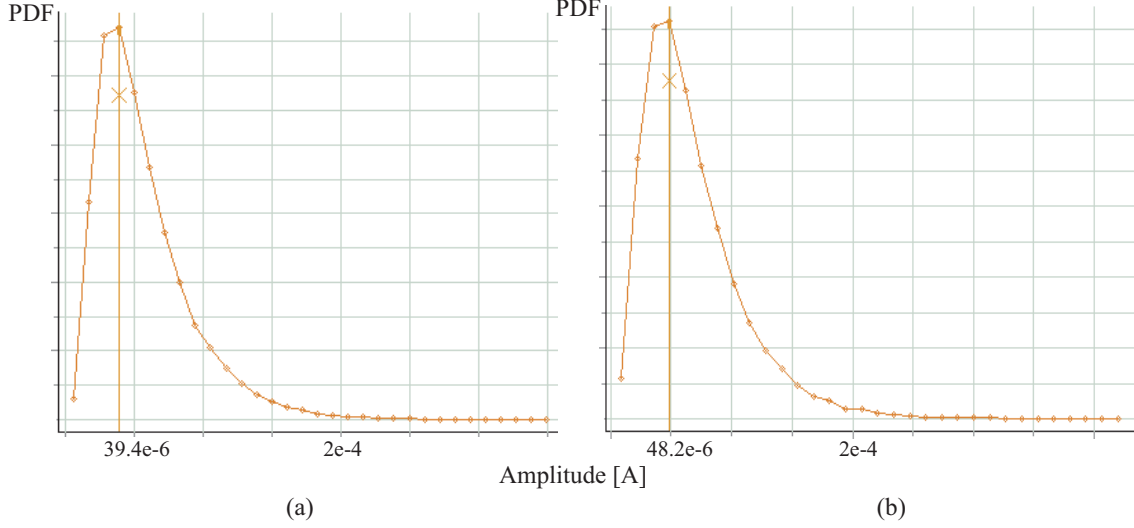
Figure 1.30: Propability density function (PDF) of '0' bits for (a) SPolSK and (b) OOK system with optical amplification (at an RIP of $P = -49.1\,\mathrm{dBm}$)

1.4.4 Balanced polarization shift keying system

A balanced PolSK system using a receiver with optical preamplification is shown in Fig.(1.31). The parameters are the same as for the BPolSK system without optical preamplifier (see Tab.(1.1) and Tab.(1.5)).

An BER estimator designed for balanced detection is used. The simulation uses the χ^2 assumption for signal-ASE and ASE-ASE beat noise. For example, when a logical '1' is received, the optical signal mixes with optical ASE noise and ASE mixes with ASE at the detector in the upper branch, leading to signal-ASE and ASE-ASE beating. No signal is present in the lower branch and there occurs only ASE-ASE beat noise at the detector. The signal samples at the inputs of the balanced detection BER module are divided into two groups, one corresponding to the detection of optical signals mixed with noise, and another corresponding to the detection of noise only. Each of these groups of samples is fitted by a noncentral χ^2 distribution (see Appendix B.2.2) [18].

The subtraction of the signal in the upper branch and the signal in the lower branch is realized in the balanced detection BER estimator. I designed a special clock recovery for the '0' branch, where the data sequence is inverted compared to the transmitted pattern. As shown in Fig.(1.32) the signal has to be inverted before and after the VPI clock recovery module.

The achievable receiver sensitivity of an BPolSK system at $BER = 10^{-9}$ in the case of ASE limited operation is $S_{RX} = -51.55\,\mathrm{dBm}$, independent of the thermal noise evoked in the receiver's electronics. Thus, it has no influence how the electronic part of the receiver is realized. Either a photodiode with TIA in each branch or two photodiodes and one differential amplifier can be used [1]. In comparison with SPolSK a gain of 2.46 dB in receiver sensitivity is achieved. A gain of 3 dB like in systems without optical amplification is not possible because additional beating noise terms impair the performance. In the BPolSK system the noise terms
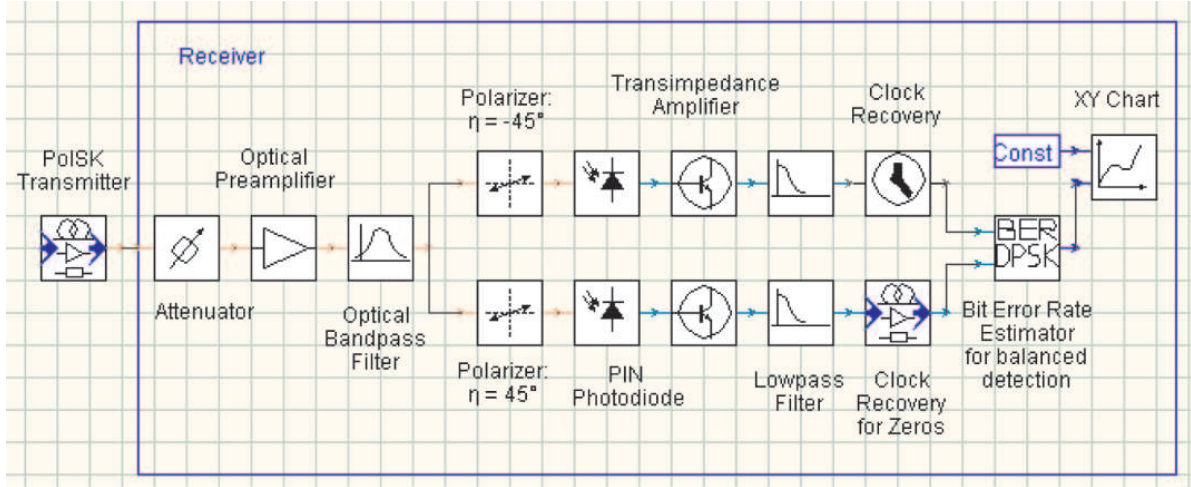
Figure 1.31: Balanced PolSK system with optical amplification (η ... azimuth)
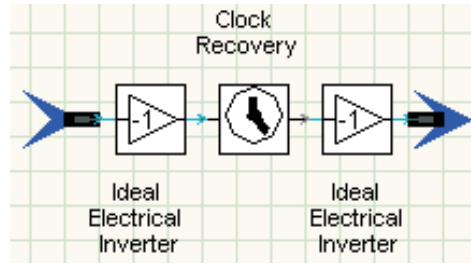
Figure 1.32: Clock recovery for '0' branch

at the decision element include signal-ASE/2 and two times the ASE/2-ASE/2 noise (see Fig.(1.33)), while in an SPolSK system the noise current is only due to signal-ASE/2 and ASE/2-ASE/2 for a logical '1' and due to ASE/2-ASE/2 for a logical '0' (see Fig.(1.28)).

Figure (1.34) gives the RX sensitivity in photons per bit [ppb] versus the optical filter bandwidth in multiples of the bit rate [R]. The optimum filter bandwidth is $B_o = 1.3\,\text{GHz}$, leading to 53 photons per bit ($S_{RX} = -51,72\,\text{dBm}$ @ $R = 1\,\text{Gbit/s}$) necessary to achieve a BER of 10^{-9}.

Comparison of systems with optically preamplified receivers

In Table (1.6) the required receiver input (peak) power at an $BER = 10^{-9}$ for systems with optical preamplifiers is listed.

In Tab.(1.7) the gain in receiver sensitivities of PolSK systems compared to an OOK system with polarization control is listed.

This shows that in ASE noise limited systems PolSK outperforms OOK systems in terms of peak power. SPolSK reaches a gain of $0.4\,\text{dB}$ compared to OOK systems because of less beating noise in the receiver. The performance of the BPolSK RX is $2.9\,\text{dB}$ better than that of the OOK RX. A $3\,\text{dB}$ gain is not reached because of additional beating noise terms in the BPolSK RX.
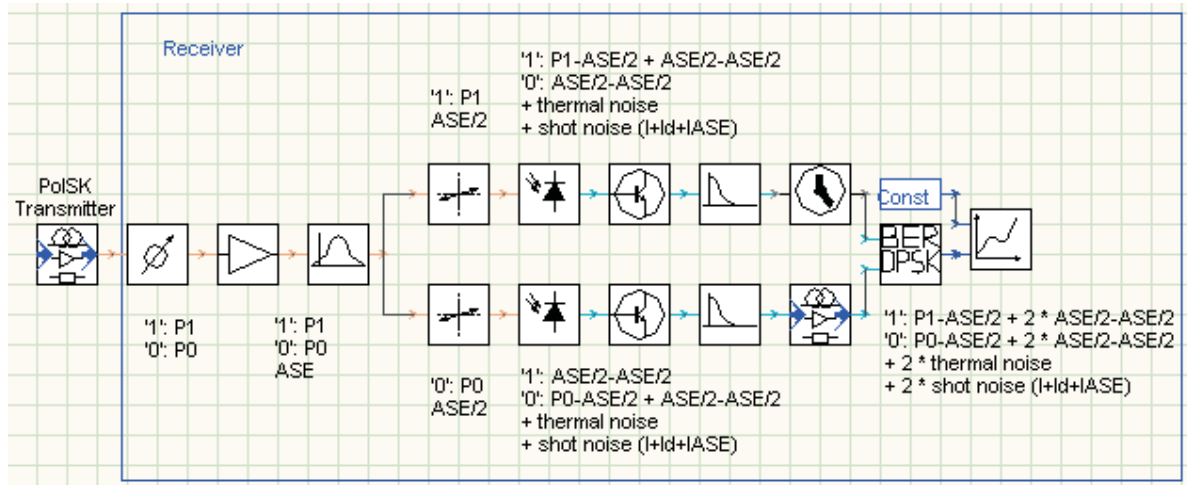
Figure 1.33: BPolSK system with optical preamplification (P_0 ... power level '0' bit, P_1 ... power level '1' bit, ASE ... amplified spontaneous emission, I ... electrical current due to signal, I_D ... dark current, I_{ASE} ... electrical current due to ASE noise)
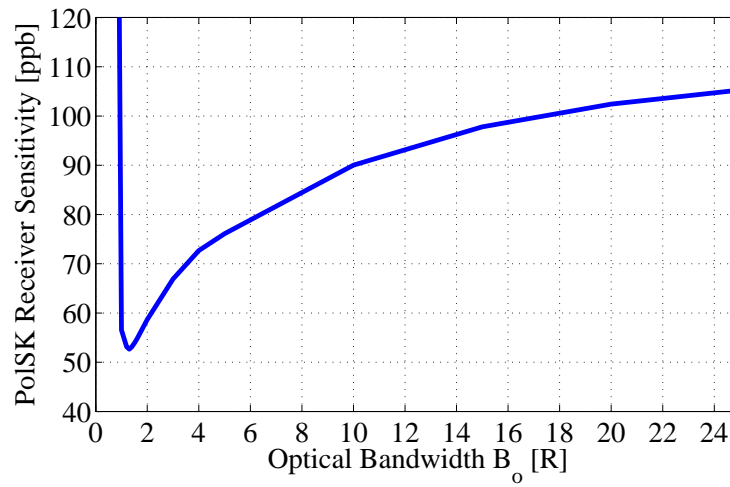

Figure 1.34: BPolSK receiver sensitivity in photons per bit [ppb] versus optical filter bandwidth (R ... bit rate)

	Noise statistics	RX sensitivity [dBm]	RX sensitivity [ppb]
OOK	χ^2	−48.2	118
OOK (with polarization control)	χ^2	−48.7	106
SPolSK	χ^2	−49.1	96
BPolSK	χ^2	−51.6	54

Table 1.6: Receiver sensitivity in the case of ASE noise limited operation (ppb ... photons per bit)

	Gain in receiver sensitivity [dB]
OOK (with polarization control)	0
SPolSK	0.4
BPolSK	2.9

Table 1.7: Gain in receiver sensitivity in the case of ASE noise limited operation

1.5 Non-idealities in the BPolSK receiver

In this section I investigate the non-idealities of components within the BPolSK receiver (which was presented in Section 1.4.4) to allow for a realistic performance estimation. The non-idealities correspond to non-ideal optical and electrical devices used in practical realizations of the receiver (see also Chapter 3).

A balanced PolSK receiver, as implemented in my simulations, is shown in Fig.(1.35). The polarization modulated optical input signal first enters an optical amplifier followed by an optical bandpass filter. Then the signal enters a polarization beam splitter. The PBS is realized with two polarizers, which pass through $-45°$ polarized light (equivalent to logical '1's) in the upper branch and $+45°$ polarized light (equivalent to logical '0's) in the lower branch. The optical power in both branches is then converted into an electrical current by a PIN photodiode with an TIA. After low pass filtering the two electrical signals are subtracted. The electrical signal after clock recovery is then passed to a decision unit.
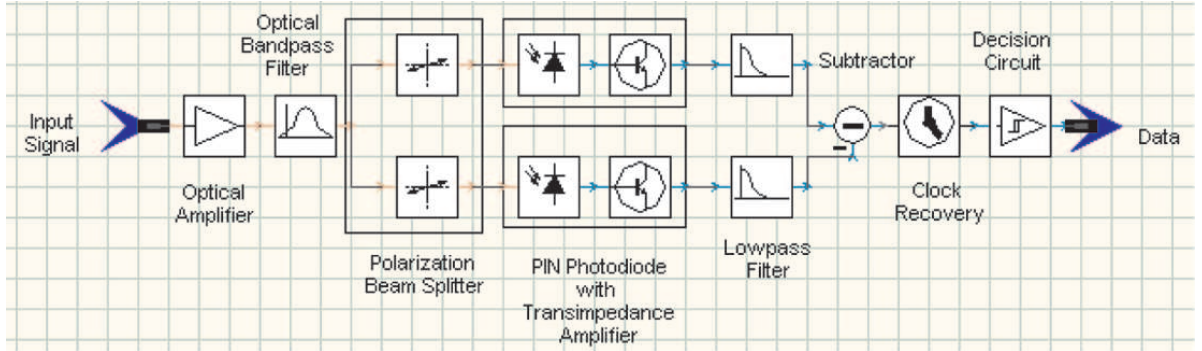
Figure 1.35: BPolSK receiver with optical preamplification

1.5.1 Non-ideal polarization beam splitter

In Fig.(1.36) an ideal polarization beam spitter is depicted. A non-ideality in the PBS can be a deviation of the polarizers transmission axes (see Section 1.2.2) from the incident polarized light, which is $-45°$ linear polarized for a logical '1' and $+45°$ linear polarized for a logical '0'.

Figure (1.37) depicts the penalty in receiver sensitivity versus an offset angle γ from the transmission axis of the $+45°$ linear polarized light, i.e., the logical '1' is perfectly detected, while the logical '0' is not. The two curves, which are plotted in Fig.(1.37), represent the cases of using an adaptive threshold and an absolute decision threshold of $D = 0\,\mathrm{A}$ (see Appendix B.2). The receiver's performance experiences more losses when an absolute threshold is applied.
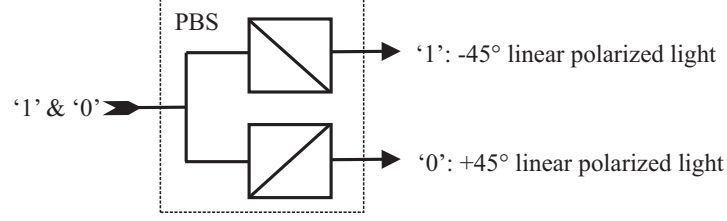
Figure 1.36: Schematic of an ideal PBS
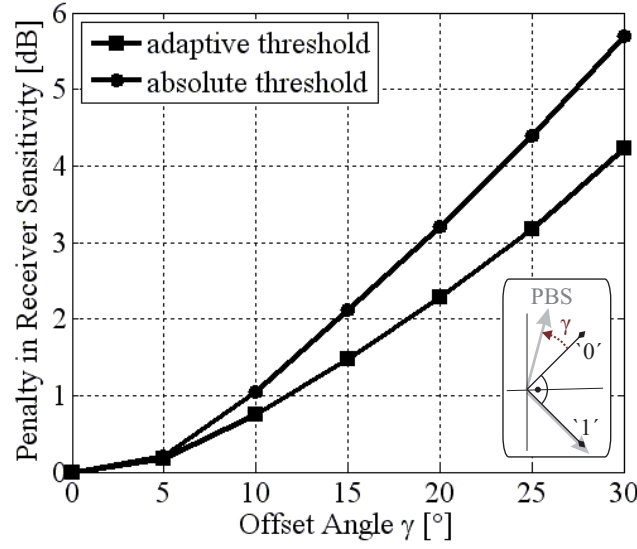
Figure 1.37: Sensitivity penalty in BPolSK RX versus offset angle γ relative to $+45\,^\circ$ polarized light

In Fig.(1.38) the penalties in RX sensitivity using adaptive thresholding are plotted versus an offset angle γ of the transmission axis of one or both polarizers from the state of polarization of the incoming light. The dashed curve is assigned to a deviation of the transmission axis of one polarizer, which is equivalent to the deviation plotted in Fig.(1.37). The solid curve represents the penalty in RX sensitivity versus a total offset angle of the transmission axes of both polarizers, e.g., an offset angle of $\gamma = 10\,^\circ$ relates to a deviation of one transmission axis of $\gamma/2 = 5\,^\circ$. The latter curve does not depend on the kind of threshold used.

The explanation for the different performances in Fig.(1.38) lies in plane geometry. In Fig.(1.39) the projections of a $60\,^\circ$ linear polarizer on $45\,^\circ$ linear polarized light and the projection of a $-60\,^\circ$ linear polarizer on $-45\,^\circ$ linear polarized light can be seen. This is equivalent to a total offset angle of $\gamma = 30\,^\circ$. Furthermore, a projection of a $75\,^\circ$ linear polarizer on the incident light is depicted, which also corresponds to an offset angle of $\gamma = 30\,^\circ$. The difference of '1' and '0' levels in the first case is bigger than the difference in the second case. Thus, the BER probability is higher for a deviation of the transmission axis of only one polarizer compared to an equal total deviation of the transmission axes of both polarizers.

Figure (1.40) shows the penalty in receiver sensitivity plotted over an total offset angle γ of
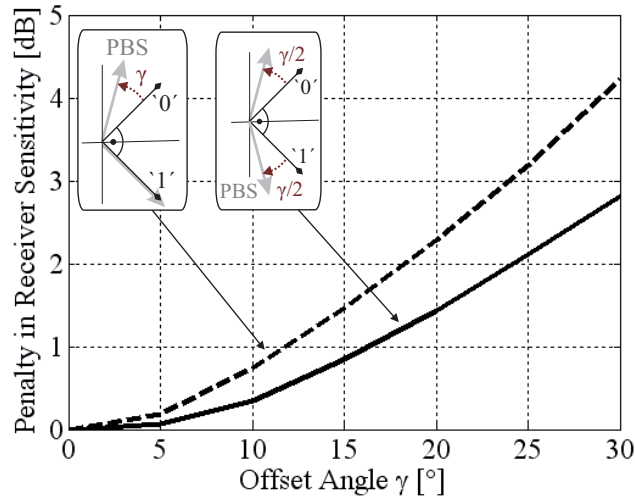
Figure 1.38: Sensitivity penalty in BPolSK RX versus offset angle γ of one or both polarizers from the state of polarization of the incoming light (adaptive thresholding)

Offset Angle 30°

Deviation of both polarizers
+60° and -60°:
'1' branch: '1': 0.97
            '0': 0.26
'0' branch: '1': 0.26
            '0': 0.97
Subtraction: '1': 0.97-0.26=0.71
             '0': 0.26-0.97=-0.71
Difference '1'-'0' levels: 1.42

Deviation of one polarizer +75°:
'1' branch: '1': 1
            '0': 0
'0' branch: '1': 0.5
            '0': 0.87
Subtraction: '1': 1-0.5=0.5
             '0': 0-0.87=-0.87
Difference '1'-'0' levels: 1.37
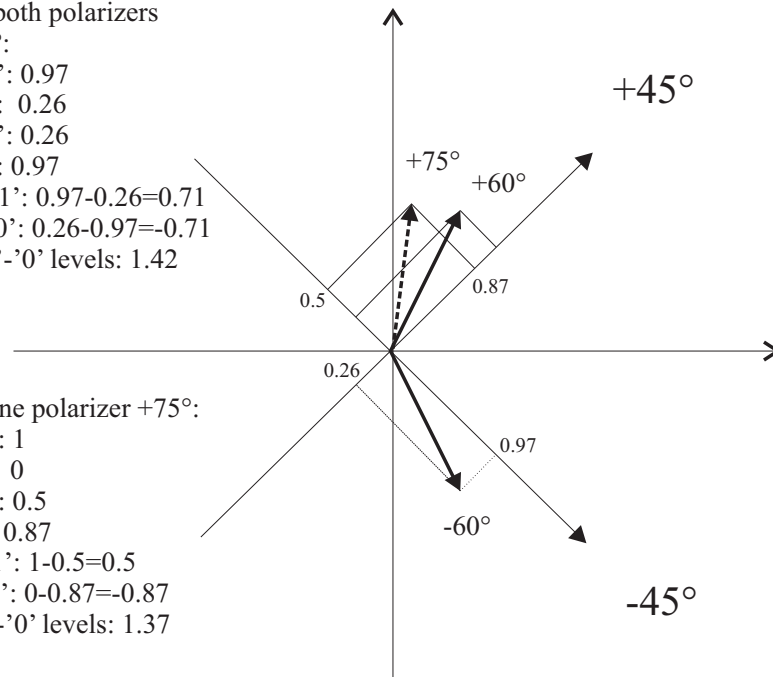
Figure 1.39: Projections of polarizers on incident light

the transmission axes of both polarizers. The two curves represent an orthogonality-preserving deviation of the transmission axes and a non-orthogonal deviation of the transmission axes. The performances are similar for both kinds of deviations because the projections of the

transmission axes of the polarizers on the incident light are equal. The difference between the curves of maximal 0.15 dB are due to a limited simulation accuracy of the software. Both curves does not depend on the kind of threshold used (see Fig.(1.38) and Fig.(1.41)).
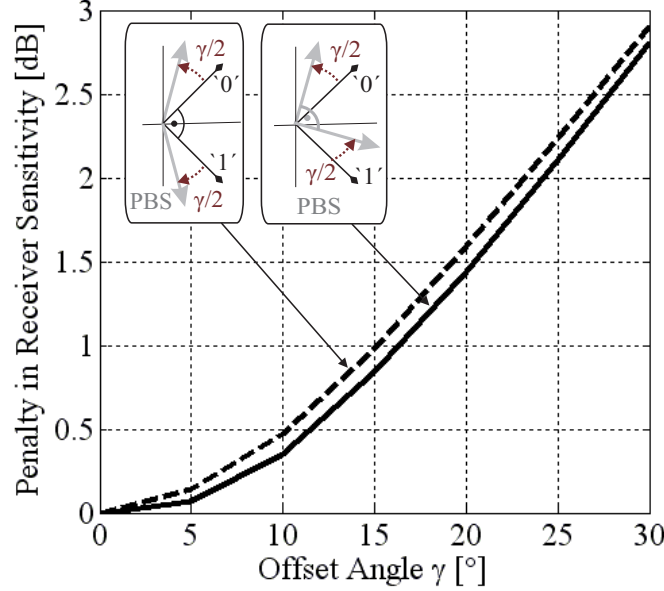
Figure 1.40: Sensitivity penalty in BPolSK RX versus total offset angle γ of both polarizers from the state of polarization of the incoming light

In Fig.(1.41) the penalty in RX sensitivity is plotted versus a total offset angle γ of the transmission axes of both polarizers. Here, the orthogonality of the polarizers is preserved. The two curves represent an adaptive threshold of the decision unit and an absolute threshold of 0 A. There is no difference in the RX performances for both curves within the allowed simulation accuracy of 0.15 dB.

1.5.2 Non-ideal PIN photodiode with transimpedance amplifier

Other non-idealities in the BPolSK RX arise in PIN photodiodes with TIAs (see Fig.(1.35)). For example, there can be a deviation in the gain of the TIAs in both branches relative to each other. Figure (1.42) shows the penalty in receiver sensitivity versus a gain offset in the TIA of one branch with an initial gain of 26 dB. It is shown that the performance of the receiver is much better for an adaptive decision threshold than for an absolute threshold of 0 A.

Another non-ideality that can occur in PIN photodiodes with TIAs may be a difference in the responsivities of the photodiodes. It can be described with a *responsivity imbalance*, β, which is defined as [24]

$$\beta = \frac{S_A - S_B}{S_A + S_B}, \tag{1.49}$$

where S_A and S_B are the PIN photodiodes responsivities in the upper and in the lower branch of the BPolSK receiver. Balanced detection, where β is equal to 0, is reached for $S_A = S_B$. Figure (1.43) shows the penalty in the RX sensitivity for an adaptive and an absolute decision threshold (0 A) versus a responsivity imbalance. For $\beta = 1$, i.e., the responsivity of the
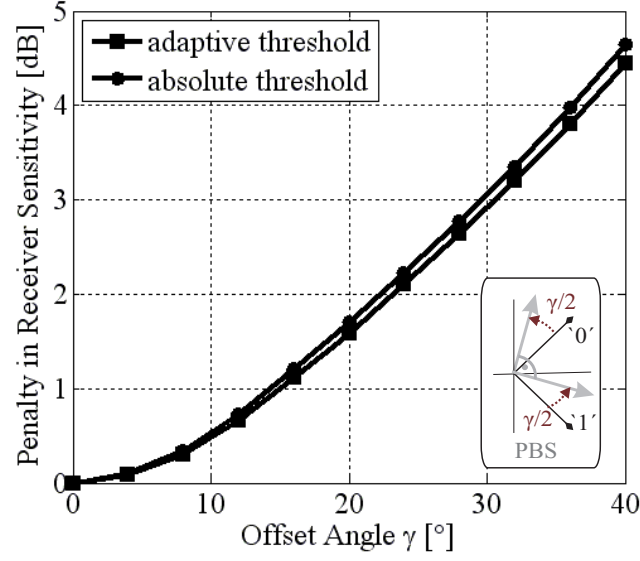
Figure 1.41: Sensitivity penalty in BPolSK RX versus total offset angle γ of both polarizers from the state of polarization of the incoming light
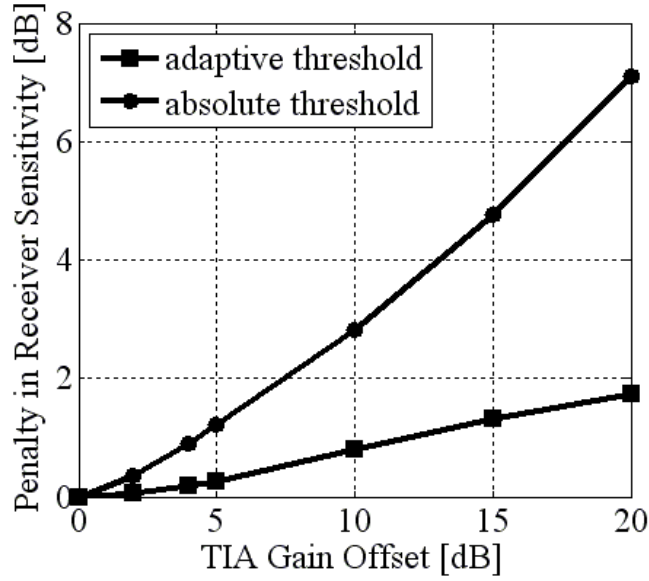
Figure 1.42: Sensitivity penalty in BPolSK RX versus TIA gain offset in one branch

photodiode in the lower branch is set to zero ($S_B = 0$), the BPolSK RX is equivalent to the SPolSK RX introduced in Section 1.4.3. Thus, the penalty in the sensitivity of the BPolSK RX for $\beta = 1$ should be 2.5 dB, this is equivalent to the gain of 2.5 dB in the receiver sensitivity of the BPolSK RX compared to the SPolSK RX (see Tab.(1.7)). According to Fig.(1.43) there occur a penalty of 2.6 dB, the 0.1 dB difference is due to an inaccuracy of the simulation of

the systems in VPItransmissionMaker.
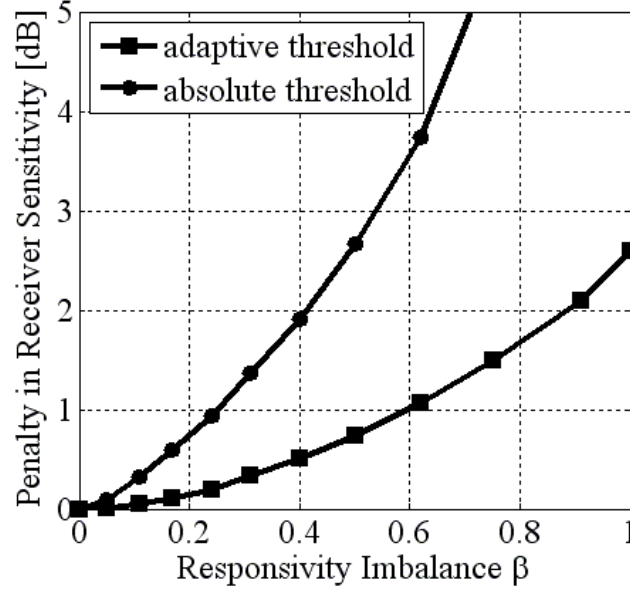
Figure 1.43: Sensitivity penalty in BPolSK RX versus responsivity imbalance

1.5.3   Non-ideal optical and electrical wires

Finally, there can occur non-idealities in the optical and electrical wires of the BPolSK RX. Thus, I simulate a delay difference in the detector branches of the receiver shown in Fig.(1.44). In Fig.(1.45) the penalty of the RX sensitivity versus a delay difference, τ, in the receiver branches is depicted. The τ is plotted in multiples of $1/R$. There is no difference in the performance of the RX for an adaptive or an absolute $(0\,\mathrm{A})$ decision threshold.
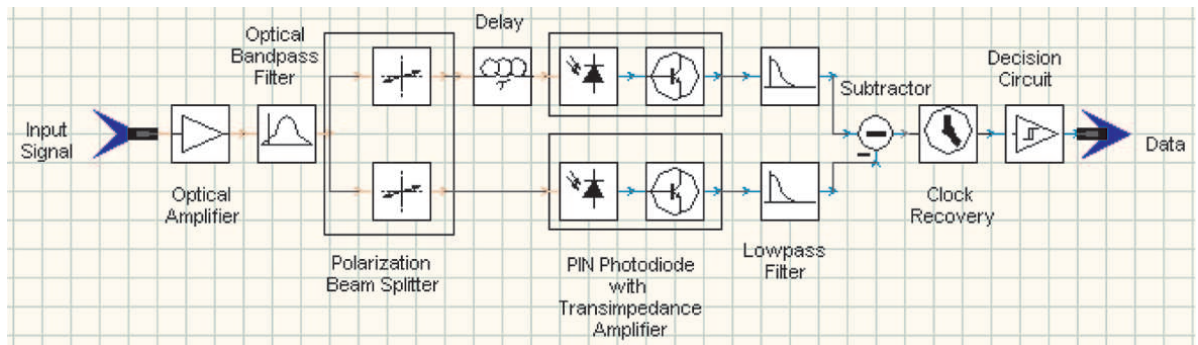
Figure 1.44: BPolSK receiver with optical preamplification and a delay τ in the upper branch
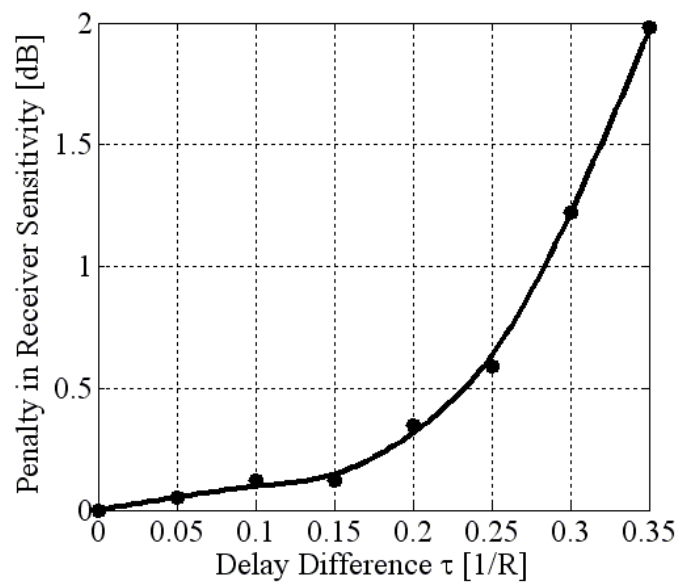
Figure 1.45: Sensitivity penalty in BPolSK RX versus a delay τ in detector branches

Chapter 2

Impact of the Atmosphere on Polarization

2.1 Introduction

Systems employing polarization modulation can be used for communication links between ground stations on earth, high-altitude platforms, and satellites [23]. Thus, the potential influence of the atmosphere on the polarization of a laser beam has to be assessed. In this chapter I present some literature research on this topic. First, I introduce the optical coherence theory, which describes random light, especially the concept of partial polarization and depolarization. Then, four possible impacts of the atmosphere on the polarization of a laser beam are presented, namely depolarization, birefringence, rotation of the angle of linear polarization, and polarization filtering. Quantitatively this effects can be assessed by means of polarimetry, a field of research in astronomy.

2.2 Optical coherence

The study of the random fluctuations of light is known as the theory of optical coherence. Randomness in light arises because of unpredictable fluctuations of the field of the light source or of the medium through which light propagates (e.g., it propagates through the random atmosphere) [13]. Even light from a well stabilized light source, such as a laser, will exhibit some random fluctuations, since the effect of spontaneous emission is never entirely absent [25].

In the preceding chapter it was assumed that light is deterministic or "coherent". An example of coherent light is the monochromatic wave, $E(\vec{r}, t) = \Re[E(\vec{r})e^{j\omega t}] = \Re[E_c(\vec{r}, t)]$ (scalar version of Eqn.(1.8)) with the complex wavefunction $E_c(\vec{r}, t)$, for which the complex amplitude $E(\vec{r})$ is a deterministic complex function, e.g., $E(\vec{r}) = E(\vec{k})e^{-j\vec{k}\cdot\vec{r}}$ in the case of a plane wave (scalar version of Eqn.(1.10)). The dependence of the wavefunction on time and position is perfectly periodic and predictable. On the other hand, for random light the dependence of the wavefunction on time and position is not totally predictable and cannot generally be described without resorting to statistical methods [13].

2.2.1 Temporal coherence

Consider the fluctuations of stationary light at a fixed position $\vec{r}$ as a function of time. The complex wavefunction, $E_c(t)$ (the $\vec{r}$ dependence is dropped, since $\vec{r}$ is fixed), is now modeled as a stationary stochastic process [25]. A random process is statistically stationary, when its statistical averages are invariant to the absolute time, t [26].

The random fluctuations of $E_c(t)$ are characterized by a time scale representing the "memory" of the random function. Fluctuations at points separated by a time interval longer than the memory time are independent, so that the process "forgets" itself. A quantitative measure of this temporal behavior is established by defining a statistical average known as the autocorrelation function [13]

$$G(\tau) = \langle E_c^*(t) E_c(t + \tau) \rangle, \tag{2.1}$$

where the symbol $\langle \cdot \rangle$ denotes an ensemble average over many realizations of the random process. For an ergodic process [25], the statistical averaging operation can then be determined by time averaging over a long time duration, T, with [13]

$$\langle \cdot \rangle = \lim_{T \to \infty} \frac{1}{2T} \int_{-T}^{T} (\cdot) \, dt. \tag{2.2}$$

In optical coherence theory the autocorrelation function, $G(\tau)$, is known as the temporal coherence function [13]. This function carries information about both the intensity of stationary light, $I_0 = G(0)$, and the degree of correlation (coherence), $g(\tau)$. The complex degree of temporal coherence is defined as [13]

$$g(\tau) = \frac{G(\tau)}{G(0)} = \frac{\langle E_c^*(t) E_c(t + \tau) \rangle}{\langle E_c^*(t) E_c(t) \rangle}. \tag{2.3}$$

It's absolute value cannot exceed unity, $0 \leq |g(\tau)| \leq 1$. When the light is deterministic and monochromatic, i.e., $E_c(t) = A \exp(j\omega t)$, where A is a constant, Eqn.(2.3) gives $g(\tau) = \exp(j\omega\tau)$, so that $|g(\tau)| = 1$ for all τ. The variables $E_c(t)$ and $E_c(t + \tau)$ are then completely correlated for all time delays τ.

Usually, $|g(\tau)|$ drops from its largest value as τ increases and the fluctuations become uncorrelated for a sufficiently large time delay. The value τ_c at which the function $|g(\tau)|$ drops to the value $1/2$ serves as a measure of the memory time of the fluctuations known as the coherence time (see Fig.(2.1)) [13].

The autocorrelation function, $G(\tau)$, of the stationary random process and the power spectral density (or power spectrum), $S(f)$, of the process form a Fourier transform pair [25][13]

$$S(f) = \int_{-\infty}^{\infty} G(\tau) \exp(-j2\pi f\tau) d\tau. \tag{2.4}$$

This relation is known as the Wiener-Khinchin theorem. The spectral width, or linewidth of the light is the width, Δf, of the power spectrum. Because of the Fourier transform relation between $S(f)$ and $G(\tau)$, their widths are inversely related. A light source of broad spectrum has a short coherence time, whereas a light source with narrow linewidth has a long coherence time.

In the limiting case of monochromatic light the temporal autocorrelation function is $G(\tau) = I_0 \exp(j2\pi f_0\tau)$, so that the corresponding spectral density, $S(f) = I_0\delta(f - f_0)$, contains only a single frequency component, f_0. Thus, $\tau_c = \infty$ and $\Delta f = 0$ [13].

Light for which the coherence time is much longer than the differences of the time delays encountered in the optical system of interest is effectively completely temporal coherent. That is, the coherence length, $l_c = c\tau_c$ (c is the velocity of the light), is much greater than all optical path length differences encountered. In this case the light is said to be quasi-monochromatic [13], i.e., its bandwidth, Δf, is small compared to its mean frequency, f_0 (see Fig.(2.1)) [25].
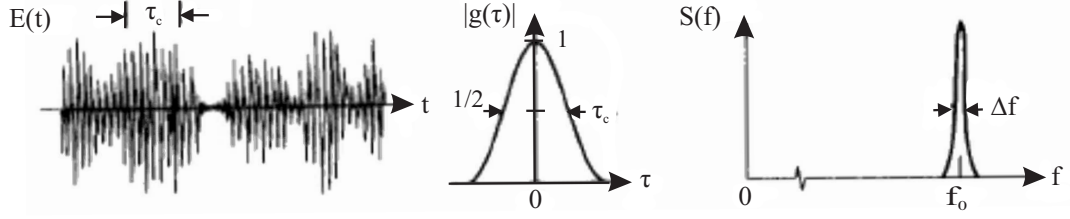
Figure 2.1: The magnitude of the complex degree of temporal coherence, $|g(\tau)|$, and the spectral density, $S(f)$, of a quasi-monochromatic random wave, $E(t) = \Re[E_c(t)]$, with coherence time, τ_c, and linewidth, $\Delta f \ll f_0$ [13].

2.2.2 Spatial coherence

An important descriptor of the spatial and temporal fluctuations of the random function $E_c(\vec{r}, t)$ is the cross-correlation function of $E_c(\vec{r}_1, t)$ and $E_c(\vec{r}_2, t)$ at pairs of positions $\vec{r}_1$ and $\vec{r}_2$ [25],

$$G(\vec{r}_1, \vec{r}_2, \tau) = \langle E_c^*(\vec{r}_1, t) E_c(\vec{r}_2, t + \tau) \rangle. \tag{2.5}$$

It is known as the *mutual coherence function* (MCF). The spatial correlation of light is assessed by examining the dependence of the MCF for a fixed time delay τ, in many situations the point $\tau = 0$ is the most appropriate [13],

$$G(\vec{r}_1, \vec{r}_2) = \langle E_c^*(\vec{r}_1, t) E_c(\vec{r}_2, t) \rangle. \tag{2.6}$$

It is known as the mutual intensity.

When the light is quasi-monochromatic (see previous section), the mutual coherence function is a harmonic function of time and $G(\vec{r}_1, \vec{r}_2)$ describes the spatial coherence completely [25],

$$G(\vec{r}_1, \vec{r}_2, \tau) = G(\vec{r}_1, \vec{r}_2) \exp(j2\pi f_0\tau). \tag{2.7}$$

The normalized mutual intensity is [13]

$$g(\vec{r}_1, \vec{r}_2) = \frac{G(\vec{r}_1, \vec{r}_2)}{\sqrt{I(\vec{r}_1)I(\vec{r}_2)}}, \tag{2.8}$$

where $I(\vec{r}) = G(\vec{r}, \vec{r}, 0)$ is the intensity at position $\vec{r}$. Its magnitude, $|g(\vec{r}_1, \vec{r}_2)|$, is bounded between zero and unity and is regarded as a measure of the degree of spatial coherence. If the complex wavefunction, $E_c(\vec{r}, t)$, is deterministic, $|g(\vec{r}_1, \vec{r}_2)| = 1$ for all $\vec{r}_1$ and $\vec{r}_2$, so that the light is completely correlated everywhere.

The area within which the function $|g(\vec{r}_1, \vec{r}_2)|$ is greater than the value $1/2$ is called the coherence area, A_c (see Fig.(2.2)). It represents the spatial extent of $|g(\vec{r}_1, \vec{r}_2)|$ as a function of $\vec{r}_1$ for fixed $\vec{r}_2$. In the ideal limit of coherent light the coherence area is infinite. If the area of
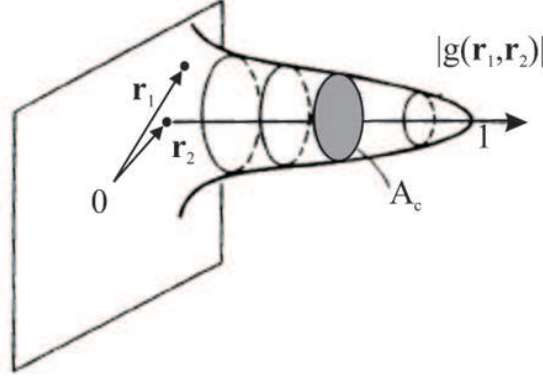
Figure 2.2: An example of the magnitude of the normalized mutual intensity, $|g(\vec{r}_1, \vec{r}_2)|$, as a function of the position vector $\mathbf{r}_1$ in the vicinity of a fixed point $\mathbf{r}_2$, the coherence area, A_c, is depicted [13].

coherence is greater than the size of the aperture through which light is transmitted, so that $|g(\vec{r}_1, \vec{r}_2)| \approx 1$ at all points of interest, the light may be regarded as spatially coherent [13].

In the following it is assumed that the light of the laser, which is used for communications through the atmosphere, is quasi-monochromatic and spatially coherent.

2.2.3   Partial polarization

The scalar coherence theory of light presented in the previous sections is inadequate for the statistical theory of random light including the effects of polarization. The theory of partial polarization is based on characterizing the components of the optical field vector by correlations and cross-correlations [13].

Spatial effects are not included here. The light is described by a transverse electromagnetic plane wave traveling in the z-direction. The electric field vector has two components in the x- and y-directions with complex wavefunctions $\tilde{E}_x(t)$ and $\tilde{E}_y(t)$ (see Eqn.(1.13)) that are generally random. Each function is characterized by its autocorrelation function (the temporal coherence function, see Eqn.(2.1)) [13]:

$$
\begin{aligned}
G_{xx}(\tau) &= \langle \tilde{E}_x^*(t)\tilde{E}_x(t+\tau)\rangle, & (2.9) \\
G_{yy}(\tau) &= \langle \tilde{E}_y^*(t)\tilde{E}_y(t+\tau)\rangle. & (2.10)
\end{aligned}
$$

An additional descriptor of the wave is the cross-correlation function of $\tilde{E}_x(t)$ and $\tilde{E}_y(t)$ [13],

$$
G_{xy}(\tau) = \langle \tilde{E}_x^*(t)\tilde{E}_y(t+\tau)\rangle. \tag{2.11}
$$

The normalized function [13]

$$
g_{xy}(\tau) = \frac{G_{xy}(\tau)}{\sqrt{G_{xx}(0)G_{yy}(0)}} \tag{2.12}
$$

is the cross-correlation coefficient. It satisfies the inequality $0 \leq |g_{xy}(\tau)| \leq 1$. When the two components are uncorrelated at all times, $|g_{xy}(\tau)| = 0$, and when they are correlated at all times, $|g_{xy}(\tau)| = 1$.

For quasi-monochromatic light all dependencies on τ are approximately of the form $\exp(j2\pi f_0\tau)$, so that the polarization properties are described by the values at $\tau = 0$. The three numbers $G_{xx}(0)$, $G_{yy}(0)$, and $G_{xy}(0)$, hereafter denoted by G_{xx}, G_{yy}, and G_{xy}, are then used to describe the polarization of the wave. Note that $G_{xx} = I_x$ and $G_{yy} = I_y$ are real numbers that represent the intensities of the x- and y-components, but G_{xy} is complex and $G_{yx} = G_{xy}^{\star}$. It is convenient to write the four variables in the form of a 2×2 Hermitian matrix [13],

$$\mathbf{G} = \begin{pmatrix} G_{xx} & G_{xy} \\ G_{yx} & G_{yy} \end{pmatrix} = \begin{pmatrix} \langle \tilde{E}_x^*(t)\tilde{E}_x(t)\rangle & \langle \tilde{E}_x^*(t)\tilde{E}_y(t)\rangle \\ \langle \tilde{E}_y^*(t)\tilde{E}_x(t)\rangle & \langle \tilde{E}_y^*(t)\tilde{E}_y(t)\rangle \end{pmatrix}, \tag{2.13}$$

called the coherency matrix or polarization matrix [25]. The trace of the matrix is the total intensity, $tr(\mathbf{G}) = G_{xx} + G_{yy} = I_x + I_y = \hat{I}$.

The coherence matrix, $\mathbf{G}$, defined in Eqn.(2.13), characterizes the correlation properties of an uniform, quasi-monochromatic beam of electromagnetic radiation. It is adequate to describe the state of polarization of the beam [25].

Unpolarized light (natural light)

Light of intensity $\hat{I}$ is said to be unpolarized if its two components have the same intensity and are uncorrelated, $I_x = I_y = \hat{I}/2$ and $G_{xy} = 0$, i.e., the magnitude of the cross-correlation coefficient at $\tau = 0$ is $|g_{xy}| = 0$. The coherency matrix is then [13]

$$\mathbf{G} = \frac{\hat{I}}{2}\begin{pmatrix} 1 & 0 \\ 0 & 1 \end{pmatrix}. \tag{2.14}$$

Unpolarized light therefore has an electric field vector that is statistically isotropic, it is equally likely to have any direction in the (x,y) plane [13] and thus to have any SOP (see Section 1.2.1). Unpolarized light is also called natural light, because such light is generated by sources that are commonly encountered in nature [25].

Completely polarized light

If the cross-correlation coefficient at $\tau = 0$ has unit magnitude, $|g_{xy}| = 1$, the two components of the optical field are perfectly correlated and the light is said to be completely polarized. Since $g_{xy} = G_{xy}/\sqrt{I_xI_y}$, the coherency matrix takes the form [13]

$$\mathbf{G} = \begin{pmatrix} I_x & \sqrt{I_xI_y}exp^{j\phi} \\ \sqrt{I_xI_y}exp^{-j\phi} & I_y \end{pmatrix}, \tag{2.15}$$

where ϕ is the phase difference between the two components of the electric field vector (see Section 1.2.1) and the argument of g_{xy}. The coherency matrix for linear polarized light in the x-direction with intensity $\hat{I}$ looks like

$$\mathbf{G} = \hat{I}\begin{pmatrix} 1 & 0 \\ 0 & 0 \end{pmatrix} \tag{2.16}$$

and the coherency matrix for right-hand circularly polarized light with intensity $\hat{I}$ is

$$\mathbf{G} = \frac{\hat{I}}{2}\begin{pmatrix} 1 & j \\ -j & 1 \end{pmatrix}. \tag{2.17}$$

Degree of polarization

Partial polarization is a general state of random polarization that lies between the two ideal limits of unpolarized and polarized light. A partially polarized wave can always be regarded as a mixture of two uncorrelated waves, a completely polarized wave and an unpolarized wave [13]. The coherency matrix, $\mathbf{G}$, can be uniquely expressed as the sum of two matrices, one of which represents completely unpolarized light, $\mathbf{G}^{unpol}$, and the other completely polarized light, $\mathbf{G}^{pol}$ [25],

$$\mathbf{G} = \mathbf{G}^{unpol} + \mathbf{G}^{pol}. \tag{2.18}$$

The ratio of the intensity of the polarized portion of the wave to its total intensity is called the *degree of polarization* (DOP) [25][13],

$$DOP = \frac{tr(\mathbf{G}^{pol})}{tr(\mathbf{G})} = \sqrt{1 - \frac{4\,det(\mathbf{G})}{tr(\mathbf{G})^2}}, \tag{2.19}$$

$$DOP = \sqrt{1 - 4\left[\frac{I_x I_y}{(I_x + I_y)^2}\right](1 - |g_{xy}|^2)}, \tag{2.20}$$

where $det(\mathbf{G})$ is the determinant of the matrix. The degree of polarization, DOP, satisfies $0 \leq DOP \leq 1$. For polarized light the degree of polarization has its highest value of 1, as can easily be seen by substituting $|g_{xy}| = 1$ into Eqn.(2.20). For unpolarized light it has its lowest value, $DOP = 0$, since $I_x = I_y$ and $g_{xy} = 0$ [13]. In Fig.(2.3) the fluctuations of the electric field vector for unpolarized, partially polarized and completely polarized light are shown.

(a)   (b)   (c)
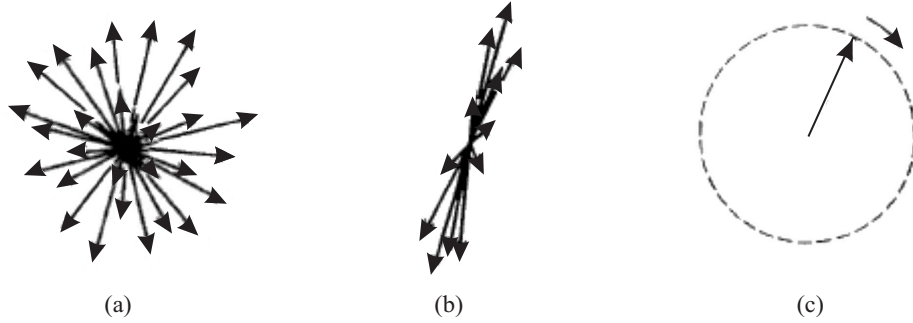
Figure 2.3: Fluctuations of the electric field vector for (a) unpolarized light, (b) partially polarized light, and (c) polarized light with circular polarization [13]

The DOP can be also expressed in terms of the four Stokes parameters. As introduced in Section 1.2.1, S_0 is the optical intensity, while S_1, S_2, and S_3 determines the SOP. The DOP is now defined as [12][25]

$$DOP = \frac{\sqrt{\langle S_1 \rangle^2 + \langle S_2 \rangle^2 + \langle S_3 \rangle^2}}{\langle S_0 \rangle}. \tag{2.21}$$

For signals whose state of polarization does not change in time, the DOP is one, $DOP = 1$. It immediately follows from equation (2.21) that for a completely polarized beam [25]

$$\langle S_0 \rangle^2 = \langle S_1 \rangle^2 + \langle S_2 \rangle^2 + \langle S_3 \rangle^2. \tag{2.22}$$

For completely polarized light the various SOPs can be mapped on the surface of the Poincaré sphere. $DOP = 0$ denotes completely unpolarized beams [25],

$$\langle S_1 \rangle = \langle S_2 \rangle = \langle S_3 \rangle = 0. \tag{2.23}$$

An intermediate value of DOP means that some of the optical power is polarized and the remaining power is not [12].

2.3 Impacts of the atmosphere

There are four possible impacts of the atmosphere on the polarization of a laser beam, which are depicted in Fig.(2.4). A quasi-monochromatic, spatially coherent, and completely polarized laser beam with a certain SOP (e.g., a linear SOP) is transmitted through the random medium "atmosphere". At the RX the polarization of the laser beam may have changed:

- One possible impact that can occur is depolarization of the completely polarized laser beam (see Fig.(2.4a)). The laser beam is then partially polarized at the receiver (see Section 2.2.3). It depends on the degree of polarization, if the initial SOP can be still recognized at the receiver.

- Another effect can be that the atmosphere is acting like a birefringent medium (see Fig.(2.4b)). The x- and y-components of the electric field vector experience different phase velocities (see Eqn.(3.1)) and thus have a certain phase difference at the receiver, i.e., in general the SOP at the RX is elliptic (see Section 1.2.1).

- The atmosphere can also rotate the angle of linear polarization (see Fig.(2.4c)). There occur an offset angle between the direction of the electric field vector at the TX and the RX.

- The fourth effect can be that the atmosphere is acting like a polarization filter, it transmits a particular SOP while the orthogonal SOP is attenuated, e.g., see Fig.(2.4d).

These possible effects can be assessed with the aid of polarimetry. Polarimetry is a field in astronomy. Light from an astronomical object that is scattered from a flattened cloud of electrons, atoms, molecules, or grains can lead to (partially) linearly polarized light. For example, light from distant stars is polarized by magnetically aligned, elongated dust grains. The distribution of the polarization reveals the direction of the galactic field, while the wavelength dependance of the polarization carries information about sizes and shapes of the interstellar grains. In polarimetry, stars of well-known polarization ("polarization standards") are observed to calibrate the measuring devices [27]. In such polarimetric observations the degree of polarization (see Section 2.2.3), DOP, and the angle of linear polarization, the azimuth, (see Section 1.2.1), η, are measured [28].

The light of a star can be compared to a laser beam. It is spatially coherent because of the wide distance of the star from Earth and it is quasi-monochromatic when filters are used in the measurements.

For the *Hubble space telescope* (HST), which is orbiting the Earth at a height of $589\,\mathrm{km}$, a program was sponsored to obtain complete and accurate polarimetry data of a variety of celestial targets for in-flight calibration of its polarimetric instruments. The target list emphasized hot stars with reasonably well-understood polarizing mechanisms. These observations
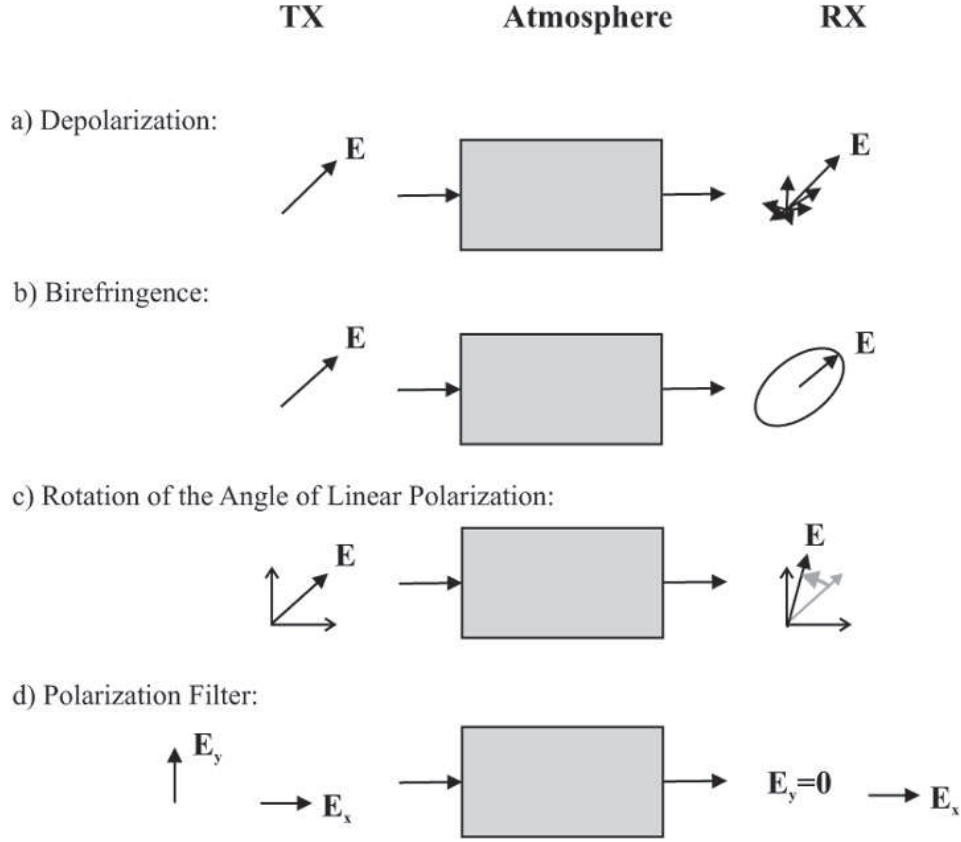
Figure 2.4: Four possible atmospheric impacts on the polarization of a laser beam: (a) depolarization, (b) birefringence, (c) rotation of the angle of linear polarization, and (d) filtering of a certain SOP ($\mathbf{E}$ ... electric field vector, $\mathbf{E}_x$, $\mathbf{E}_y$ ... electric field vectors of x- and y-polarized light)

were obtained in eight observation runs between 30. October 1985 and 16. November 1987 using the Mount Lemmon telescope in Tucson, Arizona (USA) [29].

In Table (2.1) the polarized standard stars BD +59°389, HD 19820, HD 161056, and HD 204827 from the HST target list are given [29]. DOP and η are mean values measured with a bandpass filter with a center wavelength of 540 nm [30]. The standard deviations are also given. The final column denotes the number of observations of each star. Multiple measurements of each of the polarized targets were obtained to assess any variability which may be present. Such variability could result from the motion of intervening interstellar clouds across the line of sight or due to the atmosphere. Each of the objects listed in Tab.(2.1) showed no evidence of polarimetric variability to a limit of $\Delta DOP \approx 0.05\%$ and $\Delta\eta \approx 0.5°$ in data obtained at a minimum of three observations during the two year period of the program [29]. From this observations it follows, that if there occurs an atmospheric effect it is only in the range of $\Delta DOP \approx 0.05\%$ and $\Delta\eta \approx 0.5°$.

The atmosphere doesn't act like a birefringent element, because the linear polarized light of the stars is also linear polarized, when it goes through the atmosphere and is measured on the ground. This can be seen in Tab.(2.1), where η is the same for different observations over time.

Star	DOP [%]	η [°]	N
BD +59°389	6.701 ± 0.015	98.09 ± 0.07	4
HD 19820	4.787 ± 0.028	114.93 ± 0.17	3
HD 161056	4.030 ± 0.025	66.93 ± 0.18	3
HD 204827	5.322 ± 0.014	58.73 ± 0.08	4

Table 2.1: List of standard stars (DOP ... mean degree of polarization, η ... mean angle of linear polarization, N ... number of observations) [29]

Some results and details of ground based polarimetry observations, as well as the results of the polarimetric measurements of HST, are presented in Tab.(2.2) [31]. The polarization

	ground based		space based	
Star	DOP [%]	η [°]	DOP [%]	η [°]
HD 283812	1.31 ± 0.07	35 ± 2	1.32 ± 0.04	33 ± 7
			1.38 ± 0.09	29 ± 5

Table 2.2: Polarimetric measurements on Earth and on HST of the star HD 283812 (DOP ... mean degree of polarization, η ... mean angle of linear polarization) [31]

properties of HD 283812 have been reported to be $DOP = 1.31\,\% \pm 0.07\,\%$ at $\eta = 35\,° \pm 2\,°$ on ground, based on measurements at a wavelength of $\lambda = 2.04\,\mu$m. Two measurements on board of the HST report polarization properties at a wavelength of $\lambda = 2.05\,\mu$m. They are also listed in Tab.(2.2). The differences in the ground and space spaced measurements can be seen in Tab.(2.3). Although a part of the differences may arise from the not fully sophisticated measuring instruments in the HST or the slightly different wavelengths [31], I assume here that all differences arise from an effect of the atmosphere in the worst case.

Star	ΔDOP [%]	$\Delta \eta$ [°]
HD 283812	0.01 ± 0.11	2 ± 9
	0.07 ± 0.16	6 ± 7

Table 2.3: Differences in ground and space based polarimetric measurements (ΔDOP ... difference in the degree of polarization, $\Delta \eta$ ... difference in the angle of linear polarization)

The polarimetric measurements of the HST don't include an effect of the atmosphere on the polarization. Thus, the comparison of the space based and ground based measurements can help to assess an atmospheric influence in terms of penalties in receiver sensitivity:

- Depolarization: In Tab.(2.3) the biggest difference in the DOP is $\Delta DOP = 0.23\,\%$. That is, the totally polarized laser beam, which is transmitted through the atmosphere, experiences a depolarization of $0.23\,\%$. It is assumed that the total intensity of the laser beam, $\hat{I}$, remains the same when passing through the atmosphere. At the receiver the intensity of the polarized part of the laser beam is then $0.9977 \cdot \hat{I}$ and the intensity of the unpolarized part is $0.0023 \cdot \hat{I}$. Thus, after the PBS at the RX (see Section 1.5.1) one polarizer transmits $0.9977 \cdot \hat{I}$ plus $50\,\%$ of the unpolarized part (which is $11.5 \cdot 10^{-4} \cdot \hat{I}$) and the other polarizer transmits the other $50\,\%$ of the unpolarized part of the intensity. This corresponds to a deviation of $0.066\,°$ of the transmission axis of one polarizer from the ideal position and results in a negligible penalty in the receiver's sensitivity (see

Fig.(1.37)). The mean value of the DOP exhibit a maximum difference of $\Delta DOP = 0.07\,\%$. This is equivalent to a deviation of $0.02°$ and results also in a negligible penalty.

- Rotation of the angle of linear polarization: The change of η is equal to the deviation of the polarizers transmission axes in the RX from the incident polarized light (see Section 1.5.1). In Tab.(2.3) the biggest atmospheric effect is a deviation of $\Delta\eta = 13°$. This results in a penalty in RX sensitivity of $1.19\,\mathrm{dB}$ for a deviation of only one polarizer (see Fig.(1.37), adaptive threshold) and $2.49\,\mathrm{dB}$ for a deviation of both polarizers from the SOP of the incoming light (see Fig.(1.40), $\gamma/2 = 13°$), which would correspond to an attenuator. The mean value of η exhibits a maximum difference of $\Delta\eta = 6°$ and results in a penalty in the receiver's sensitivity of $0.27\,\mathrm{dB}$ for a deviation of only one polarizer (see Fig.(1.37), adaptive threshold) and about $0.73\,\mathrm{dB}$ for a deviation of both polarizers (see Fig.(1.40), $\gamma/2 = 6°$). According to the deviation of the mean value, the influence on the RX sensitivity by the rotation of η is negligible. But if there arises an effect on both orthogonal polarizations of the PolSK system, and the maximum deviation is $13°$, an attenuation is not negligible. However, an effect on both orthogonal polarizations which preserves the orthogonality can be compensated by adjusting the PBS in the receiver.

In Table (2.4) three other standard stars HD 155197, HD 147084, and HD 204827 are listed. In each case two polarimetric measurements at different observation places and different observation times are given. DOP and η are the mean values measured with a bandpass filter with a center wavelength of $540\,\mathrm{nm}$ [30]. The standard deviations of the measurements are also added in the list, which contain effects reported in [32].

Star	DOP [%]	η [°]	Year	Location	Source
HD 155197	4.32 ± 0.023	102.84 ± 0.15	2000	Tucson, Arizona (USA)	[33]
	4.38 ± 0.03	103.2	1988	La Serena (Chile)	[34]
HD 147084	4.17 ± 0.08	32.9	1988	La Serena (Chile)	[34]
	4.18 ± 0.02	32 ± 0.1	1981	Austin, Texas (USA)	[32]
HD 204827	5.36 ± 0.025	58.6	1990	Tucson, Arizona (USA)	[34]
	5.49 ± 0.02	59.3 ± 0.1	1981	Austin, Texas (USA)	[32]

Table 2.4: List of standard stars (DOP ... mean degree of polarization, η ... mean angle of linear polarization)

The differences between the two measurements of the standard stars are listed in Tab.(2.5). Because standard stars usually do not have an intrinsic variability in the polarization at all or rather have a very small negligible variability [29], it follows that the differences occur due to an effect of the atmosphere or an inaccuracy in the measurement. Observing the light at different places, the light is differently influenced by the atmosphere, because of the different ways it travels through it. Also two different observation times would lead to a varying atmospheric effect.

From Tab.(2.5) it can be seen that the atmospheric effects are very small and thus negligible:

- Depolarization: Within the three standard stars HD 204827 shows the biggest change in the degree of polarization, $\Delta DOP = 0.175\,\%$. Like in the itemization above, this depolarization corresponds to a deviation of $0.05°$ of the transmission axis of one polarizer from the ideal position and results in a negligible penalty in the receiver's sensitivity (see Fig.(1.37)). The mean value of the DOP exhibit a maximum difference of

Star	ΔDOP [%]	$\Delta\eta$ [°]
HD 155197	0.06 ± 0.053	0.36 ± 0.15
HD 147084	0.01 ± 0.1	0.9 ± 0.1
HD 204827	0.13 ± 0.045	0.7 ± 0.1

Table 2.5: Differences in standard stars (ΔDOP ... difference in the degree of polarization, $\Delta\eta$ ... difference in the angle of linear polarization)

$\Delta DOP = 0.13\,\%$. This is equivalent to a deviation of $0.037°$ and results also in a negligible penalty. The atmospheric effect of depolarization is negligible according to the measurements at different places and times presented in Tab.(2.4).

- Rotation of the angle of linear polarization: An attenuation due to the change of η is also small, HD 147084 shows a maximum shift of $\Delta\eta = 1°$. This results in a negligible penalty in RX sensitivity for a deviation of only one polarizer (see Fig.(1.37)) and in a penalty of $0.03\,$dB for a deviation of both polarizers from the SOP of the incoming light (see Fig.(1.40), $\gamma/2 = 1°$). The mean value of η exhibits a maximum difference of $\Delta\eta = 0.9°$ and results in a negligible penalty for a deviation of only one polarizer (see Fig.(1.37)) and in a penalty of $0.02\,$dB for a deviation of both polarizers (see Fig.(1.40), $\gamma/2 = 0.9°$). There occurs a negligible attenuation due to the rotation of linear polarization when standard stars are investigated on the Earth at different observation times and observation places.

A possible filtering effect introduced by the atmosphere can be assessed with the aid of two partially polarized standard stars which have two orthogonal linear polarizations. In Tab.(2.6) ground and space based measurements of the stars HD 283812 and CHA-DC-F7 are listed [31]. They have almost orthogonal polarizations, HD 283812 has an angle of about $\eta \approx 35°$ and CHA-DC-F7 has an angle of about $\eta \approx 35° + 90° = 125°$. Table (2.6) shows the measured values with the largest difference before and after the atmosphere in order to assess the worst case.

	ground based		space based	
Star	DOP [%]	η [°]	DOP [%]	η [°]
HD 283812	1.31 ± 0.07	35 ± 2	1.38 ± 0.09	29 ± 5
CHA-DC-F7	1.19 ± 0.01	126 ± 4	1.24 ± 0.03	128 ± 7

Table 2.6: Polarimetric measurements on Earth and on HST of the stars HD 283812 and CHA-DC-F7 (DOP ... mean degree of polarization, η ... mean angle of linear polarization) [31]

It can be seen in Tab.(2.7) that the mean degree of polarization of both stars exhibit almost the same differences in ground and space based measurements. Only the standard deviations show a bigger difference. From this I conclude that a filtering effect introduced by the atmosphere is negligible. Both orthogonal polarizations are treated equally by the atmosphere.

From the four polarimetric measurements presented above I conclude, that the depolarization by the atmosphere is very small and thus negligible. This conclusion coincide with the statements in [35]. Moreover, there occur no birefringent effect in the atmosphere. A

Star	ΔDOP [%]
HD 283812	0.07 ± 0.16
CHA-DC-F7	0.05 ± 0.04

Table 2.7: Differences in ground and space based polarimetric measurements (ΔDOP ... difference in the degree of polarization)

rotation of the angle of linear polarization is rather small and produces only in the worst case a considerable attenuation. A filtering effect in the atmosphere is also negligible. Thus, the polarization is the most stable characteristic of a laser beam while propagating through the atmosphere, this is also stated in [36].

Chapter 3

Practical Implementation of the BPolSK Receiver

3.1 Introduction

For the practical implementation of an BPolSK receiver as presented in Section 1.4.4, the appropriate electronic devices have to be found. This is done by a market study.

High-sensitivity receivers, which use PIN photodiodes as detectors, are realized in practice using optical preamplification. The two adequate configurations for real BPolSK RX structures can be seen in Fig.(3.1) and Fig.(3.2).
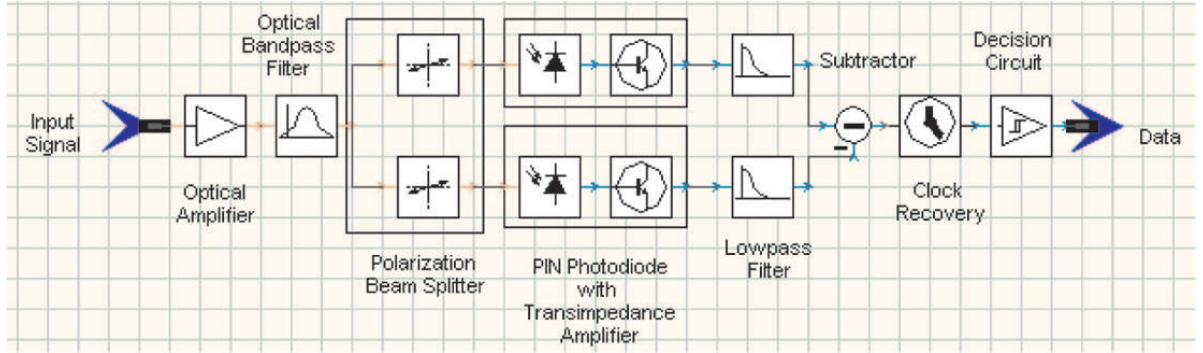
Figure 3.1: Realization 1 of BPolSK receiver with optical preamplification

In Fig.(3.1) the BPolSK receiver with optical amplification is realized with a polarization beam splitter, two PIN photodiodes with transimpedance amplifiers (one in each branch), and a subtractor. In Fig.(3.2) the BPolSK receiver is realized with an PBS, two PIN photodiodes, and a single differential amplifier.

3.2 Polarization beam splitter

An ideal PBS splits the incoming light into two orthogonal polarized parts, i.e., into x-polarized and $(x + 90°)$-polarized light. The same effect can be achieved with two polarizers oriented orthogonal to each other. The x-polarized light is then passed through the upper branch, while the $(x + 90°)$-polarized light is transmitted through the lower branch of the BPolSK RX.
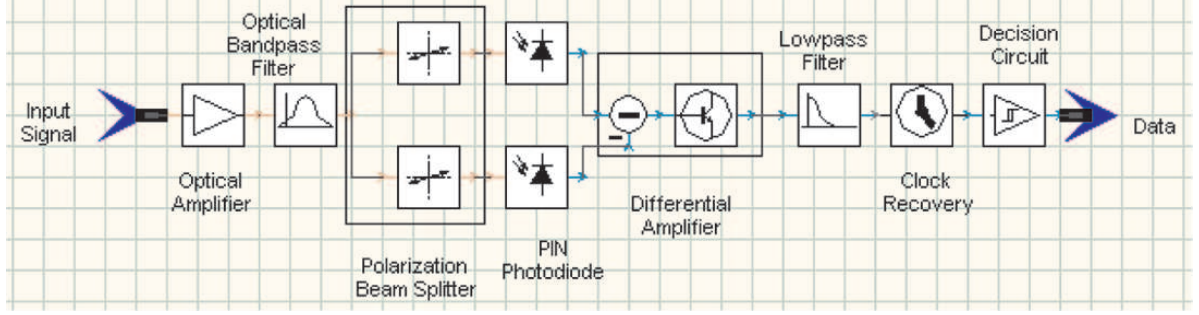
Figure 3.2: Realization 2 of BPolSK receiver with optical preamplification

Polarization beam splitters can be realized based on optical fibers or based on bulk optics.

3.2.1 Polarization beam splitter based on fiber optics

An PBS realization based on fibers is presented in this section.

Fiber optic components exhibit birefringence due to the non-perfect cylinder geometry. The orientation and the strength of the birefringence change statistically over long optical fibers. Thus, an optical fiber can be modeled as a concatenation of birefringent elements [20]. There always exist an orthogonal pair of polarization states at the output of a birefringent concatenation which are stationary in the first order in frequency. These two states are called *principle states of polarization* (PSP). That is, if the input polarization is aligned to an PSP of the fiber, then the output polarization state of the fiber is the same as the input state [12]. In an PBS based on fiber optics the incident polarization is aligned to one PSP of the fiber, the orthogonal polarization is therefore aligned to the second PSP.

There exists a differential delay between the signals launched along the PSP. This delay occurs due to different phase velocities as a consequence of different refractive indices in the PSP. With the Maxwell relation (see Section 1.2.1) the phase velocity can be expressed in terms of the refractive index [15],

$$c = \frac{1}{\sqrt{\varepsilon\mu}} = \frac{1}{\sqrt{\varepsilon_0\mu_0}} \cdot \frac{1}{\sqrt{\varepsilon_r\mu_r}} = \frac{c_0}{n}, \tag{3.1}$$

where c_0 is the velocity of light in vacuum, ε_r, and μ_r denote the relative electric permittivity and the relative magnetic permeability. The refractive index n is defined as $n = \sqrt{\varepsilon_r\mu_r}$. The aforementioned differential delay causes *polarization mode dispersion* (PMD) in optical fibers [20][12].

An example of a polarization beam splitter based on fiber optics is the device PBC/S-001, which is schematically depicted in Fig.(3.3). The parameters of this device can be seen in Tab.(3.1).

The PBC/S-001 provides an extinction ratio of $22\,\text{dB}$. The extinction ratio is defined as the optical power in one PSP, P_x, relative to the optical power in the orthogonal PSP, $P_{x+90°}$, (see Fig.(3.4)). That is, when the incident light is x-polarized, the x-polarizer transmits the whole optical input power P, while the $(x + 90°)$-polarizer passes through $0.0063 \cdot P$ of the optical power. This corresponds to a deviation of $0.4°$ of the transmission axis of the $(x+90°)$-polarizer from the ideal position. Such non-idealities were presented in Section 1.5. An offset
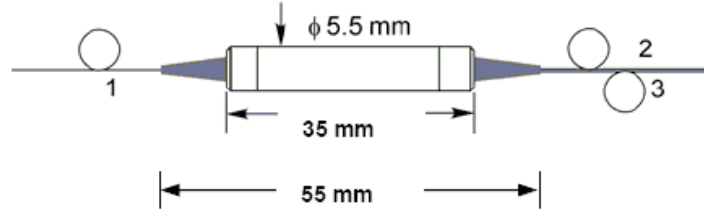
Figure 3.3: Fiber based polarization beam splitter [37]

	PBC/S-001
Fiber type	Polarization maintaining fiber
Available center wavelengths	1310 nm, 1480 nm, 1550 nm
Operating bandwidth	±40 nm
Size	Φ 5.5 mm x 35 mm
Extinction ratio (PBS only)	22 dB
Insertion loss	0.4 dB typical, 0.6 dB maximum
Return loss	50 dB
Optical power handling	500 mW
Operating temperature	−5 ° to 70 °

Table 3.1: Parameters of fiber based polarization beam combiner/splitter (Φ ... diameter) [37]

angle of the transmission axis of one polarizer of $\gamma = 0.4\,°$ results in a negligible penalty in the receiver's sensitivity, which is depicted in Fig.(1.37).
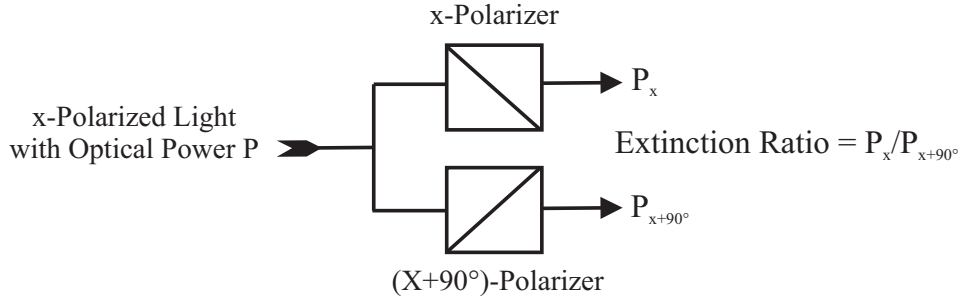
Figure 3.4: Explanation of the extinction ratio of an PBS (P_x ... optical power in one PSP, $P_{x+90°}$ ... optical power in the orthogonal PSP)

The insertion loss of the optic device PBC/S-001 of maximal 0.6 dB can be neglected. It doesn't affect the BPolSK receiver performance, since the PBS is placed behind the optical preamplifier and ASE beat noise limits the RX performance.

The device's return loss of 50 dB indicates that the reflected power from that device is always 50 dB lower than the power transmitted. That is, for an input power of −40 dBm the reflected portion is −90 dBm. Because of optical preamplification a return loss of 50 dB has no limiting effect on the receiver's performance.

The effect of PMD in the optical fibers can be neglected because of the low bit rate $R = 1$ Gbit/s and the short length of the fibers [20].

Using an optical amplifier in front of the PBS the transmitted light is already coupled into the fiber. Thus, an PBS based on fiber optics is ideal for BPolSK systems with optical preamplification.

3.2.2 Polarization beam splitter based on bulk optics

An PBS realization based on bulk optics is presented in this section.

An PBS cube is based on two transparent triangular prisms of the same material, which are cemented together (see Fig.(3.5)). The incident light reflects from the interface between these two materials. The reflectivity is different for light polarized in the plane of incidence ($(x+90°)$-polarization, labeled in Fig.(3.5)) and light polarized perpendicular to it (x-polarized light). When the incident light and the interface between the two prisms include an angle called Brewster's angle, no light polarized perpendicular to the plane of incidence (x-polarized light) is reflected from the surface, thus all reflected light must be $(x + 90°)$-polarized [14].

The parameters of an example PBS device based on bulk optics, PBS3, are presented in Tab.(3.2).
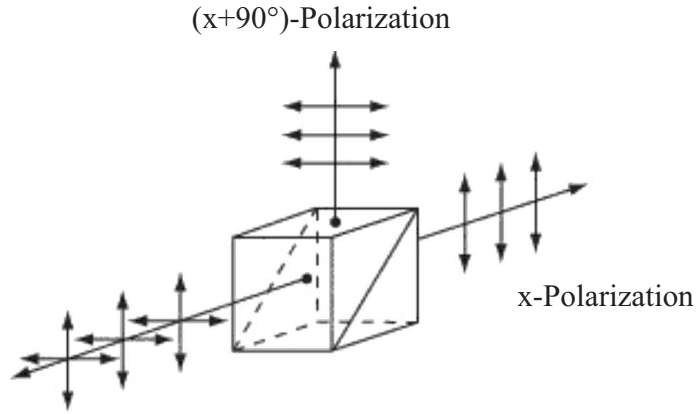
Figure 3.5: Polarizing beam splitter cube [38]

	PBS3
Substrate material	BK7 glass
Wavelength range	$1525 - 1610\,\text{nm}$
Size	$3\,\text{mm x }3\,\text{mm x }3\,\text{mm}$
Dimensional tolerance	$\pm 0.25\,\text{mm}$
Extinction ratio	$30\,\text{dB}$
Transmission efficiency	$T_x > 95\,\%$
Reflection efficiency	$R_{x+90°} > 99.9\,\%$
Reflected beam deviation	$90 \pm 0.083\,°$
Transmitted beam deviation	$< 0.083\,°$
Antireflection coating	$R < 0.25\,\%$
Clear aperture	$> 85\,\%$ of center diameter
Damage threshold	$100\,\text{W/cm}^2$ CW at $515\,\text{nm}$

Table 3.2: Polarizing beam splitter cube (T ... transmission, R ... reflection) [38]

The device provides an extinction ratio of $30\,$dB. Like in the previous section this is equivalent to a deviation of the transmission axis of one polarizer of $\gamma = 0.06\,°$. Such a small offset angle doesn't corrupt the receiver's performance, as seen in Fig.(1.37).

The transmission efficiency of x-polarized light is $T_x > 95\,\%$. The reflection efficiency for $(x+90\,°)$-polarized light is $R_{x+90°} > 99.9\,\%$. This results in an imbalance of transmitted powers in both polarization directions. This imbalance is equivalent to ideal transmission efficiencies of the polarizers plus an imbalance in the photodiodes responsivities. The loss in optical power for $(x + 90\,°)$-polarized light is neglected ($R_{x+90°} \approx 100\,\%$). The $5\,\%$ loss in optical power for x-polarized light is equivalent to $95\,\%$ of the original photodiode's responsivity, e.g., $S_B = 0.95 \cdot S_A = 0.9975\,$A/W (see Section 1.5.2). According to Eqn.(1.49) this results in a responsivity imbalance of $\beta = 0.03$ with $S_A = 1.05\,$A/W. An imbalance of $\beta = 0.03$ results in negligible penalty in the receiver performance, as shown in Fig.(1.43).

If the direction of polarization of the incident light is not perfectly aligned to the polarization beam splitter cube there will also be a penalty in the receiver's sensitivity. The orthogonality of the polarizers is maintained. In Fig.(1.41) the penalty in the receiver's performance due to such an offset angle of the transmission axes of the polarizers is plotted (see Section 1.5.1).

An PBS based on bulk optics is not ideal for an BPolSK RX with optical preamplification, because after the amplifier the light is already coupled into the fiber. However, the polarizing beam splitter cube can be used within an RX without optical preamplification, e.g, when using an *avalanche photodiode* (APD) [20].

3.3   PIN photodiode with transimpedance amplifier

The parameters of the PIN photodiode with an TIA which I used for my simulations are taken from *Electro-Optics Technology's* device ET-3000A and shown in Tab.(3.3).

	ET-3000A
Detector type	PIN
Detector material	InGaAs
Spectral range	$900 - 1700\,$nm
Responsivity	$S = 1.05\,$A/W @ $1550\,$nm
Frequency response	$30\,$kHz-$1.5\,$GHz
Dark current	$I_D < 1\,$nA
Thermal noise spectral density	$N_{th} =< 31.5\,$pA$/\sqrt{Hz}$
Transimpedance	$Z = 1000\,\Omega$
Gain	$G_{TIA} = 26\,$dB

Table 3.3: ET-3000A PIN photodetector with TIA [39]

3.4   Subtractor

The subtractor in Fig.(3.1), which subtracts the electrical signals from the lower and upper branch of the BPolSK RX, can be realized with an unity gain differential amplifier. Examples of appropriate devices are given in Tab.(3.4).

	TSH330 [40]	*THS3201* [41]	*LMH6703* [42]
Gain	1	1	1
$-3\,\mathrm{dB}\,Bandwidth$	$1500\,\mathrm{MHz}$	$1300\,\mathrm{MHz}$	$1800\,\mathrm{MHz}$
Supply voltage	$\pm2.5\,\mathrm{V}$	$\pm5\,\mathrm{V}$	$\pm5\,\mathrm{V}$
Ambient temperature	$25\,^{\circ}\mathrm{C}$	$25\,^{\circ}\mathrm{C}$	$25\,^{\circ}\mathrm{C}$
Equivalent input noise current (+)	$22\,\mathrm{pA}/\sqrt{Hz}$	$13.4\,\mathrm{pA}/\sqrt{Hz}$	$3\,\mathrm{pA}/\sqrt{Hz}$
Equivalent input noise current (-)	$16\,\mathrm{pA}/\sqrt{Hz}$	$20\,\mathrm{pA}/\sqrt{Hz}$	$18.5\,\mathrm{pA}/\sqrt{Hz}$

Table 3.4: Unity gain differential amplifiers

3.5   PIN photodiode

In realizations like in Fig.(3.2) only an PIN photodiode without TIA is needed. An appropriate device is the ET-3010. Its parameters are presented in Tab.(3.5).

	ET-3010
Detector type	PIN
Detector material	InGaAs
Spectral range	$900 - 1700\,\mathrm{nm}$
Responsivity	$S = 0.95\,\mathrm{A/W}$ @ $1550\,\mathrm{nm}$
Cutoff frequency	$> 1.5\,\mathrm{GHz}$
Dark current	$I_D < 1\,\mathrm{nA}$
Thermal noise spectral density	$N_{th} < 0.095\,\mathrm{pA}/\sqrt{Hz}$

Table 3.5: ET-3010 biased PIN photodetector [43]

3.6   Differential amplifier

The differential amplifier as used in the setup of Fig.(3.2) can be implemented with an unity gain differential amplifier (see Tab.(3.4)). There is no need for a higher gain because the receiver's performance is determined by the optical preamplifier.

3.7   Polarization diversity detector

There is another possibility to implement a receiver like in Fig.(3.2), i.e., using a *polarization diversity detector* (PDD). It detects simultaneously the power of two orthogonal polarization components. A pigtailed PBS coupled with two photodetectors can be used for such applications [44]. Although the device PDD-001 from *General Photonics* does not have the appropriate bit rate, I will present it's parameters for demonstration. The parameters can be found in Tab.(3.6).

	PDD-001
Bit rate	$R = 50\,\mathrm{MHz}$
Detector sensitivity	$S = 0.8\,\mathrm{A/W}$ @ 1550 nm for both photodiodes
Center wavelength	1310 nm, 1550 nm
Wavelength range	$\pm 75\,\mathrm{nm}$
Extinction ratio	$> 40\,\mathrm{dB}$
Minimum return loss	55 dB
Fiber	Polarization-maintaining
Maximum optical power	20 mW
Dark current	$I_D < 20\,\mathrm{nA}$ at 5 V bias at 23 °C
Thermal noise spectral density	$N_{th} = 6.6 \cdot 10^{-15}\,\mathrm{A}/\sqrt{Hz}$

Table 3.6: Polarization diversity detector [44]

Chapter 4

Summary

My investigations of polarization modulation in optical free space communications through the atmosphere show the following advantages in comparison with intensity modulated systems:

- PolSK features a constant envelope of the transmitted optical power, which makes it especially attractive for peak power limited systems (see Section 1.2.2).

- PolSK clearly outperforms OOK systems in terms of peak optical power by about $3\,\mathrm{dB}$ (see Section 1.3.4 and 1.4.4).

- The atmospheric influence on the polarization of a laser beam is negligible (see Section 2.3).

- For deviations of the polarization from the PBS transmission axes which preserve the orthogonality or for equal offset angles in both directions even that the orthogonality is not preserved, there is no difference in the PolSK RX performance when using an absolute threshold at $0\,\mathrm{A}$ or using an adaptive threshold (see Fig.(1.40)).

- If there occur non-idealities in the optical or electrical wires in the PolSK system, the performance is the same for absolute and adaptive thresholding (see Section 1.5.3).

- Non-idealities in the practical realization of an PBS do not effect the receivers performance (see Section 3.2).

The following disadvantages have been found:

- The complexity in the PolSK system is higher than the complexity of the OOK system (see Section 1.3 and 1.4).

Polarization and intensity modulated systems are equal in the following points:

- The performance of PolSK and OOK systems is about the same in average power limited systems.

- In the most cases when non-idealities arise in the PolSK RX adaptive thresholding reaches a better performance than absolute thresholding (see Section 1.5).

Although the complexity of an PolSK system is higher than that of an OOK system, the advantages of PolSK in peak power limited systems such as the constant envelope of the transmit signal and the $3\,\mathrm{dB}$ sensitivity gain predominate the disadvantages. Thus, PolSK is a promising candidate to replace OOK as modulation system in optical free communications through the atmosphere.

Appendices

Appendix A

Simulation parameters in VPItransmissionMaker

In Appendix A I want to deliver insight to the most important parameters for the correct and efficient operation of the simulations in VPItransmissionMaker. These global parameters determine the signal conversion from continuous time to discrete time signals for digital computations, e.g., they determine the temporal and spectral resolution of the signals. Moreover, I specify the signal representation, the form of data which is passed between the single modules of a simulation schematic.

A.1 Discrete conversion

The efficient representation of real-world signals as data in a computer model is an important topic in a simulation software like in VPItransmissionMaker. If the signal representations have unnecessary detail, the model will be computationally inefficient. If the representations are too abstract, the model will fail to predict important phenomena, or give inaccurate results [17].

Generally, the complex envelope of lightwaves can be described by a waveform which is continuous in time and frequency. This representation has to be approximated, since continuous signals cannot be handled by digital computation, which is discrete in nature [17].

Converting a continuous time domain description into a discrete one, means that the waveform is only considered at discrete points on the continuous time axis. These points are equally spaced in time. The spacing of adjacent points is called sampling interval, Δt. The rate at which the time samples are gathered is called the **sample rate**, denoted by f_s. The sample rate is related to the sampling interval by $f_s = 1/\Delta t$ (see Fig.(A.1)) [17].

The imposition of regular sampling does not itself cause an approximation, apart from limiting the bandwidth that can be simulated. The simulation bandwidth is equivalent to the sample rate (see Fig.(A.1)). A wide simulation bandwidth requires a short sampling interval, which is obtained by choosing to have many samples per bit, for a given bit rate, R [17].

The conversion from the discrete time to the discrete frequency domains is performed using an efficient implementation of the *discrete fourier transform* (DFT), namely the *fast fourier transform* (FFT). Sampling in the time domain representation leads to a periodical expansion of the frequency response. That is, the frequency spectrum becomes periodic with a repetition equal to the sample rate. A real continuous time waveform can be converted to a sampled complex baseband form without loss of information, if the sample rate is at least the maximum
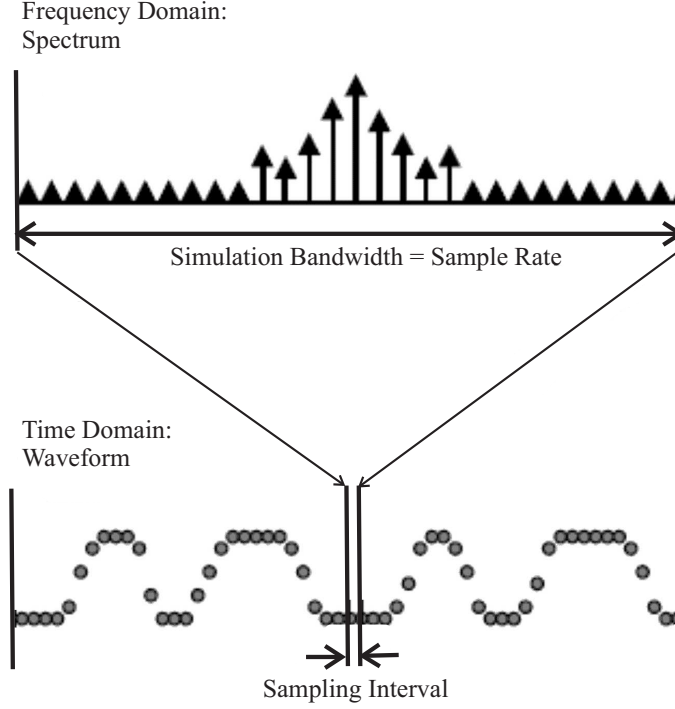
Figure A.1: Illustration of the inverse relationship between the sampling interval and the sample rate, which is equivalent to the simulation bandwidth [17]

bandwidth, B_{max}, of the continuous time waveform, $f_s \geq B_{max}$. Otherwise, aliasing errors occur, which result from an overlap of the spectra [17].

Similar to time domain sampling, one can imagine the process of sampling in the frequency domain. This is because a signal which is represented over a limited **time window** will have a limited spectral resolution, equal to the inverse of the window duration (see Fig.(A.2)).

For there to be no leakage between the frequency points during the Fourier transformation, which would reduce the accuracy of a spectrum, particularly close to a lasing peak, the time waveform has to be periodic within the time window. In this case, the transformation between time and frequency domains is exact, and can be performed without approximation [17].

For digital transmission, the length of the simulated time window can be written in terms of the number of bits, N_B, multiplied by the bit duration, T_B, which is the inverse of the bit rate [17].

A.2   Block mode signal representation

The signal representation defines in what form the data is passed between the modules of a simulation schematic (see, e.g., Fig.(1.18)). In VPItransmissionMaker the data exchange between the individual modules can be organized in blocks, that is, vectors representing the signals in the time or frequency domains, or by transmitting single samples [17]. In my simulations I used the block mode signal representation (see Tab.(1.1)) because some VPI modules I used (e.g., polarization modulator, BER estimator, etc.) work only in block mode. In this mode the simulation usually progresses from transmitter to receiver, one module at a
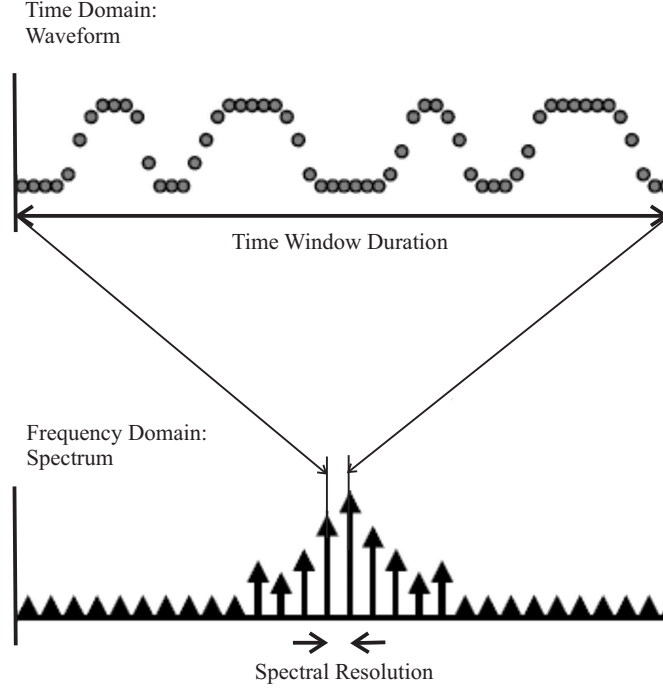
Figure A.2: Illustration of the inverse relationship between the time window duration and the spectral resolution [17]

time.

A.3 Global parameters

The global parameters **bit rate**, **sample rate**, and **time window** are common to all modules in a simulation schematic. Their values are important for the correct and efficient operation of the simulator [17].

A precise definition of these parameters is given in [17]:

- The global parameter **bit rate** is equal to the bit rate of the PRBS module, e.g., $R = 1\,\mathrm{Gbit/s}$ (see Tab.(1.1)).

- The **sample rate** is used to set the simulation bandwidth of the system (see Appendix A.1). It is usually set to a value of $(2^m * R)$ [Hz], where m is an integer. In my simulations I set the sample rate to $f_s = 16 * R$, i.e., a bit is represented by 16 samples.

- The duration of each block of data (see Appendix A.2) is determined by the value **time window** (see Appendix A.1). Each run of a simulation will simulate this amount of time. Usually the parameter is set to a value of $(2^l/R)$ [s], where l is an integer. This sets the resolution of the spectral visualizers and the accuracy of the BER estimation depends critically on the number of bits simulated. When the BER estimator uses Gaussian noise statistics (see Appendix B.2.1) a time window of $(2^{13}/R)$ [s] (2^{13} bits per simulation) is necessary to reach an accuracy in RX sensitivity of $0.05\,\mathrm{dB}$. When the BER estimator

uses χ^2 noise statistics a time window of $(2^{17}/R)$ [s] is necessary to reach an accuracy of 0.1 dB.

Appendix B

VPItransmissionMaker modules

In Appendix B I give some additionally information about those modules in VPItransmission-Maker which I used for my simulations.

B.1 Pseudo random bit sequence module

In Section 1.2.2 I introduced the parameters of a pseudo random bit sequence generator (see Tab.(1.1)), which I used in my simulations to model an information source for digital transmission. In VPItransmissionMaker the PRBS module provides a number of different types of bit streams. I used the **PRBS** type, which produces a sequence of $N_B = 2^l$ bits, which is equivalent to the specified time window multiplied by the bit rate (see Appendix A.3) [18].

B.2 BER estimation modules

The bit error rate estimation modules I used in my simulations (in Chapter 1) are presented in this section.

In order to estimate the BER, each BER estimation module needs to know the sequence of bits that was originally transmitted. This enables it to associate each received sample with a specific type of symbol, which will be either a logical '1' or a logical '0'. That's why each transmitter within VPItransmissionMaker generates a logical channel along with the 'physical' channel that represents the optical signal. The transmitted bit sequence is then attached to the logical channel [18]. The name of the logical channel is specified using the parameter **channel label**. In my work the channel label is defined in the NRZ coder (channel label = c1) of the PolSK and the OOK receiver (see Fig.(1.10) and Fig.(1.17)).

A clock recovery module is situated prior to the BER estimation module (see, e.g., Fig.(1.18)). The reason for this is that propagation effects and others sources of delay will result in the signal being shifted within the time window. Thus at the end of the simulation, the signal waveform with the sampled band is no longer correctly aligned with the bits in the logical channel. The clock recovery module in VPI realigns the signal with the bit sequence, so that the BER estimator associates the correct transmitted symbol with each sample in the received signal [18].

As I mentioned in Section 1.3.2 the BER estimator defines the sample time and the decision threshold. If the parameter **sample type** in the BER estimator module is set to *optimum* then the BER estimator automatically determines the sampling time at which the BER is

minimum. This is done by computing the BER for all possible sampling times across the bit period and selecting the sample time which produces the lowest BER result [18]. If the parameter **threshold type** is set to *optimum*, then the BER estimator determines the decision threshold for which the BER is minimum. The threshold is said to be adaptive (see Section 1.5). This parameter can also be set to *absolute*, then the decision threshold is set directly by the **threshold** parameter in the module [18]. This is done in Section 1.5, where I used an absolute threshold of $D = 0\,\mathrm{A}$ in some simulations.

B.2.1 BER estimator

In Section 1.3 I presented different receiver structures without optical preamplification. The dominant source of noise is the thermal noise in the electronics of the receiver (see Section 1.3.1). Thermal noise is Gaussian in nature, thus, the noise statistics are Gaussian (i.e., distributed according to the so-called Normal distribution).

In Section 1.4 I presented receiver structures with optical preamplification. The ASE beat noise terms dominate all other noise sources and the noise statistics after square law detection and low pass filtering are χ^2 distributed (see Section 1.4.1).

The bit error ratio in this systems can now be calculated analytically as [18]

$$BER = P_0 P_{0|1} + P_1 P_{1|0},$$

this follows from the law of total probability [10]. P_1 is the probability of receiving a '1' bit, P_0 is the probability of receiving a '0' bit, $P_{0|1}$ is the conditional error probability of deciding that a received bit is '0' when actually a '1' was sent, and $P_{1|0}$ is the conditional probability of a detected '1' when a '0' was sent [18]. In my simulations I used the same probabilities of receiving a '1' or a '0' bit, i.e., $P_1 = P_0 = 0.5$ (see Tab.(1.1)).

To calculate the conditional error probabilities, $P_{0|1}$ and $P_{1|0}$, the probability density functions $f_1(x)$ and $f_0(x)$ of the '1' and the '0' signal levels must be known, as well as the decision threshold, D. The conditional error probabilities are then obtained by integrating the density functions from the decision threshold according to [18]

$$
\begin{aligned}
P_{0|1} &= \int_{-\infty}^{D} f_1(x)dx, \\
P_{1|0} &= \int_{D}^{\infty} f_0(x)dx.
\end{aligned}
$$

The exact method used to obtain the density functions $f_1(x)$ and $f_0(x)$ depends upon the noise statistics used, i.e. either Gaussian or χ^2 statistics, as described in the following sections.

Gaussian noise statistics

A Gaussian probability density function is fully characterized by two parameters, its mean and its variance. The BER estimator module assuming Gaussian noise statistics uses a two-step process to estimate the BER [18]:

1. The means, μ_k, and variances, σ_k^2, of the received '1' and '0' bits ($k = 0{,}1$) are estimated using a sample estimator. They are determined from the statistics of the input signal at the BER estimator.

2. The dark current, I_D, is then added to the computed means, μ_k, and the thermal noise variance, σ_{th}^2, and shot noise variance, σ_{sh}^2, are added to the computed variances, σ_k^2. The probability density functions, $f_1(x)$ and $f_0(x)$, and the corresponding error probabilities, $P_{0|1}$ and $P_{1|0}$, are then assumed to be those of Gaussian distributions with the total mean and variance values calculated.

The thermal noise variance is given by [18]

$$\sigma_{th}^2 = N_{th}^2 B_e,$$

where N_{th} is the noise spectral density, and B_e is the electrical noise bandwidth equivalent to the $3\,\mathrm{dB}$ bandwidth of the electrical low pass filter of the receiver (see Tab.(1.2)). The shot noise variance for an PIN photodiode is calculated according to [18]

$$\sigma_{sh}^2 = 2e(\mu_k + I_D)B_e,$$

where $e = 1.6 \cdot 10^{-19}\,\mathrm{C}$ is the electron charge.

Parameter	Value
Estimation method	Gaussian
Sample type	Optimum
Threshold type	Optimum/Absolute
Threshold	$D = 0\,\mathrm{A}$
Dark current	$I_D = 0\,\mathrm{A}$
Include shot noise	No
Thermal noise spectral density	$N_{th} = 0\,\mathrm{pA}/\sqrt{Hz}$
Electrical noise bandwidth	$B_e = 0.75\,\mathrm{GHz}$
Channel label	c1

Table B.1: Parameters of the BER estimation module for Gaussian noise statistics as used for simulations

In Tab.(B.1) the parameters of the BER estimation module for Gaussian noise statistics as used for my simulations are listed. The parameters dark current and thermal noise spectral density are set to zero because they are already specified in the PIN photodiode with TIA.

Chi-square noise statistics

The general non-central χ^2 probability density function can be fully described by three parameters: the non-centrality parameter, the number of degrees of freedom, and a scaling factor. For simplicity, it is assumed that the input signal of the BER estimation module does not contain any additive post-detection Gaussian noise (thermal and shot noise). To achieve this, the parameters thermal noise, dark current, and shot noise should be specified in the BER estimator and set to zero in the PIN photodiode and the TIA [18]. In my simulations I found no difference in RX sensitivities between a specification of these parameters in the BER estimator or in the PIN photodiode and the TIA.

The BER in receivers with χ^2 noise statistics is estimated by a two-step process [18]:

1. The three parameters of the χ^2 distribution are estimated by performing a statistical analysis of the input signal samples. A separate analysis is performed for '1' and '0' bits in the received bit sequence.

64

2. The probability density functions, $f_1(x)$ and $f_0(x)$, and the corresponding error probabilities, $P_{0|1}$ and $P_{1|0}$, are then computed including the effect of post-detection noise processes, using numerical methods described by Marcuse [45].

The BER estimation module uses several numerical approximations when performing the BER calculation for χ^2 noise statistics. These approximations are extremely accurate in most cases and significantly improve the speed and efficiency of the algorithms. However, they are not valid at very high values of the BER, on the order of 10^{-2} and above. This limitation is not very restrictive in practice, because such high values of BERs are in any case unacceptable in a real system [18].

It is necessary to simulate a larger number of bits when using χ^2 noise statistics than when using Gaussian noise statistics, in order to obtain results that do not exhibit excessive statistical variation (see Appendix A.3) [18].

Parameter	Value
Estimation method	Chi2
Sample type	Optimum
Threshold type	Optimum/Absolute
Threshold	$D = 0\,\text{A}$
Dark current	$I_D = 1\,\text{nA}$
Include shot noise	Yes
Thermal noise spectral density	$N_{th} = 31.5\,\text{pA}/\sqrt{Hz}$
Electrical noise bandwidth	$B_e = 0.75\,\text{GHz}$
Channel label	c1

Table B.2: Parameters of the BER estimation module for χ^2 noise statistics as used for simulations

In Tab.(B.2) the parameters of the BER estimation module for χ^2 noise statistics as used in my simulations are listed.

B.2.2 Balanced detection BER estimator

In Section 1.4.4 I presented a balanced PolSK system using a receiver with optical preamplification. An BER estimation module designed for a balanced receiver is used. The signal samples at the inputs of the balanced detection BER module are divided into two groups, one corresponding to the detection of optical signals mixed with noise, and another corresponding to the detection of noise only. Each of these groups of samples is fitted by a noncentral χ^2 distribution. The fitted parameters of the distributions are used in order to construct the characteristic function of the resulting signal [18]. The characteristic function is the expectation value, $E[\cdot]$, of $\exp(j\omega O)$ [26],

$$\Phi(\omega) = E[\exp(j\omega O)] = \int_{-\infty}^{\infty} f_O(o)\exp(j\omega o)do,$$

where O is a random variable, o is its integration variable, and $f_O(o)$ is its PDF. If the two inputs at the BER estimator are statistically independent, which is fulfilled, then the resulting characteristic function in the BER estimation module is the product of both characteristic functions [26].

As mentioned in the previous section, the χ^2 assumption on signal statistics is valid only when additive optical noise is the only noise source. Therefore in order not to invalidate the results of the PDF fitting, dark current, thermal noise, and shot noise of both PIN photodiodes with TIAs should be set zero. These quantities instead should be specified by the parameters **dark current**, **thermal noise**, and **include shot noise** in the balanced detection BER module. This implies that these quantities are identical for both detectors [18]. In my simulations there is no difference in the RX sensitivity, when the specification of the post-detection noise parameters is done in the PIN photodiodes with TIAs or if it is done in the balanced detection BER module.

A Gaussian assumption is used on thermal and shot noise statistics, the parameters of the Gaussian distribution are used to construct the characteristic function of the post-detection noise.

The characteristic functions of the detected optical signal with beating noise and the receiver's post-detection noise are combined together to produce the total characteristic function of the detected signal. The BER is calculated from this characteristic function by the saddle point approximation method [46].

Parameter	Value
Optical filter bandwidth	$B_o = 1.6\,\text{GHz}$
Sample type	Optimum
Threshold type	Optimum/Absolute
Threshold	$D = 0\,\text{A}$
Dark current	$I_D = 1\,\text{nA}$
Include shot noise	Yes
Thermal noise spectral density	$N_{th} = 31.5\,\text{pA}/\sqrt{Hz}$
Electrical noise bandwidth	$B_e = 0.75\,\text{GHz}$
Channel label	c1

Table B.3: Parameters of the balanced detection BER estimation module as used for simulations

In Tab.(B.3) the parameters of the balanced detection BER estimation module I used in my simulations are stated.

B.3   Optical amplifier module

The optical amplifier module I used in my simulations in Chapter 1 is an amplifier model with fixed gain shape. It can act as a gain-controlled, power-controlled, or saturable amplifier. These modes can be selected via the **amplifier type** parameter [18]. I chose a gain-controlled amplifier type (see Tab.(1.5)). The amplifier module consists of an ideal amplifying unit characterized by a gain, G, according to

$$\vec{E}_{out}(t) = \vec{E}_{in}(t) \cdot \sqrt{G},$$

where $\vec{E}_{in}(t)$ is the electrical field input vector and $\vec{E}_{out}(t)$ is the electrical field output vector (see Fig.(B.1)). In gain-controlled mode the pump power is variable and the port to port gain of the amplifier, G, is defined differently for low and high input powers. At low input powers the amplifier provides a power-independent gain, $G = 39\,\text{dB}$. This small-signal gain is frequency-independent. At high input powers, the amplifier's output power (averaged over one block)

will be limited, as in a real device, by setting a maximum output power, $P_{out(max)} = 14.5\,\text{dBm}$. Additionally, the amplifier corrupts the output signal, $\vec{E}_{out}$, by ASE noise (see Fig.(B.1)). The
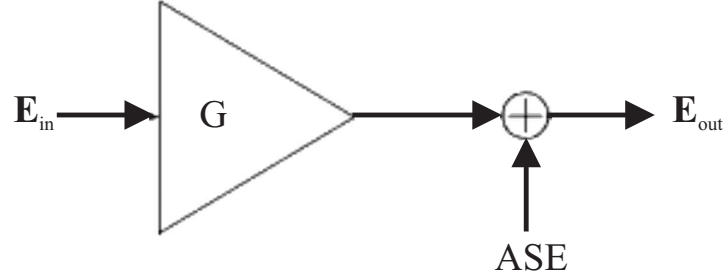
Figure B.1: Optical amplifier in the gain-controlled mode ($\mathbf{E}_{in}$ ... electrical field input vector, $\mathbf{E}_{out}$ ... electrical field output vector, G ... gain, and ASE ... amplified spontaneous emission noise) [18]

resulting noise figure, $F = 3.8\,\text{dB}$, is related to the single sided spectral noise density, N_{ASE}, via the spontaneous emission factor, n_{sp} (see Eqn.(1.40) and Eqn.(1.39)).

Appendix C

Abbreviations, constants, and symbols

C.1   List of abbreviations

AM	amplitude modulator
APD	avalanche photodiode
ASE	amplified spontaneous emission
ASK	amplitude shift keying
BER	bit error ratio
BPolSK	balanced polarization shift keying
CW	continuous wave
DFT	discrete fourier transform
DOP	degree of polarization
DPSK	differential phase shift keying
EDFA	Erbium-doped fiber amplifier
ESA	European Space Agency
FFT	fast fourier transform
FSK	frequency shift keying
HST	Hubble space telescope
InGaAs	Indium Gallium Arsenide
LHC	left-hand circular
MCF	mutual coherence function
NRZ	non return to zero
OOK	on-off keying
PBC	polarization beam combiner
PBS	polarization beam splitter
PDD	polarization diversity detector
PDF	probability density function
PIN	p-type, intrinsic, n-type
PM	phase modulator
PMD	polarization mode dispersion
PolM	polarization modulator
PolSK	polarization shift keying

ppb	photons per bit
PRBS	pseudo random bit sequence
PSK	phase shift keying
PSP	principal state of polarization
RHC	right-hand circular
RIP	receiver input power
RX	receiver
SOP	state of polarization
SPolSK	single polarization shift keying
TIA	transimpedance amplifier
TX	transmitter

C.2 List of physical and mathematical constants

$c_0 = 2.9979 \cdot 10^8$ m/s	velocity of light in vacuum
$e = 1.602 \cdot 10^{-19}$ As	charge of a single electron
$h = 6.6262 \cdot 10^{-34}$ Js	Planck's constant
$j = \sqrt{-1}$	imaginary unit
$k = 1.3807 \cdot 10^{-23}$ J/K	Boltzmann's constant
$\pi = 3.1416$	pi
$\varepsilon_0 = 8.854 \cdot 10^{-12}$ As/Vm	electric field permittivity in vacuum
$\mu_0 = 4\pi \cdot 10^{-7}$ Vs/Am	magnetic field permeability in vacuum

C.3 List of Latin symbols

a	major axis of the polarization ellipse
A	constant
A_c	coherence area
b	minor axis of the polarization ellipse
B_{ASE}	noise bandwidth of the optical amplifier
B_e	bandwidth of the electrical filter
BER	bit error ratio
B_{max}	maximum bandwidth
B_o	bandwidth of the optical bandpass filter
c	phase velocity
$data(t)$	electrical modulation signal
∂_t	partial derivative with respect to t
∂_x	partial derivative with respect to x
∂_y	partial derivative with respect to y
∂_z	partial derivative with respect to z
D	decision threshold
DOP	degree of polarization
$\vec{e}_x$	x-direction in the cartesian coordinate system
$\vec{e}_y$	y-direction in the cartesian coordinate system
$\vec{e}_z$	z-direction in the cartesian coordinate system
$\mathbf{E}$	electric field vector

$E_c(\vec{r},t)$	complex scalar electric field
$\vec{E}_c(\vec{r},t)$	complex electric field vector
$E_c(\vec{r}_1,t)$	complex scalar electric field at a fixed position $\vec{r}_1$
$E_c(\vec{r}_2,t)$	complex scalar electric field at a fixed position $\vec{r}_2$
$E_c(t)$	complex scalar electric field at a fixed position $\vec{r}$
$\mathbf{E}_{in}$	electrical field input vector
$\vec{E}_{in}(t)$	electrical field input vector
$\vec{E}_J$	Jones vector
$E(\vec{k})$	complex envelope of the scalar electric field
$\vec{E}(\vec{k})$	complex envelope of the electric field vector
$\mathbf{E}_{out}$	electrical field output vector
$\vec{E}_{out}(t)$	electrical field output vector
$E(\vec{r})$	complex amplitude of the scalar electric field for time-harmonic processes
$\vec{E}(\vec{r})$	complex amplitude of the electric field vector for time-harmonic processes
$E(\vec{r},t)$	scalar electric field
$\vec{E}(\vec{r},t)$	electric field vector
$E(t)$	real scalar electric field at a fixed position $\vec{r}$
E_x	magnitude of the x-component of the complex envelope of the electric field vector
$\mathbf{E}_x$	electric field vector of x-polarized light
$\tilde{E}_x(t)$	x-component of the complex electric field vector
E_y	magnitude of the y-component of the complex envelope of the electric field vector
$\mathbf{E}_y$	electric field vector of y-polarized light
$\tilde{E}_y(t)$	y-component of the complex electric field vector
E_z	magnitude of the z-component of the complex envelope of the electric field vector
$\tilde{E}_z(t)$	z-component of the complex electric field vector
$\vec{E}(z,t)$	electric field vector for a plane wave traveling in the z-direction
E_0	magnitude of a component of the complex envelope of the electric field vector
E_1	lower energy level
E_2	upper energy level
f	frequency
$f_O(o)$	PDF of random variable O
f_s	sample rate
f_0	mean frequency
$f_0(x)$	probability density function of the '0' signal level
$f_1(x)$	probability density function of the '1' signal level
F	noise figure of the optical amplifier
$g(\vec{r}_1,\vec{r}_2)$	normalized mutual intensity
$g(\tau)$	degree of correlation (coherence)
$g_{xy}(\tau)$	cross-correlation coefficient
G	gain of the optical amplifier
$\mathbf{G}$	coherency matrix
$\mathbf{G}^{pol}$	coherency matrix of completely polarized light
$G(\vec{r}_1,\vec{r}_2)$	mutual intensity
$G(\vec{r}_1,\vec{r}_2,\tau)$	mutual coherence function
G_{TIA}	gain of the transimpedance amplifier
$\mathbf{G}^{unpol}$	coherency matrix of completely unpolarized light

G_{xx}	autocorrelation function at $\tau = 0$
G_{xy}	crosscorrelation function at $\tau = 0$
G_{yy}	autocorrelation function at $\tau = 0$
$G(\tau)$	autocorrelation function
$G_{xx}(\tau)$	autocorrelation function of the x-component of the complex electric field vector
$G_{xy}(\tau)$	crosscorrelation function of the x- and y-component of the complex electric field vector
$G_{yy}(\tau)$	autocorrelation function of the y-component of the complex electric field vector
$h(t)$	Gaussian-shaped filter
$\vec{H}(\vec{r}, t)$	magnetic field vector
i	index of the components of the Stokes vector
I	electrical current
$\hat{I}$	total intensity
I_{ASE}	electrical current according to ASE noise
$I^2_{ASE-ASE}$	quadratic noise current according to ASE-ASE term
I_D	dark current
$I^2_n(t)$	quadratic noise current at the output of the PIN photodiode
$I(\vec{r})$	intensity at position $\vec{r}$
$I(\vec{r_1})$	intensity at position $\vec{r_1}$
$I(\vec{r_2})$	intensity at position $\vec{r_2}$
I_{sat}	saturation current of the PIN photodiode
I_{sh}	shot noise
$I^2_{sh}(t)$	quadratic noise current according to shot-noise
$I^2_{Signal-ASE}$	quadratic noise current according to Signal-ASE term
$I(t)$	electrical current over time
I_{th}	thermal noise
$I^2_{th}(t)$	quadratic noise current according to thermal noise
I_x	intensity of the x-component of the complex electric field vector
I_y	intensity of the y-component of the complex electric field vector
I_0	intensity
k	wave number
$\vec{k}$	wave vector
l	integer
l_c	coherence length
m	integer
n	refractive index
n_{sp}	spontaneous emission factor
N	number of observations
N_{ASE}	one-sided spectral density according to ASE noise
N_B	number of bits
$N_{sh}(t)$	one-sided spectral density according to shot noise
$N_{th}(t)$	one-sided spectral density according to thermal noise
N_1	population density of the lower energy level
N_2	population density of the upper energy level
o	integration variable
O	random variable
p	number of polarizations present at the output of the optical amplifier
P	optical power

P_{ASE}	power according to ASE noise
$P_{average}$	average power
$\vec{P}_{in}(t)$	input power of the modulator
$P_{out(max)}$	maximum output power of the optical amplifier
$\vec{P}_{out}(t)$	output power of the modulator
P_{peak}	peak power
$P(t)$	optical power over time
P_x	optical power in one PSP
$P_{x+90°}$	optical power in the orthogonal PSP
P_0	power level '0' bit
P_0	probability of receiving a '0' bit
$P_{0|1}$	conditional probability of a detected '0' when a '1' was sent
P_1	power level '1' bit
P_1	probability of receiving a '1' bit
$P_{1|0}$	conditional probability of a detected '1' when a '0' was sent
$\vec{r}$	position vector
$\mathbf{r}_1$	position vector
$\vec{r}_1$	position vector
$\mathbf{r}_2$	position vector
$\vec{r}_2$	position vector
R	bit rate
R	reflection
$R_{x+90°}$	reflection efficiency for $(x+90°)$-polarized light
s_i	ith normalized component of the Stokes vector
s_1	normalized component of the Stokes vector
s_2	normalized component of the Stokes vector
s_3	normalized component of the Stokes vector
S	responsivity of the PIN photodiode
$\vec{S}$	Stokes vector
S_A	responsivity of the PIN photodiode in the upper branch of the BPolSK receiver
S_B	responsivity of the PIN photodiode in the lower branch of the BPolSK receiver
$S(f)$	power spectral density
S_i	ith component of the Stokes vector
S_{RX}	receiver sensitivity
S_0	component of the Stokes vector
S_1	component of the Stokes vector
S_2	component of the Stokes vector
S_3	component of the Stokes vector
t	absolute time
T	absolute temperature
T	time duration
T_B	bit duration
T_x	transmission efficiency of x-polarized light
u	u-coordinate of the polarization ellipse
v	v-coordinate of the polarization ellipse
V_d	voltage at the PIN photodiode
x	x-coordinate

$x(t)$	input pulse
y	y-coordinate
$y(t)$	output pulse
z	z-coordinate
Z	transimpedance

C.4 List of Greek symbols

β	responsivity imbalance
ΔDOP	difference in the degree of polarization
Δf	laser linewidth
Δt	sampling interval
$\Delta t_{10/90}$	10/90-rise time
$\Delta\eta$	difference in the angle of linear polarization
$\Delta\varphi$	phase difference between marks and spaces
γ	offset angle
ε	electric field permittivity
ε_r	relative electric field permittivity
ϵ	ellipticity
ζ	quantum efficiency
η	azimuth
κ	electric conductivity
λ	wavelength
λ_0	wavelength in vacuum
μ	magnetic field permeability
μ_I	mean of electrical current
μ_r	relative magnetic field permeability
μ_0	mean of received '0' bits
μ_1	mean of received '1' bits
σ_I	standard deviation of electrical current
σ_I^2	variance of electrical current
σ_{sh}^2	variance according to shot noise
σ_{th}^2	variance according to thermal noise
σ_0^2	variance of received '0' bits
σ_1^2	variance of received '1' bits
τ	time delay
τ_c	coherence time
ϕ	phase difference
ϕ_x	phase of the x-component of the complex envelope of the electric field vector
ϕ_y	phase of the y-component of the complex envelope of the electric field vector
ϕ_z	phase of the z-component of the complex envelope of the electric field vector
Φ	diameter
$\Phi(\omega)$	characteristic function
χ	random variable of chi-squared distribution
ω	angular frequency
$\vec{\nabla}$	vectorial differential operator Nabla
∇^2	Laplace operator

Bibliography

[1] S. Betti, G. D. Marchis, and E. Iannone, "Polarization modulated direct detection optical transmission systems," *Journal of Lightwave Technology*, Vol. 10, no. 12, pp. 1985–1997, 1992.

[2] S. Benedetto, R. Gaudino, and P. Poggiolini, "Direct detection of optical digital transmission based on polarization shift keying modulation," *IEEE Journal on Selected Areas in Communications*, Vol. 13, no. 3, pp. 531–542, 1995.

[3] E. Hu, Y. Hsueh, K. Wong, M. Marhic, L. Kazovsky, and K. Shimizu, "4-level direct-detection polarization shift-keying (DD-PolSK) system with phase modulators," in *Proceedings of Optical Fiber Communication Conference and Exposition (OFC), Atlanta, USA*, Vol. 2, 2003, pp. 647–649.

[4] A. Carena, V. Curri, R. Gaudino, N. Greco, P. Poggiolini, and S. Benedetto, "Polarization modulation in ultra-long haul transmission systems: A promising aternative to intensity modulation," in *Proceedings of European Conference on Optical Communication (ECOC), Madrid, Spain*, September 1998, pp. 429–430.

[5] J. J. Lepley, J. G. Ellison, S. G. Edirisinghe, S. D. Walker, and A. S. Siddiqui, "Excess penalty impairments of polarization shift keying transmission format in presence of polarization mode dispersion," *Electronics Letters*, Vol. 36, no. 8, pp. 736–737, 2000.

[6] A. S. Siddiqui, S. G. Edirisinghe, J. J. Lepley, J. G. Ellison, and S. D. Walker, "Dispersion-tolerant transmission using a duobinary polarization-shift keying transmission scheme," *IEEE Photonics Technology Letters*, Vol. 14, no. 2, pp. 158–160, 2002.

[7] N. Chi, L. Xu, S. Yu, and P. Jeppesen, "Generation and transmission performance of 40 Gbit/s polarization shift keying signal," *Electronics Letters*, Vol. 41, no. 9, 2005.

[8] S. Benedetto and P. Poggiolini, "Theory of polarization shift keying modulation," *IEEE Transactions on Communications*, Vol. 40, no. 4, pp. 708–721, 1992.

[9] ——, "Polarization shift keying: An efficient coherent optical modulation," in *Proceedings of Telecommunications Symposium, Rio de Janeiro, Brazil*, Vol. 2, 1990, pp. 14–20.

[10] F. Hlawatsch, "Modulations- und Detektionsverfahren," Lecture Notes, Institut für Nachrichtentechnik und Hochfrequenztechnik, TU Wien, 2005.

[11] S. B. Alexander, *Optical Communication Receiver Design*, ser. Tutorial texts in optical engineering. Bellingham, Washington: SPIE Optical Engineering Press, 1997, Vol. TT22.

[12] J. N. Damask, *Polarization Optics in Telecommunications*, ser. Springer series in optical sciences. New York: Springer Science and Business Media, Inc., 2005, Vol. 101.

[13] B. Saleh and M. C. Teich, *Fundamentals of Photonics*. New York: John Wiley and Sons, Inc., 1991.

[14] A. Scholtz, "Wellenausbreitung," Lecture Notes, Institut für Nachrichtentechnik und Hochfrequenztechnik, TU Wien, 2004.

[15] B. Dehlink, "Atmospheric impact on laser beam propagation," Master Thesis, Institut für Nachrichtentechnik und Hochfrequenztechnik, TU Wien, 2004.

[16] G. Reider, *Photonik - Eine Einführung in die Grundlagen*. Vienna, New York: Springer, 1997.

[17] *WDM User's Manual*, VPIsystems, Inc., 2007.

[18] *Photonic Modules Reference Manual*, VPIsystems, Inc., 2007.

[19] A. Taklaya, "Wandering laser beam in a turbulent atmosphere," *Sov. J. Quantum Electron.*, pp. 87–89, 1978.

[20] W. R. Leeb, "Optische Nachrichtentechnik," Lecture Notes, Institut für Nachrichtentechnik und Hochfrequenztechnik, TU Wien, 2005.

[21] N. A. Olsson, "Lightwave systems with optical amplifiers," *Journal of Lightwave Technology*, Vol. 7, pp. 1071–1082, 1989.

[22] D. Marcuse, "Derivation of analytical expressions for the bit-error probabiliy in lightwave systems with optical amplifiers," *Journal of Lightwave Technology*, Vol. 8, no. 12, pp. 1816–1823, 1990.

[23] F. Fidler, "Optical communications from high-altitude platforms (HAPs)," Doctoral Thesis, Institut für Nachrichtentechnik und Hochfrequenztechnik, TU Wien, 2007.

[24] A. H. Gnauck and P. J. Winzer, "Optical phase-shift-keyed transmission," *Journal of Lightwave Technology*, Vol. 23, no. 1, pp. 115–130, 2005.

[25] L. Mandel and E. Wolf, *Optical Coherence and Quantum Optics*. New York: Cambridge University Press, 1995.

[26] M. Rupp, "Verarbeitung stochastischer Signale," Lecture Notes, Institut für Nachrichtentechnik und Hochfrequenztechnik, TU Wien, 2004.

[27] J. Landstreet, "Standardization of optical polarization measurements: a simple introduction," in *Proceedings of Workshop on future of astronomical standardization, Blankenberge, Belgium*, 2006.

[28] D. Clarke and J. Naghizadeh-Khouei, "A reassessment of some polarization standard stars," *The Astronomical Journal*, Vol. 108, no. 2, pp. 687–693, 1994.

[29] G. D. Schmidt, R. Elston, and O. L. Lupie, "The Hubble Space Telescope northern-hemisphere grid of stellar polarimetric standards," *The Astronomical Journal*, Vol. 104, no. 4, pp. 1563–1567, 1992.

[30] K. Serkowski, D. S. Mathewson, and V. L. Ford, "Wavelength dependence of interstellar polarization and ratio of total to selective extinction," *The Astrophysical Journal*, Vol. 196, pp. 261–290, 1975.

[31] D. Batcheldor, A. Robinson, D. Axon, D. C. Hines, W. Sparks, and C. Tadhunter, "The NICMOS polarimetric calibration," *The Publications of the Astronomical Society of the Pacific*, Vol. 118, no. 842, pp. 642–650, 2006.

[32] M. Breger and J.-C. Hsu, "On standard polarized stars," *The Astrophysical Journal*, Vol. 262, pp. 732–738, 1982.

[33] University of Arizona. (2008, January) Interstellar-polarized standard stars. [Online]. Available: http://chinadoll.as.arizona.edu/ schmidt/spol/polstds.html

[34] D. A. Turnshek, R. L. W. I. R. C. Bohlin, O. L. Lupie, and J. Koornneef, "An atlas of Hubble Space Telescope photometric, spectrophotometric, and polarimetric calibration objects," *The Astronomical Journal*, Vol. 99, no. 4, pp. 1243–1261, 1990.

[35] Y. Kravtsov, "Propagation of electromagnetic waves through a turbulent atmosphere," *Reports on Progress in Physics*, pp. 39–112, 1992.

[36] A. Anufriev, Y. Zimin, A. Vol'pov, and I. Matveev, "Change in the polarization of light in a turbulent atmosphere," *Soviet Journal of Quantum Electronics*, Vol. 13, no. 12, pp. 1627–1628, 1983.

[37] General Photonics. (2007, October) Polarization beam combiner/splitter. [Online]. Available: www.generalphotonics.com/pdf/PMCombiner.pdf

[38] Thorlabs. (2007, October) 3mm polarizing beam splitting cube. [Online]. Available: www.thorlabs.com/NewGroupPage9.cfm?ObjectGroup_ID=739

[39] EOT Electro-Optics Technology. (2007, October) Amplified photodetectors. [Online]. Available: www.eotech.com/store/pdf/Amplified_Detectors.pdf

[40] STMicroelectrionics. (2007, October) 1.1 GHz low-noise operational amplifier. [Online]. Available: www.st.com/stonline/products/literature/ds/10960/tsh330.pdf

[41] Texas Instruments. (2007, October) 1.8 GHz low distortion current feedback operational amplifier. [Online]. Available: http://focus.ti.com/lit/ds/symlink/ths3201.pdf

[42] National Semiconductor. (2007, October) 1.2 GHz low distortion op amplifier with shutdown. [Online]. Available: www.national.com/ds/LM/LMH6703.pdf

[43] EOT Electro-Optics Technology. (2007, October) Biased ingaas photodetectors. [Online]. Available: www.eotech.com/store/pdf/Biased_InGaAs_Detectors.pdf

[44] General Photonics. (2007, October) Polarization diversity detector. [Online]. Available: www.generalphotonics.com/pdf/PDD.pdf

[45] D. Marcuse, "Calculation of bit-error probability for a lightwave system with optical amplifiers and post-detection gaussian noise," *Journal of Lightwave Technology*, Vol. 9, no. 4, pp. 505–513, 1991.

[46] M.-K. Liu, A. C. Vrahas, and M.-J. B. Moretti, "Saddle point bit error rate computations for optical communication systems incorporating equalizers," *IEEE Transactions on Communications*, Vol. 43, no. 2/3/4, pp. 989–1000, 1995.